FIRST YEAR REPORT

Annual Report on Contract PH-43-67-1136

by
J. W. Melvin, Project Engineer
V. L. Roberts, Project Director

Highway Safety Research Institute
The University of Michigan
Ann Arbor

ACKNOWLEDGMENTS

The authors of this report wish to acknowledge the assistance of the following persons in carrying out the research outlined in this progress report: P. M. Fuller, J. L. Wood, I. Barodawala, D. E. Bendure, and M. L. Dunlap of the Biomechanics-Biomedical Department of the Highway Safety Research Institute; A. Engin, Y. K. Liu, and I. K. McIvor of the Department of Engineering Mechanics at The University of Michigan; T. Fallenstein and A. Huntress of Dow-Corning Corporation; D. F. Huelke, Professor, and F. G. Evans, Professor of the Department of Anatomy of The University of Michigan; and P. W. Gikas, Chief of Clinical Laboratory Services at the Veterans Administration Hospital in Ann Arbor, Michigan and R. C. Hendrix, Professor of Pathology at The University of Michigan whose assistance is proving most valuable in obtaining tissues at autopsy.

TABLE OF CONTENTS

APPENDICES

LIST OF FIGURES

Main Report

Appendices

LIST OF TABLES

MAIN REPORT

INTRODUCTION

The report covers the progress made on the Head Injury Model Project in the second six months of the contract. The activity in the first six months was covered in the report previously submitted. This report uses the same format as the previous report in that it is broken down into this section, the "Main Report", and into a section of Appendices. The Main Report is a summary of the last six months progress and the Appendices detail the work.

In the past six months there have been significant advances made in three areas which bear directly on the achievement of the objectives of the project. These areas are high speed physical properties testing, histology of hard and soft tissues, and in vivo dynamic property testing of brain material. In addition, advances have been made in analytical studies of head models and in promising new measurement techniques.

The six month report discussed the evolutionary steps in getting the program under way. They were:

1. Establishment of bibliographies on hard and soft tissue.
2. Establishment of sources of fresh and embalmed materials and the attendant catloging procedures.
3. Development of testing procedures.

This report discusses the following-up and expansion of these steps and the projection of the work into the second year of the project.

In the physical testing program on hard materials, testing has been carried into the impact range. Because of the very short time duration of the tests,new grips, recording techniques and test procedures had to be developed. The Plastechon High Speed Universal Testing Machine (Fig. 1) is now being used in many of the tests. It has a continuously variable ram speed range from 20 inches/minute to 30,000 inches/minute. Statistical models have been developed to facilitate the analysis of the test data in regards to rate of loading effects, position effects and head to head effects.

A laboratory devoted exclusively to histological examination of hard and soft tissues has been set-up. It includes all the normal equipment for processing soft tissues plus a hard tissue slicer for bone specimens. A 100% examination program on tensile and compressive tests of bone is under way. The purpose of the histology lab is to correlate the microstructure of a specimen with its mode of failure. The laboratory is in the process of being equipped to do complete chemical analysis.

Dow-Corning engineers have developed a portable dynamic property device known as the Dynamic Probe Apparatus (DPA). The DPA permits in vivo brain testing in primates and allows testing to continue through time of death to study post mortem effects. A refined version of the DPA could possibly be used in human in vivo tests.

Significant progress has been made towards the analytical solution of the head impact problem. A solution has been obtained for the case of a fluid-filled spherical shell of uniform thickness subjected to a symmetric impulse. Work is continuing on the refinement and application to more complex systems.

The following papers will be written in the next six months by the Biomechanics Deaprtment based on the work performed for the Head Injury Project.

1. Mechanical Properties of the Brain
   Fallenstein, Melvin, Hulse

2. Tensile Properties of Skull Cortical Bone
   Robbins, Melvin, Wood

3. Compression Properties of Skull Cancellous Bone
   Melvin, Robbins, Roberts

4. Shear Properties of Skull Cancellous Bone
   Melvin, Fuller, Robbins

5. The Effect of Micro-structure on the Mechanical Properties of Bone
   Fuller, Melvin, Robbins, Roberts

6. Mathematical Model of Skull Impact
   Engin, Liu, Robbins

A progress schedule showing the next years activity on the Head Injury Project is shown in Fig. 2.

Experimental Research Program

A. Sources of Biological Specimens

The arrangements made with the University of Michigan Medical Center, the Veterans Administration Hospital and the Anatomy Department of the University for the acquisition of fresh human autopsy material, embalmed human material and living primates have proven quite satisfactory. The system for material acquisition was detailed in the six month report. Table 1 lists the supply of human autopsy material acquired during the last six months.

B. Experiments and Results

1. Tension Tests

The tension test has undergone considerable development in the past six months. Improved techniques now make it possible to take a bone plug, machine

out a specimen, strain gage it and test it in less than an hour. Gripping techniques have been proven well into the range of dynamic impact loading.

Statistically planned test series are being used to study the relative effects of strain rate and skull to skull variation on the tensile properties of compact skull bone. A detailed discussion of the analysis of variance models used in the study is in Appendix D.

Comprehesive histological studies are also being made on each tensile specimen. We feel that specimens containing structural flaws, obvious only under histological examination, should not be analyzed statistically with relatively unflawed specimens. Figs. 3, 4, and 5 point this out markedly. Fig. 3 shows the stress-strain curves for two specimens from the same bone plug with grossly different behavior. Examination of the failure micrographs of the specimens pinpoint the reason for the differing behavior. Fig. 4 shows that specimen VA 13 PL 5 failed in a reasonably uniform region of bone. Fig. 5 shows that specimen VA 13 PL 1 failed in a region which was rich in flaws. For meaningful statistical analysis of mechanical properties these two specimens can not be classed together.

Details of the tension testing program can be found in Appendix A.

2. Compression Tests

The compression test determines the crushing characteristics of the diploe layer. Work in the past six months has centered on improving the test specimen configuration and developing equipment for high speed tests.

The compression specimen now consists of diploe layer only. All specimens in a test series are machined to a constant height. By standardizing the specimens we have eliminated much of the data scatter present in earlier testing. Figs. 6 and 7 show the effectiveness of this approach. These graphs show an

obvious relationship between crushing strength and modulus of elasticity. We feel the key to this relationship is the density of the diploe layer. Histological examination including density determination is being made to validate this concept.

The data from the tests has been analyzed according to two way analysis of variances in order to investigate the relative effects of strain rate and skull to skull variation on the mechanical properties. This work is detailed in Appendix B.

3. Shear Tests

The purposes of the shear test is measurement of the capacity of the diploe layer to resist shear in terms of shear strength. An improved technique has been developed for obtaining uniform specimens from embalmed calvariums and fresh bone plugs quickly. The shear test grips have been modified to improve the loading of the specimens.

Statistically planned tests have been run on embalmed material using the Plastechon high speed universal testing machine. The purpose of the tests was to investigate the relative importance of the effects of strain rate, position in the skull, and skull to skull variation on the shear strength properties. A limited number of tests have been run on frozen, fresh autopsy material. The results of the tests are detailed in Appendix C.

A useful means for displaying shear strength as a function of position in the skull has been developed. The three-dimensional bar graph show in Fig. 8 was drawn by a computer. The height of each bar represents the shear strength. The coordinate system along the sides of the display indicate the specimen position in the skull. The letters on the top of each bar indicate the strain rate

used in testing that specimen. Fig. 8 is a front view of the skull and some of the data is obscured from view. The computer can view the data from any position and in Fig. 9 it is viewing in from the rear. Note that data obscured in Fig. 8 is now visible. We feel that this technique will prove quite valuable in displaying a variety of information related to position in the skull.

4. Mechanical Properties of Brain

In the past six months there have been three major areas of investigation on the mechanical properties of human brain. Effort was directed toward the determination of the complex dynamic shear modulus and secant bulk modulus of human brain tissue. A new device, designed to measure a complex dynamic modulus of the brain in vivo, was constructed and used for preliminary investigations of two monkey brains in vivo.

The effort to determine the complex dynamic shear modulus of human brain tissue was begun during the first six months of the contract, utilizing Dow Corning's Dynamic Mechanical Apparatus (DMA). These results were published in the Six Month Report of the contract. Research since that time has been directed toward reducing observed differences in the measured modulus thought to be due to such physiological mechanisms as drying and shear degradation. Latest data indicate that these effects can be minimized by utilizing a high-relative-humidity sample environment in conjunction with a thin silicone coating on the exposed tissue surface. Based on all available data it is thought that the elastic (G'), and viscous loss (G") components of the complex dynamic shear modulus ($G^* = G' + iG''$) of human brain tissue lie between 6-11 x 10^3 dynes/cm^2 and 3.5-6.0 x 10^3 dynes/cm^2, respectively. Tan δ, or G"/G' is thought to lie in the range 0.40-0.55.

In order to measure a complex dynamic modulus of brain tissue in vivo, a device was constructed for in vivo testing through a 1/4-inch hole in the skull. Termed the Dynamic Probe Apparatus (DPA), this device has been used to test the brains of two anesthetized live monkeys. The monkeys were sacrificed during the test and measurements were continued until approximately two hours post-sacrifice in order to find a correlation between the in vivo modulus and that observed in tests of autopsy specimens as used on the DMA. Histological investigation of the sample tissue was also conducted in order to ascertain if any brain damage resulted from the testing. The data is currently being reduced and will be reported at a later date. It is now felt that this device is the potentially most-useful approach for determination of the true in vivo modulus of the brain as it encompasses the variables of amplitude and frequency, and therefore shear rate. It also allows rapid testing, as the results are recorded photographically.

The determination of the secant bulk modulus of human brain tissues for applied hydrostatic stresses of 0-1000 psi was the object of considerable testing. High pressure tests in a two-phase system (human brain tissue plus carrier fluid) were also continued for an increased test population. Severe variations in the modulus had been observed in preliminary tests conducted at low pressures, under 1000 psi, on an Instron tensile machine. These variations were though to be due to air entrapped within the vascular structure of the test tissues or to effects attributable to the selection of carrier fluid. A number of low pressure tests were conducted using both silicone fluid and water as the carrier fluids. Some of the samples were degassed at low pressure immediately preceding actual testing. Results indicate that the degassing procedure caused gaseous voids in the samples which led to erroneous low modulus values. The carrier fluids selection does not seem to be very critical except for the possibility

of trapping small air bubbles on the tissue surface when using a silicone fluid. (One test was invalidated for this reason.) The values for the secant bulk modulus obtained in other non-degassed low pressure tests form a smooth curve when mated to values obtained at high (>1000 psi) pressures. This work is detailed in Appendix E.

D. Future Work

The basic bone tests (tension, compression, and shear) will be extended into the range of dynamic impact. The resulting data will be sorted and classified according to the findings of the parallel histological studies. Finally, the sorted data will be statistically analyzed in order to produce meaningful values of the properties of skull bone as a function of strain rate and to indicate the effect microstructure has on these properties. This information will be used in the analytical development of constitutive equations for skull bone.

An additional test on skull bone will be incorporated during the coming year. A four point bending test will be performed on beams machined from fresh bone plugs. The upper and lower surfaces of the beam will be the upper and lower tables of the skull bone. Both specimens with and without sutures will be tested. In the case of specimens with sutures in the test section, the object of the test is to characterize the bending moment transmission along the beam through the suture. This information is needed for construction of whole skull mechanical models. The case where no suture is present in the test section is even more important to the goals of the Head Injury Project. This is because the bending specimen is the first step towards the construction of a whole skull model. The bending test incorporates the features of all the three basic bone tests (tension, compression, and shear) into what is essentially a working model.

The values of the mechanical properties determined in the basic tests can be used in simple beam theory to predict how the bending specimen will behave under load. Depending on the loading conditions, the beam failure can be due to tensile failure of the outer table in the test section, compressive failure of the diploe layer near the loading pins or shear failure of the diploe layer between the loading pins. Thus, the observed and measured behavior of the actual beam can be compared with the behavior predicted from the basic tests.

Testing of the soft tissues of the head except brain material will be done in the coming year. The first step in developing these tests will be the development of a phototransitonzed extensometer that will enable strain measurements to be made that will be independent of specimen slippage in the grips. The majority of the work will be done in tension, with some work done in shear. Blood vessels will be included in this testing.

A series of in vivo primate brain tests is planned using the DPA. The results of the tests will be compared with in vitro primate tests. The resulting information will be used in an analytical study to correlate the properties obtained by both testing methods. This correlation will then allow concentrated tests to be performed on human brain material in vitro with the assurance that they can be related to in vivo conditions. The concentrated testing will be concerned with structural and directional effects in the brain material. Investigation of the possibility of impulsive testing of brain material will be made.

The dynamic bulk modulus of human brain material and CSF will be determined using the test cylinder of Dow-Corning in the Plastechon testing machine. The material will be subjected to cyclic loading at frequencies up to 100 HZ. CSF viscometry will also be carried out using standard and capillary viscometers. A schedule of these efforts is shown in Fig. 2.

Theoretical Program

A. Mathematical Model for Head Injury

Since the time of the Six Month Report most of the analytical effort has been directed at the impact problem of a fluid-filled shell. This work is described in Appendix F. The problem which was solved, involves a spherical elastic shell of uniform thickness subjected to a symmetric impulse. The fluid is a linear, aconstic medium not possessing any viscoelastic behavior. Computer evaluation of the solution is nearly finished. The uniqueness of this problem rests in the fact that it is a transient problem which means that the initial wave passing through the skull and brain can be studied. The next step in the analytical effort will involve placing a viscoelastic fluid in the shell.

This analytical work is serving to satisfy the requirement for a PhD in the Department of Engineering Mechanics at the University of Michigan. Mr. Ali Engin who is carrying out the study has recently joined the staff of the Biomechanics Department where he will devote full time to studies in impact dynamics.

B. Future Work

Continuing efforts will be made towards refining the present head model analysis to achieve the goal of an accurate mathematical representation of the human head. Once sufficient data on the rate sensitive properties of skull bone have been gathered, work will renewed on developing constitutive equations to represent this behavior. The analytical techniques described in the six month report will be used in this effort.

An analytical correlation of in vivo brain testing and in vitro brain testing is planned. This work will follow the completion of the planned series of in vivo primate tests mentioned in the experimental section.

The scheduling of these efforts is shown in Fig. 2.

TABLE 1. SUMMARY OF HUMAN MATERIAL

Bone Specimen	Age	Race	Sex	Cause of Death
VA-33-PR	48	C	M	Heart attack
VA-34-PL	70	C	M	Cancer of throat
VA-35-PR	69	C	M	Cancer of colon
VA-36-PL	47	C	M	Cancer of lung
VA-37-PR	74	C	M	Vascular disease
VA-38-PL	80	C	M	Drug overdose
VA-39-PR	47	C	M	Multiple myiloma
VA-40-PR	50	C	M	Respiratory death
VA-41-PL	49	C	M	Emphysema
VA-42-PL	73	C	M	Cancer of lung and liver
VA-43-PR	72	C	M	Cancer
VA-44-PR	54	C	M	Kidney failure
VA-45-PR	36	C	M	Kidney failure
VA-46-PL	71	C	M	Diabetes
VA-47-PL	27	C	M	Malignant melenoma
VA-48-PR	26	C	M	Chronic renal failure
VA-49-PL	71	C	M	Malignant melenoma
VA-50-PR	53	C	M	Cancer
VA-51-PL	90	C	M	Acute Granulocytic Leukemia
VA-52-PR	83	C	M	Cancer
VA-53-PR	45	C	M	Di Gulielma Syndrome Leukemia
VA-54-PR	73	C	M	Infection from operation

Bone Specimen	Age	Race	Sex	Cause of Death
VA-55-PR	76	C	M	Right pulmonary embolism
VA-56-PL	35	C	M	Acute Leukemia
VA-57-PR	53	C	M	Brain Cancer
VA-58-FR	81	C	M	Mesenteric thrombosis
VA-59-FR	68	C	M	Brain Tumor
VA-60-PL	51	C	M	Metastatic carcinoma
VA-61-PR	58	C	M	Acute Aneurysm
VA-62-PR	48	N	M	Unknown
EM-89	82	C	F	Heart disease
EM-90	90	C	M	Heart disease
EM-91	65	C	F	Terminal Metastatic carcinoma
EM-94	71	C	M	Coronary thrombosis
EM-95	65	C	F	Metastatic carcinoma
EM-96	63	C	M	Chronic renal insufficiency
EM-97	68	C	M	Cerebral vascular accident
EM-99	66	C	M	Bronchopneumonia
EM-100	75	C	M	Ruptured aorta
EM-108	19	C	F	Acidosis
EM-115	52	C	M	Bronchogenic carcinoma
UM-18-P(2)	60	N	F	D.O.A. - hypertension
UM-19-P(2)	14	C	F	Hodgkini disease
UM-20-P(2)	76	C	M	Cirrhosis of liver
UM-21-P	35	C	M	Acute Gastrointestisnal hemorrhage

Bone Specimen	Age	Race	Sex	Cause of Death
UM-23-P(2)	Unknown	C	F	Unknown
UM-24-P(2)	55	C	M	Renal failure
UM-25-P(2)	30	Indian	M	Massive brain damage
UM-26-P(2)	71	C	F	Cancer
UM-27-T(2)	43	C	F	Cancer
UM-28-F(2)	40	C	M	Cancer
UM-29-F(2)	25	N	F	Pneumonia
UM-30-T(2)	45	C	M	Neurogenic shock
UM-31-PR(2)	14	C	M	Metastatic Hemangio
UM-32-F(2)	52	C	M	Lung Cancer
UM-33-F(2)	64	C	F	Renal failure
UM-34-P(2)	73	C	M	Pulmonary hemorrhage
UM-35-P(2)	55	C	F	Cardiac arrhythmia

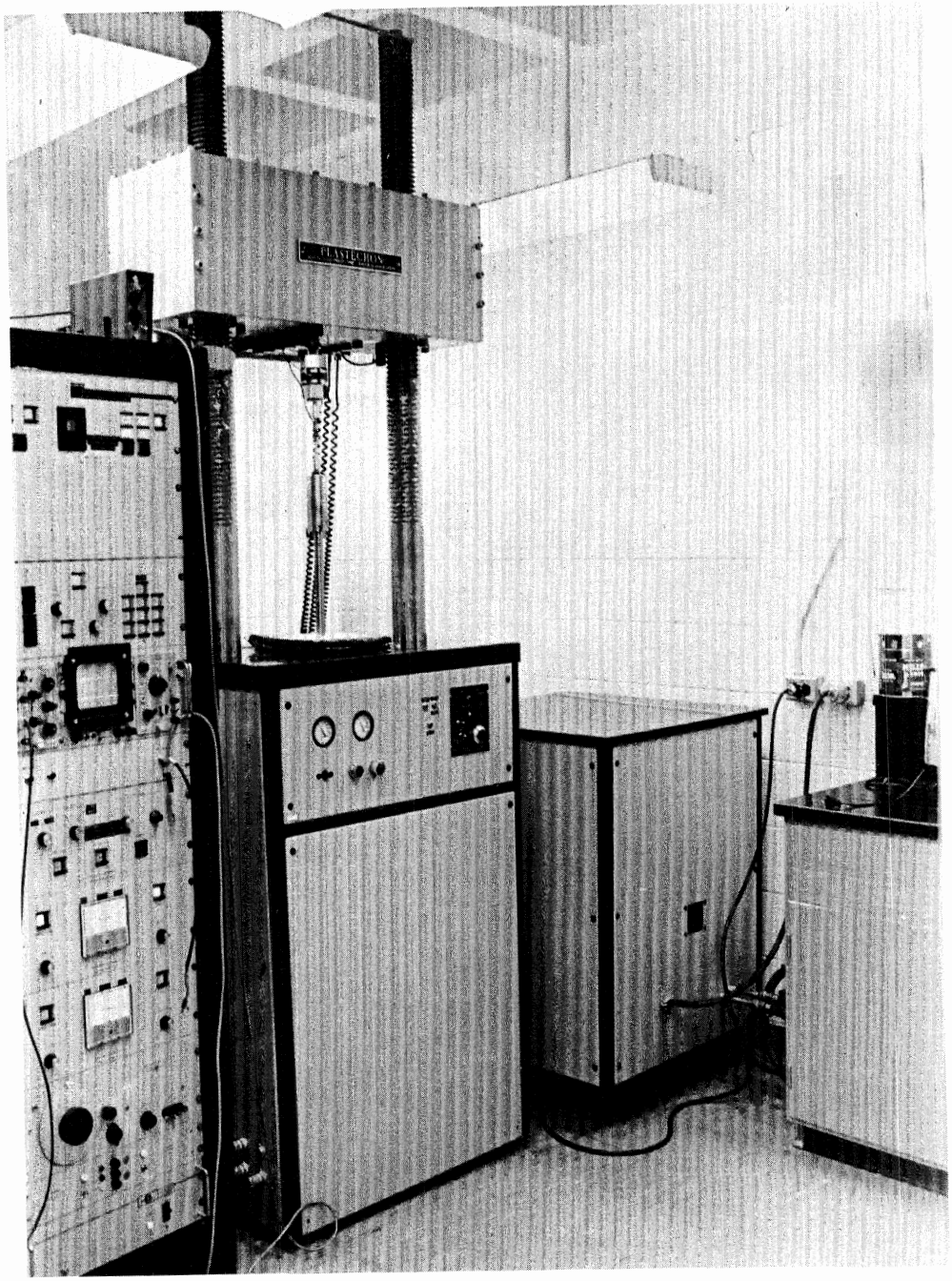

Fig. 1 Plastechon High Speed Universal Testing Machine Facility.

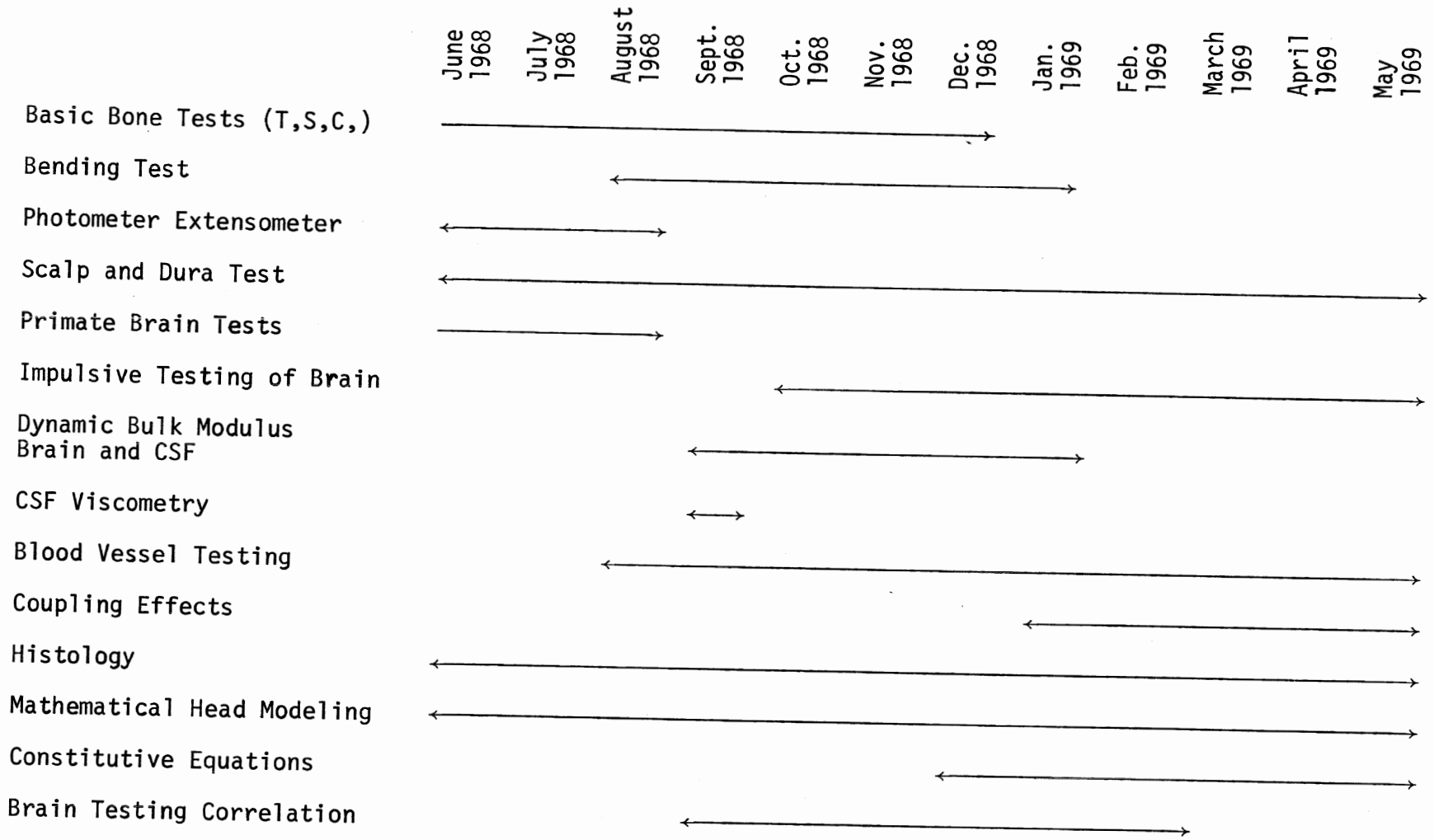

Fig. 2 WORK SCHEDULE FOR SECOND YEAR

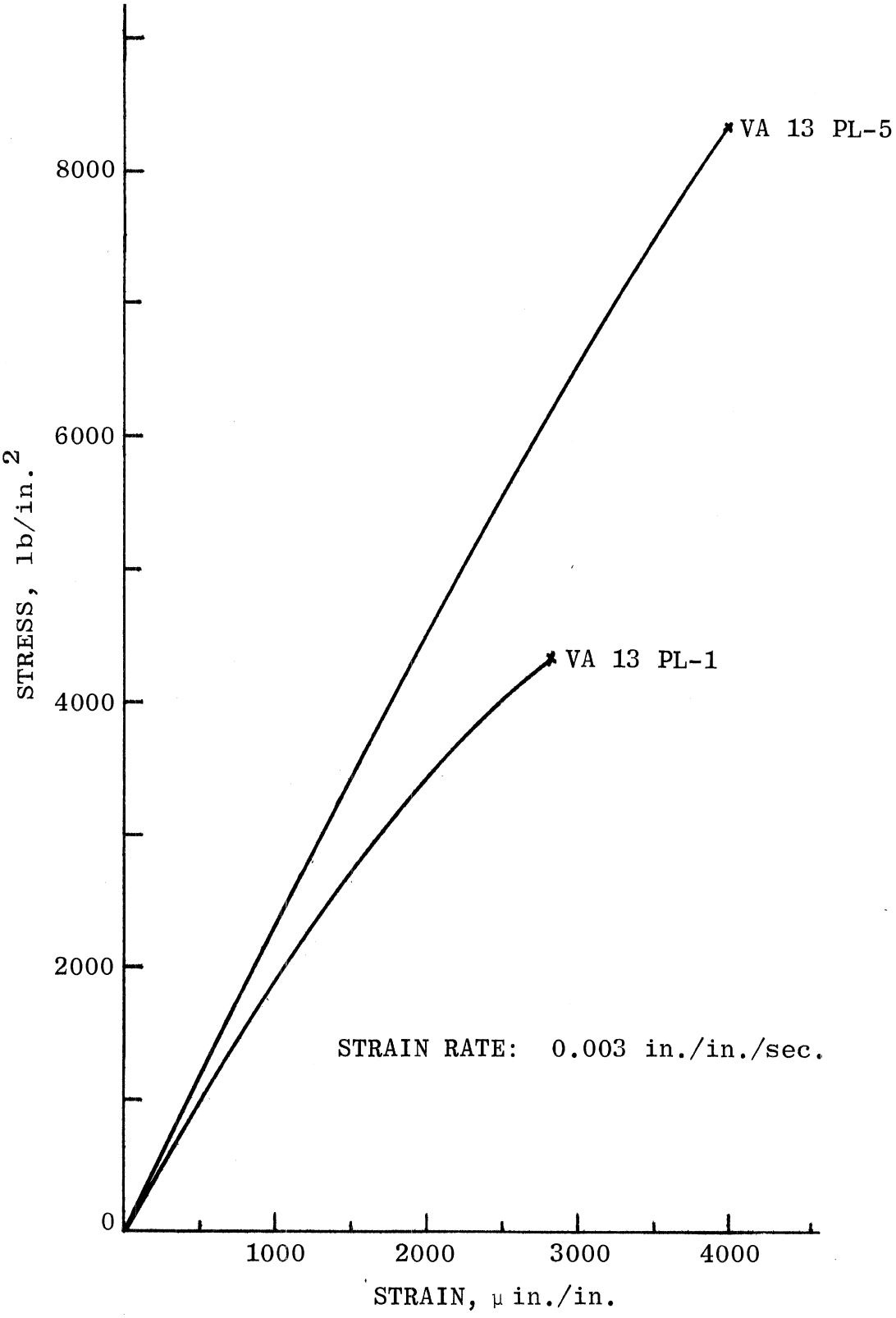

Fig. 3 Stress-Strain Curves for Two Tensile Specimens from the same Bone Plug.

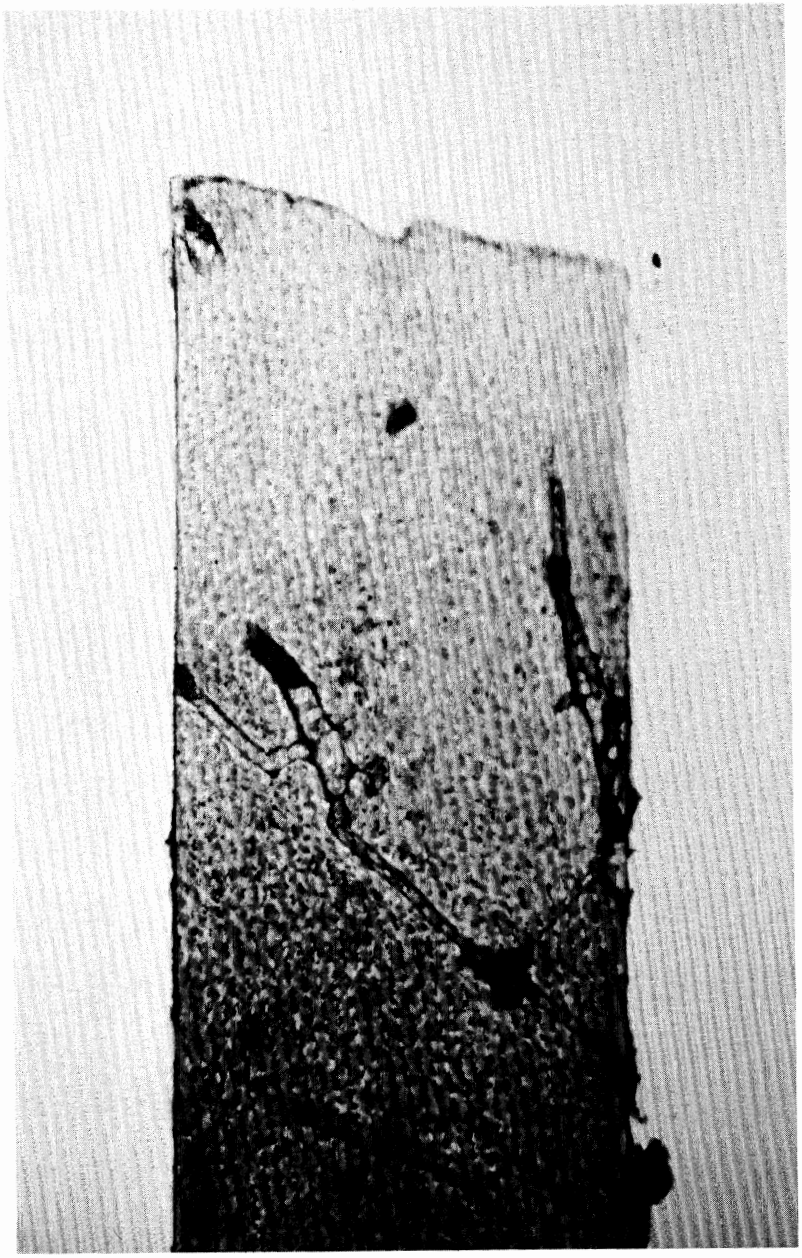

Fig. 4 Micrograph of Specimen VA 13 PL 5 (40X)

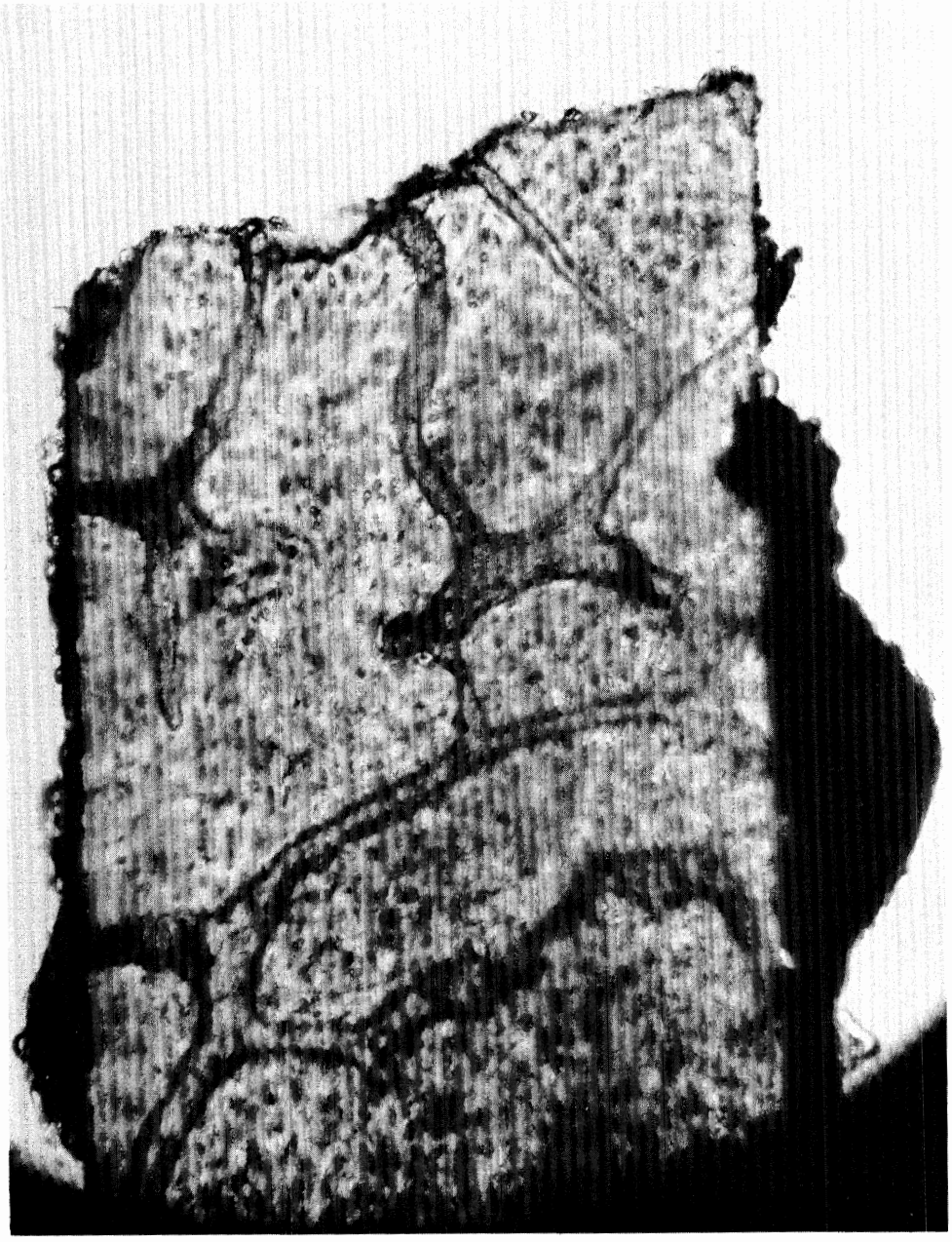

Fig. 5 Micrograph of Specimen VA 13 PL 1 (40X)

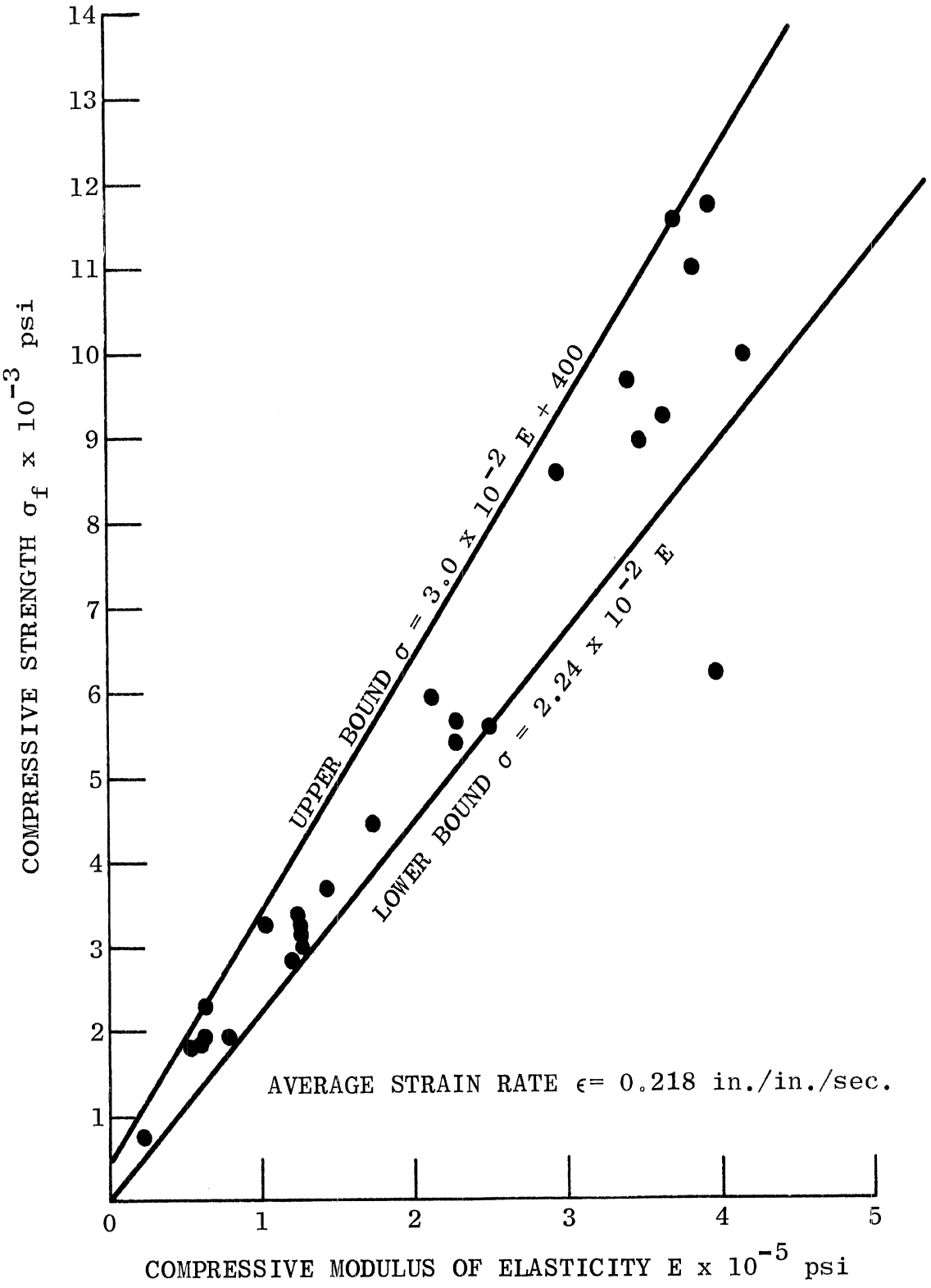

Fig. 6 Compressive Strength vs. Compressive Modulus of Elasticity for Spongy Skull Bone Tested at 0.218 in/in/sec Strain Rate.

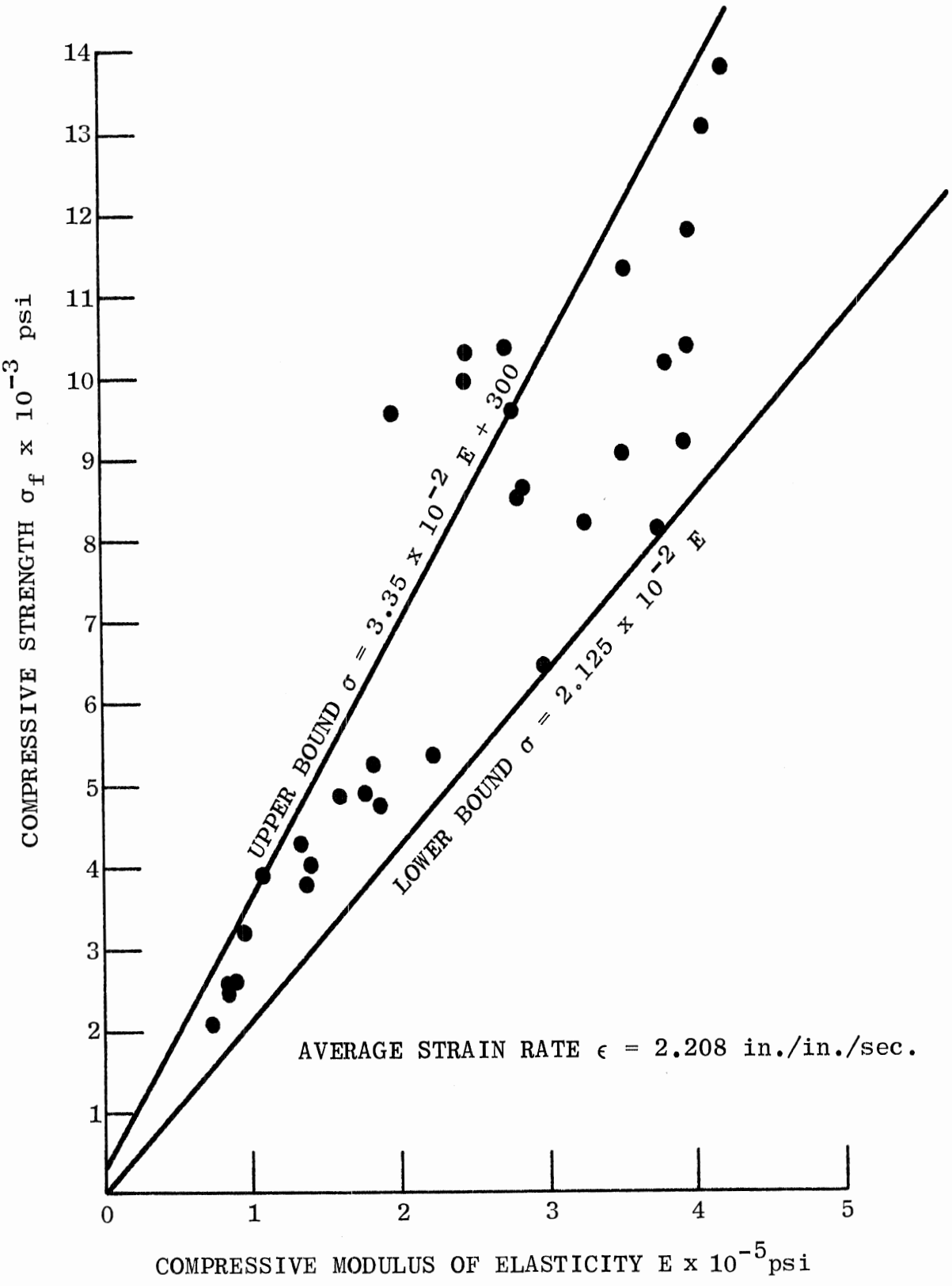

Fig. 7 Compressive Strength vs. Compressive Modulus of Elasticity for Spongy Skull Bone Tested at 2.208 in/in/sec Strain Rate.

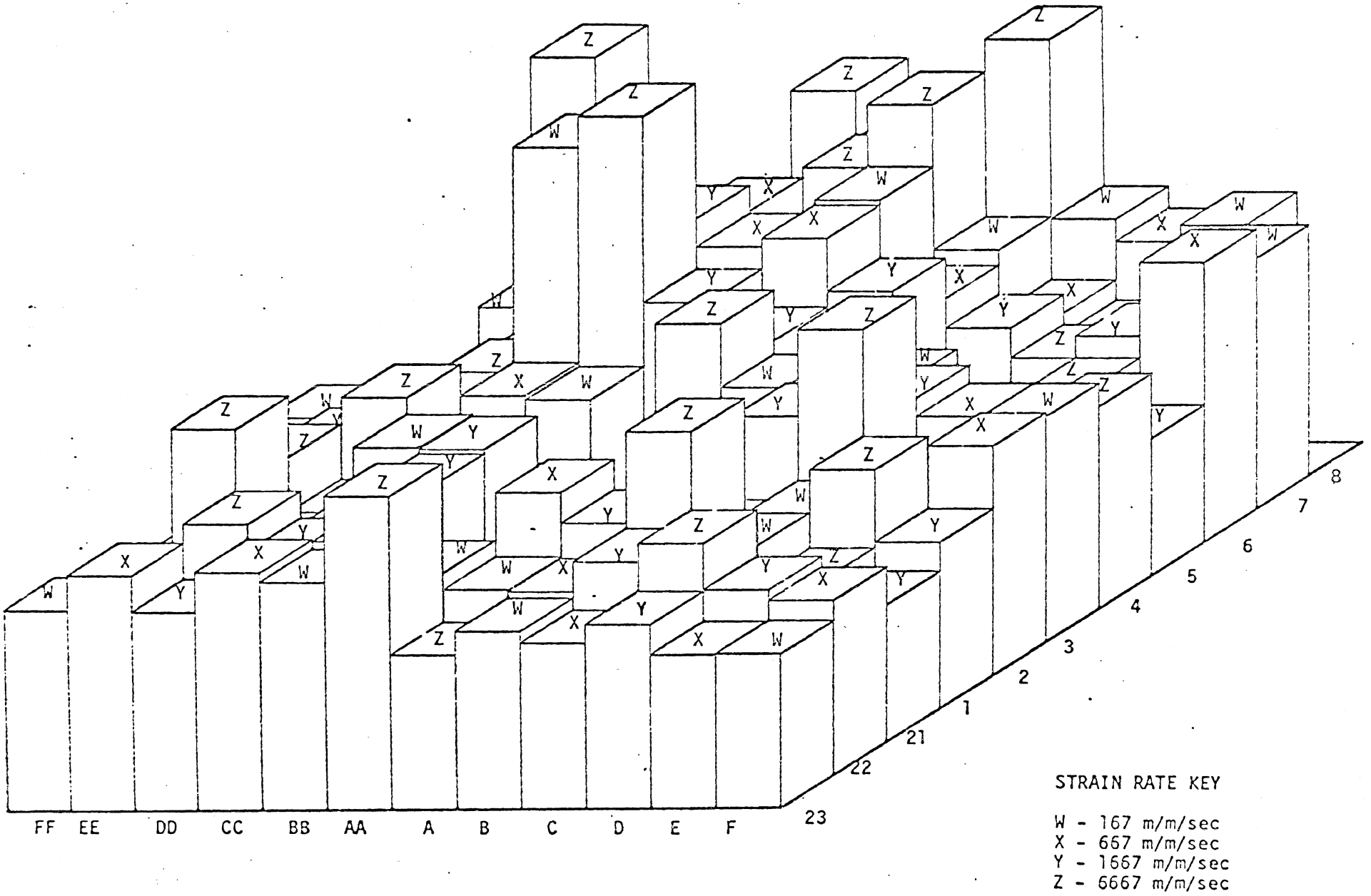

HSRI

SKULL NUMBER 115

Fig. 8 Shear Strength as a Function of Position in the Skull-Front View.

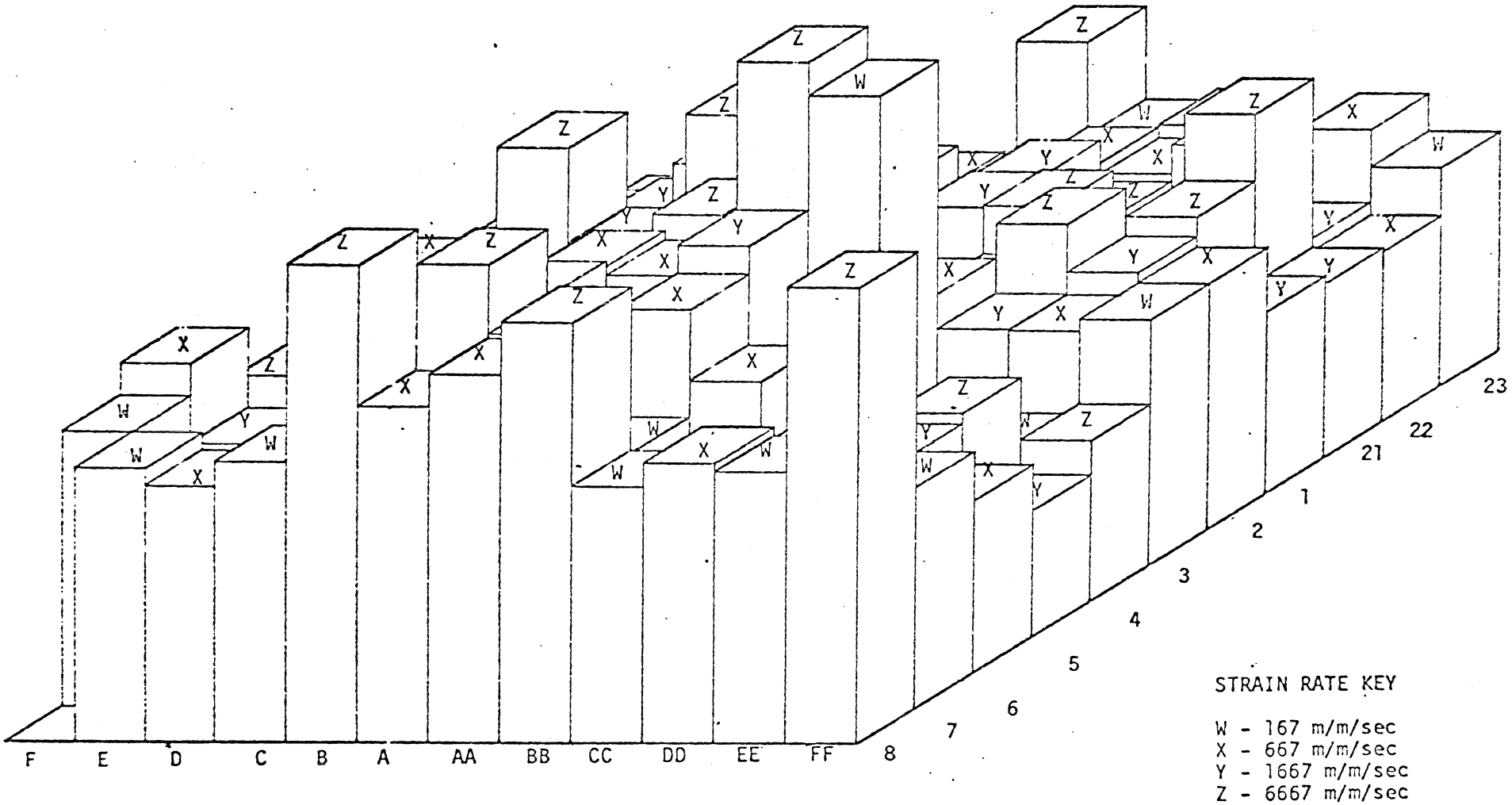

Fig. 9 Shear Strength as a Function of Position in the Skull-Rear View.

APPENDIX A

TENSION TESTS

DYNAMIC TENSION TEST

The tension test is the most sophisticated mechanical property test now being performed on the hard tissues of the skull. It is a time consuming and delicate test, but the engineering information obtained far outweighs the difficulties. At the time of the six months report the tension test program was in its early stages. Since then the test design has been proven from static loading conditions to well into the range of dynamic impact loading.

The latest techniques in specimen preparation are shown beginning with a bone plug as taken at autopsy in Fig. 1. The plug can either be fresh from autopsy or stored at -10^{0} c until needed for testing. The cross on the plug indicates the orientation of the plug in the skull as discussed in the six month report. Fig. 2 shows the layout of the specimen blanks with identification numbers in place. The blanks are sliced out carefully to avoid excessive machining heat (Fig. 3) and then a horizontal slice is taken from the outer table, diploë or inner table. The sliced specimen blanks are then milled to a uniform thickness and machined to the conventional tensile test shape shown in Fig. 4. The finished specimens are stored in the freezer until needed for testing, although some are taken directly to the strain gaging area where they are gaged with two small strain gages (Fig. 5) and then tested. The time from bone plug to finished test is less than an hour. This time is considerably less than the times mentioned in the six month report where it took two hours just to strain gage one specimen. This is due to the continued improvement of machining and strain gaging techniques. Also, the number of unsuccessful

tests has diminished appreciably due to improved testing techniques.

The dynamic tension test procedure consists now of the following steps: 1. mount specimen in the grips 2. solder strain gage leads into recorder circuitry 3. balance strain gage carrier amplifier 4. check circuit stability 5. check for bending strains induced in the specimen 6. perform a tension test to failure at a selected strain rate.

The test can be performed in either of two testing machines. For crosshead speeds from 0.02 inches per minute to 20 inches per minute the Instron 10,000 lb. capacity floor model universal testing machine is used. For crosshead rates from 20 inches per minute to 30,000 inches per minute the Plastechon high speed universal testing machine shown in Fig. 6 is used. Because of the short duration of the tests at higher rates, an oscilloscope is used to record the load-strain curve of the test. By cycling the intensity of the electron beam of the oscilloscope with an oscillation at a given frequency (known as z-axis modulation), the load-strain curve appears as a series of dots. The time duration between dots is known from the oscillator frequency and thus load, strain and time (or effectively strain rate) are recorded all on the same trace. A typical tension test data sheet is shown in Fig. 7.

A parallel study of each tension specimen is made histologically. Upon the completion of the machining of a tensile specimen, and before strain gaging, microphotographs of the four sides of the straight test section are made at a magnification of 40x. A typical example is shown in Fig. 8. After testing to failure the four-sides are again photographed with the two halves of the broken specimen in proximity as shown in Fig. 9. The photos are examined to find structural reasons for the failure occuring in the region

where it did and in the manner in which it did. In order to pinpoint the exact initiation site of the failure the fracture surface must be examined in addition to the sides of the specimen. Figs. 10 and 11 are electron micrograph replicas of a small portion of such a typical surface. The magnification is 19900x. It is felt that a lower magnification would allow better viewing of the whole fracture surface but light microscopes do not have the depth of field necessary to resolve the rough fracture surface. Plans are under way at this time to obtain the use of a scanning electron microscope for making fractographs of the entire fracture surface at about 50 to 100x. The scanning scope has no depth of field problem and the results should be spectacular.

In addition to the above histological work, one half of the tested specimen is sliced on a hard tissue slicing machine (Fig. 12) and then ground down to about 100 microns in thickness. The surfaces of the specimen can then be examined with transmitted light on a microscope for histologically significant effects of testing. For further study the other half can be decalcified and sliced on a microtome to 10 micron thickness. Chemical analysis will also be done on the specimens to determine mineral content, water content and density. In cases where the chemical analysis can not be performed on the specimen itself, the remaining material from the bone plug used to produce the specimen will be analyzed.

The results of the dynamic tensile tests will be analyzed according to the two-way analysis of variance described in Appendix D. This analysis will compare the effects of strain rate and the effects of skull to skull variation on the modulus of elasticity and the tensile strength of outer table compact skull bone. The replication of this series of tests is not complete at this time, but the data at two strain rates is available as shown in Table 1.

The average value of the modulus of elasticity for 11 specimens tested at a crosshead speed of 2 inches/minute on the Instron was 1.85×10^6 psi. The average breaking stress at that rate for 9 of the specimens was 10,194 psi. A total of 7 specimens were tested at 20 inches/minute on the Instron with an average modulus of elasticity of 2.01×10^6 psi and an average breaking stress of 10,850 psi. Both the modulus and the breaking stress showed a slight increase apparently due to strain rate effects. But, until the test series is complete with rates at 200 inches/minute and 2,000 inches/minute on the Plastechon and the entire series analyzed by the statistical model the results can only be considered tentative. The raw data from these tests is shown in Table 1 and summarized in Table 2.

TABLE 1. RAW TENSION TEST DATA

Cross Head Rate in/min.	Specimen No.	Modulus of Elasticity	Ultimate Stress psi
2.0	VA-24-PL-2	1.68×10^6	8,800
2.0	VA-18-PR-4	1.86×10^6	13,500
2.0	VA-19-PL-5	2.33×10^6	9,700
2.0	VA-21-PL-2	2.29×10^6	
2.0	VA-21-PL-3	2.09×10^6	
2.0	VA-21-PL-4	2.00×10^6	13,500
2.0	VA-21-PL-5	2.06×10^6	13,800
2.0	VA-22-PL-5	1.63×10^6	8,950
2.0	VA-22-PL-6	1.55×10^6	7,450
2.0	VA-22-PL-7	1.56×10^6	8,350
2.0	VA-22-PL-8	1.34×10^6	7,700
20	VA-28-PR-3	1.45×10^6	7,000
20	VA-17-PR-1	2.42×10^6	14,600
20	VA-17-PR-7	2.38×10^6	10,900
20	VA-17-PR-8	2.11×10^6	13,500
20	VA-18-PR-1	1.82×10^6	
20	VA-18-PR-5	1.88×10^6	
20	VA-19-PL-4	2.04×10^6	12,450

TABLE 2. SUMMARY OF TENSION TEST DATA ON COMPACT BONE

Tensile Modulus of Elasticity, E

	Strain Rate = 0.02 in/in/sec	Strain Rate = 0.140 in/in/sec
Mean Value	1.853×10^6 psi ($1.33 \times 10^9 kg/m^2$)	2.014×10^6 psi ($1.42 \times 10^6 kg/m^2$)
Standard Deviation	0.325×10^6 psi ($0.228 \times 10^9 kg/m^2$)	0.337×10^6 psi ($0.237 \times 10^6 kg/m^2$)
High Value	2.33×10^6 psi ($1.64 \times 10^9 kg/m^2$)	2.42×10^6 psi ($3.44 \times 10^6 kg/m^2$)
Low Value	1.34×10^6 psi ($0.94 \times 10^9 kg/m^2$)	1.45×10^6 psi ($1.04 \times 10^6 kg/m^2$)

Tensile Breaking Stress, G_f

	Strain Rate = 0.02 in/in/sec	Strain Rate = 0.140 in/in/sec
Mean Value	10,194 psi ($7.10 \times 10^6 kg/m^2$	10,850 psi ($7.63 \times 10^6 kg/m^2$)
Standard Deviation	2,640 psi ($1.85 \times 10^6 kg/m^2$)	2,810 psi ($1.97 \times 10^6 kg/m^2$)
High Value	13,800 psi ($9.70 \times 10^6 kg/m^2$)	14,600 psi ($10.04 \times 10^6 kg/m^2$)
Low Value	7,700 psi ($5.40 \times 10^6 kg/m^2$)	7,000 psi ($4.92 \times 10^6 kg/m^2$)

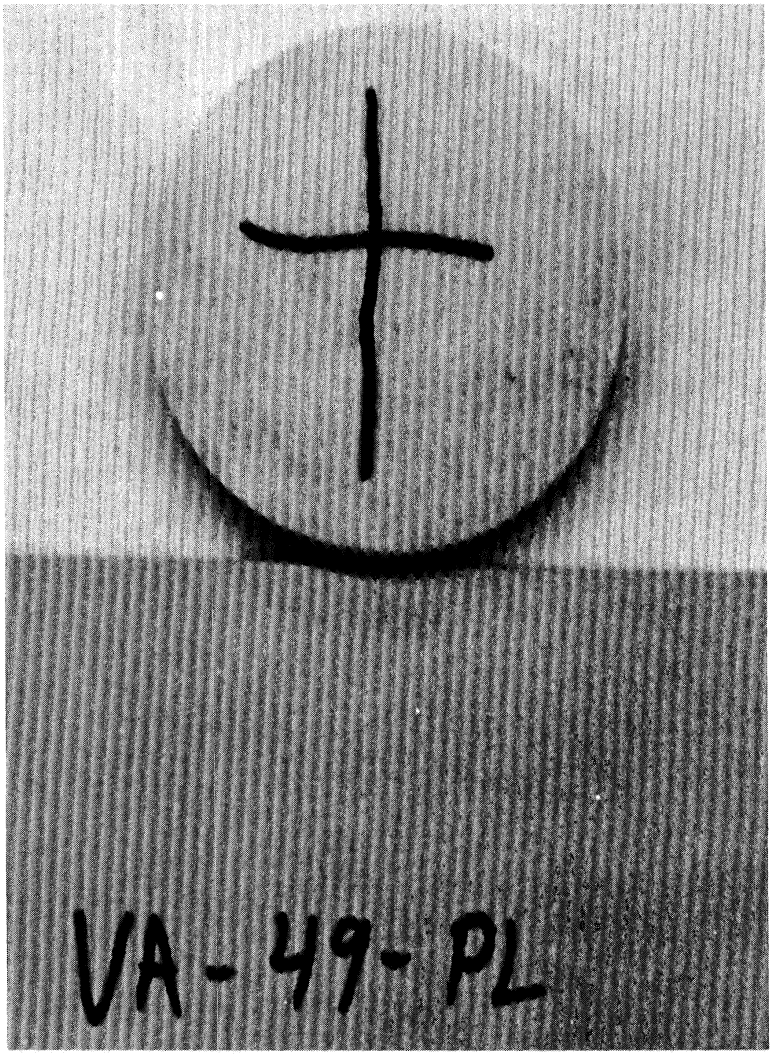

Fig. 1. Fresh Skull Bone Plug from Autopsy

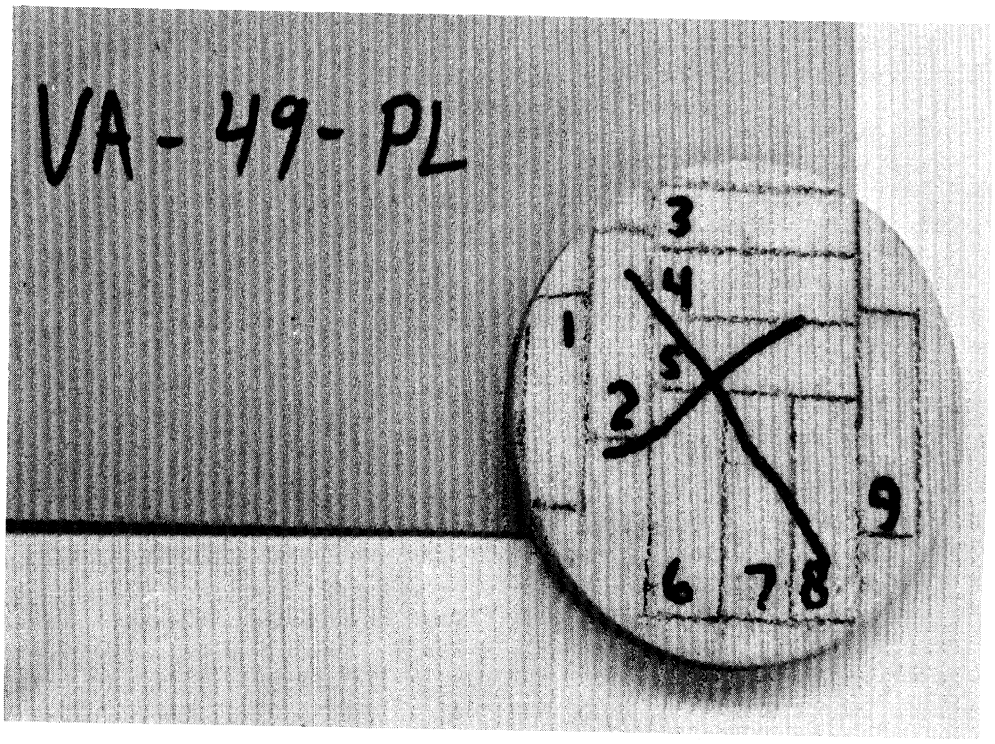

Fig. 2. Rough Specimen Lay-out on Bone Plug.

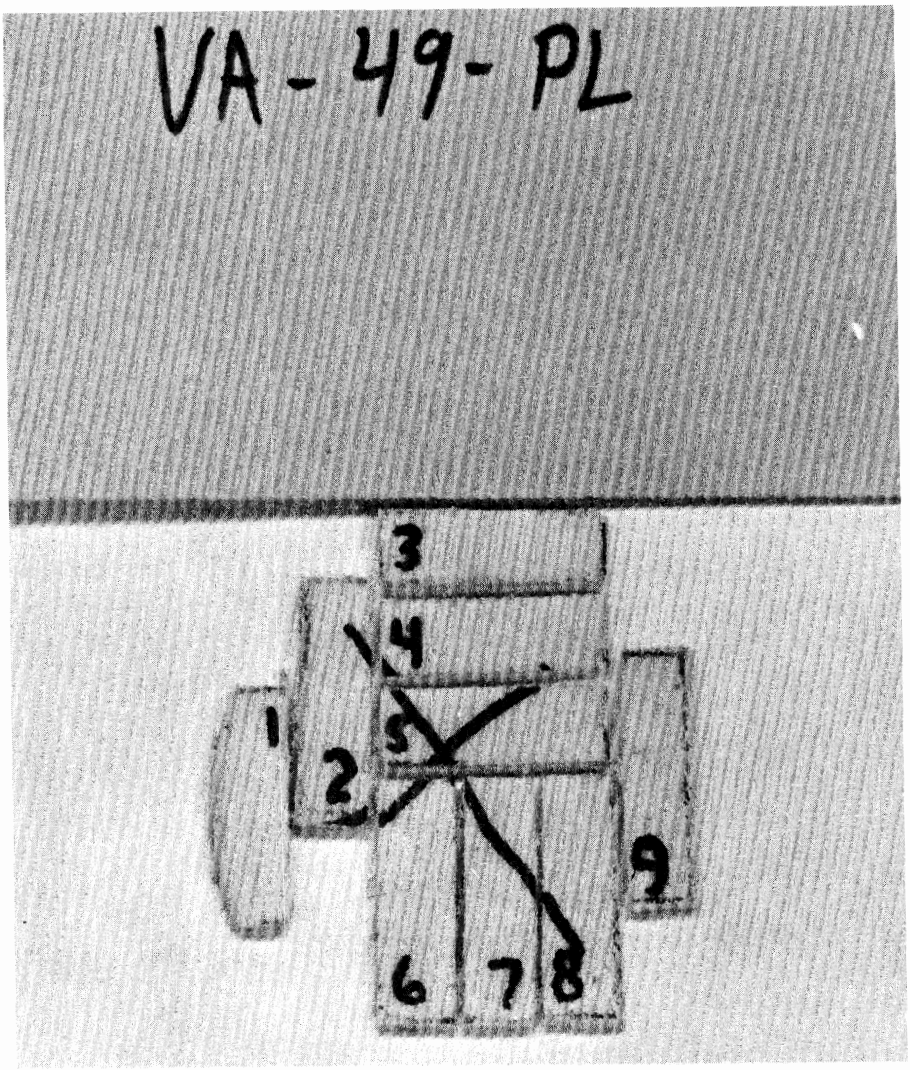

Fig. 3. Specimen Blanks Cut from Bone Plug

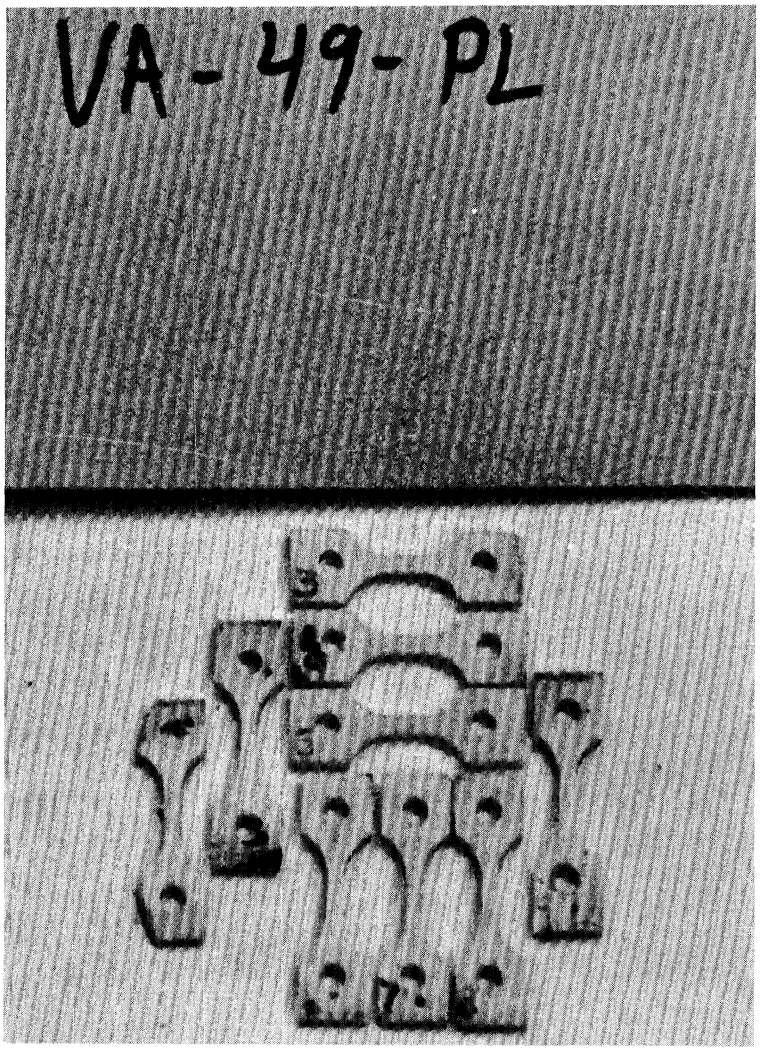

Fig. 4. Finished Tensile Specimens

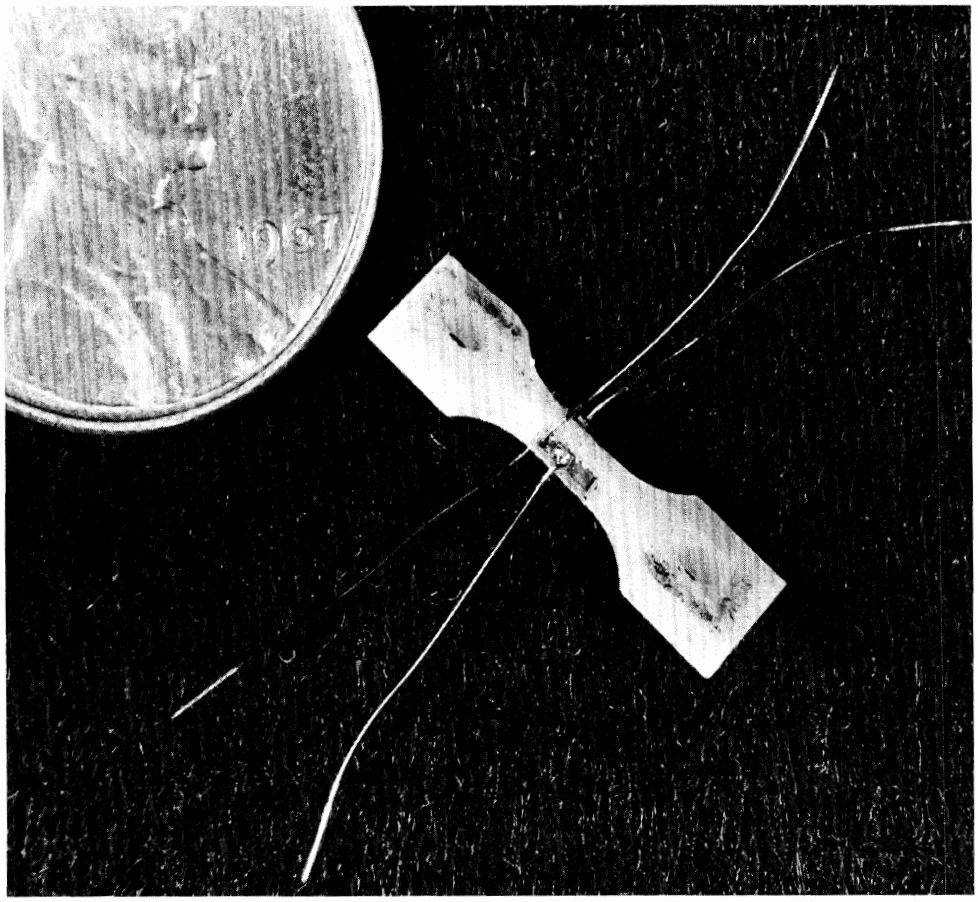

Fig. 5. Strain Gaged Tensile Specimen

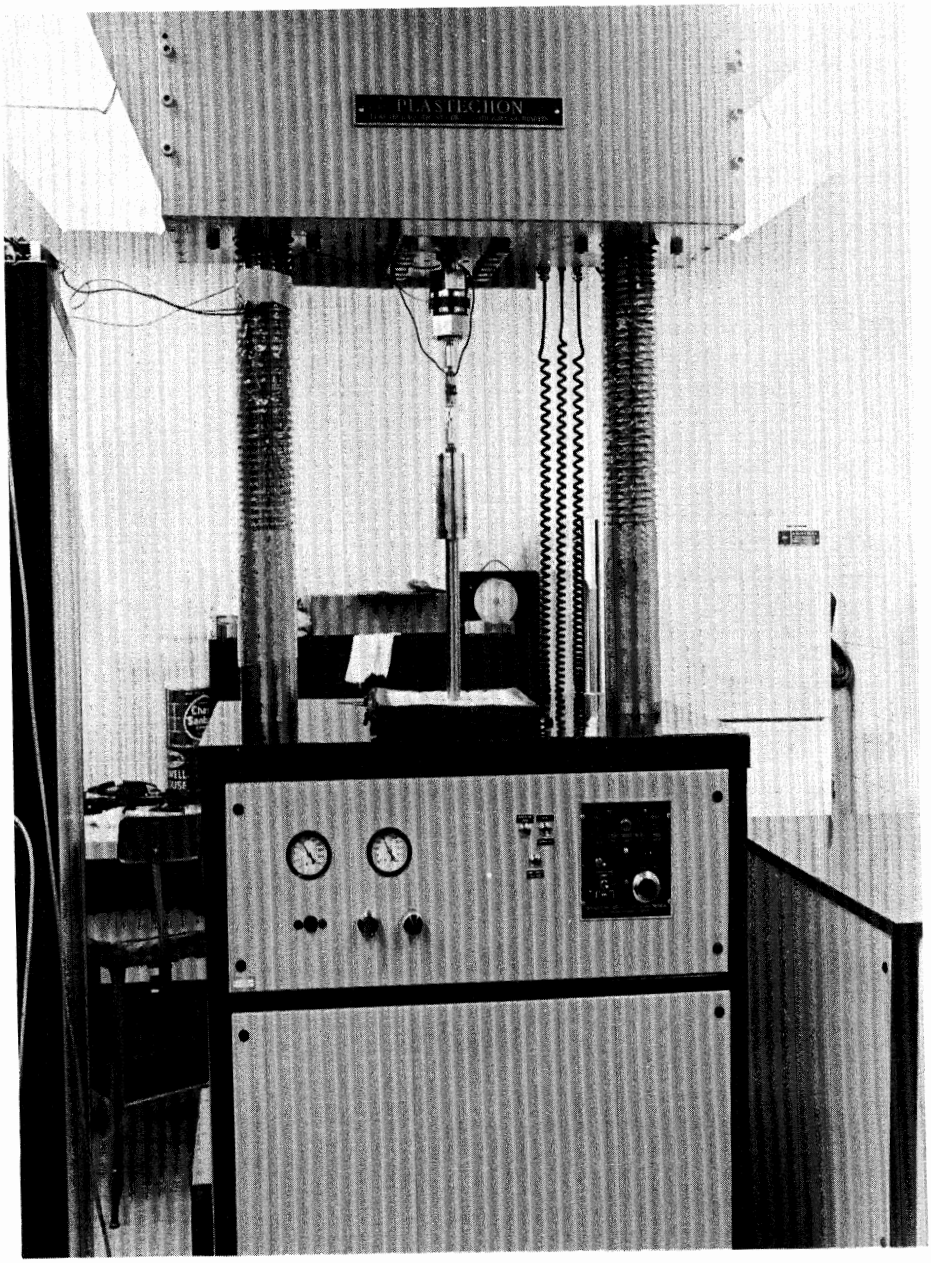

Fig. 6. Tensile Specimen Ready to be Tested in Plastechon High Speed Testing Machine

MECHANICAL PROPERTIES DATA SHEET

SPECIMEN NO. VA-17-PR-1

DATE TESTED 15 April 1968

CROSSHEAD RATE 0.05 & 20 in/min

I.M. FREQUENCY 1200 Hz

TEST SECTION
DIMENSIONS 0.053 in x 0.049 in

ADDITIONAL DATA

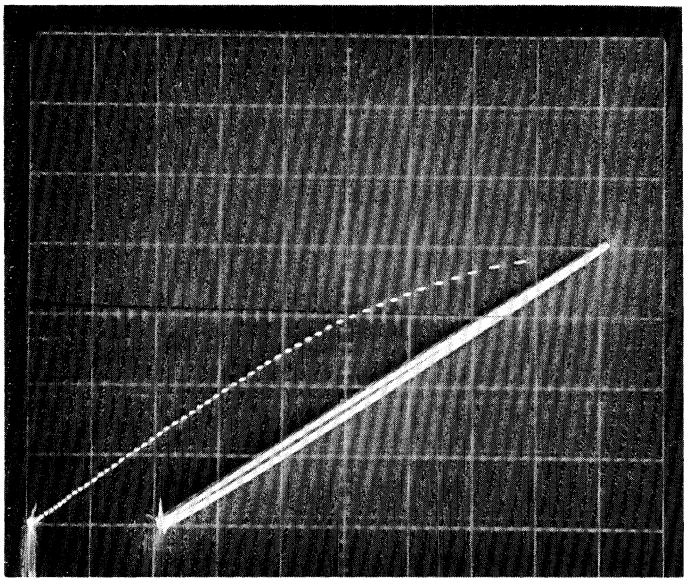

2 & 10 lbs/cm

200 & 1000 μin/in/cm

CALCULATED DATA

STRAIN RATE 0.18 in/in/sec

MODULUS OF ELASTICITY 2.42×10^6 lb/in^2

ULTIMATE STRESS 14,600 lb/in^2

ULTIMATE STRAIN 7,800 μin/in

Fig. 7. Typical Tensile Test Data Sheet

HISTOLOGICAL COMMENTS

Compact bone

TEST COMMENTS

Solid line gives initial modulus at low cross-head rate

vertical scale: 2 lb/cm
horizontal scale: 200 μin/in/cm

Dashed line from test to failure at higher cross-head rate

vertical scale: 10 lb/cm
horizontal scale: 1000 μin/in/cm

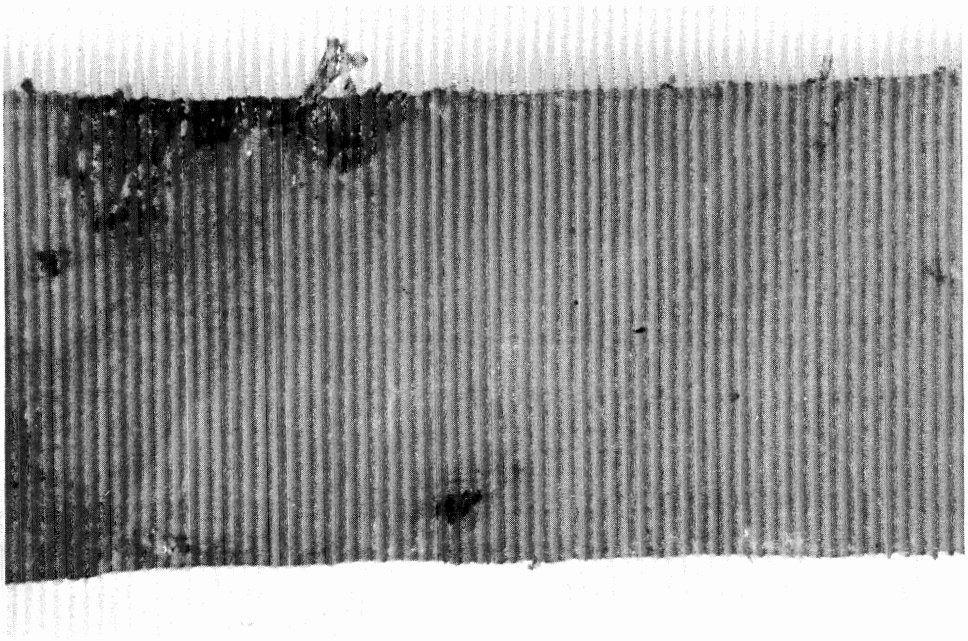

Fig. 8. Tensile Specimen VA-17-PL-5 Posterior View Before Testing

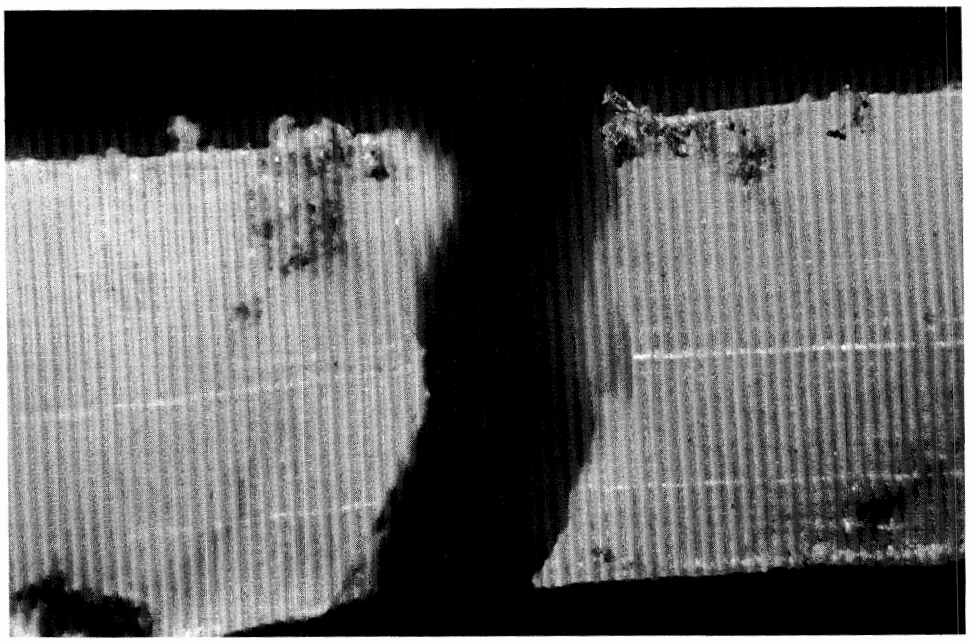

Fig. 9. Tensile Specimen VA-17-PL-5 Posterior View After Testing

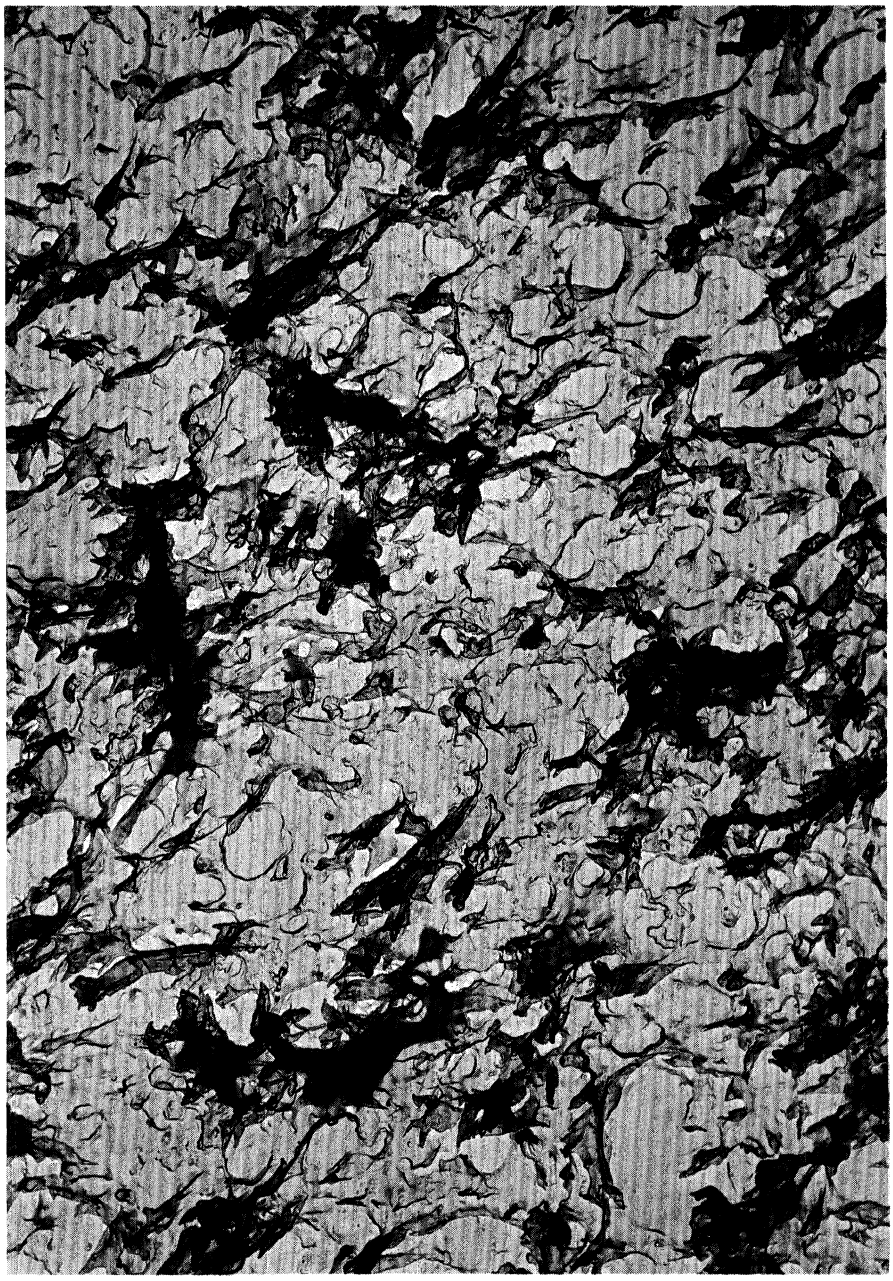

Fig. 10 Transmission Electron Micrograph of Tensile Specimen Fracture Surface Replica (19900X)

Fig. 11 Transmission Electron Micrograph of Tensile Specimen Fracture Surface Replica (19900X)

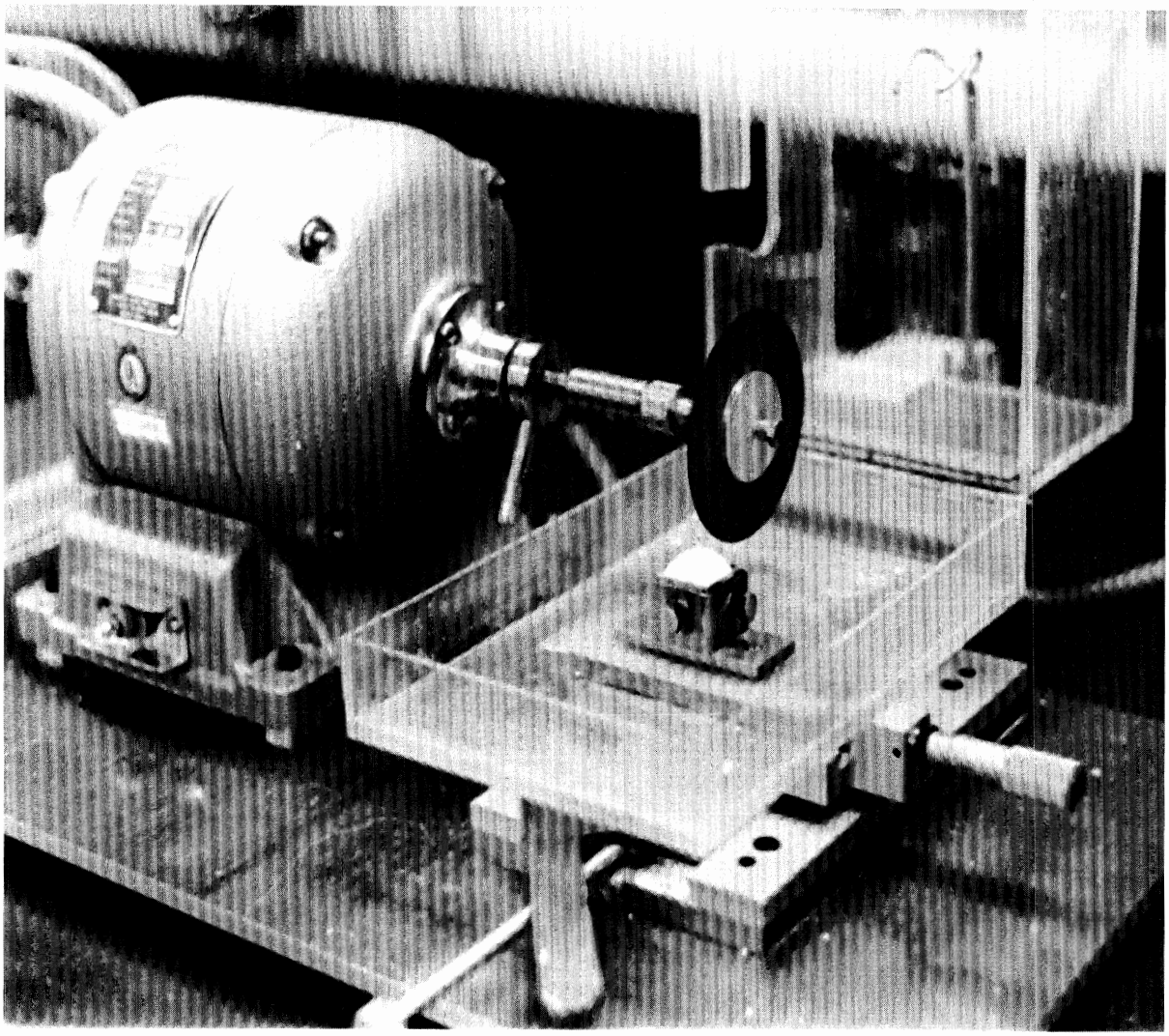

Fig. 12 Hard Tissue Slicer with Tested Tensile Specimen Mounted for Slicing

APPENDIX B

COMPRESSION TESTS

DYNAMIC COMPRESSION TEST

The compression test is basically a crush test of the diploe layer of the skull bone. The test is conducted on rectangular blocks of skull bone with the direction of loading perpendicular to the surface of the skull. In the first six months of the program the specimens consisted of diploe layer with portions of the inner and outer layers of compact bone intact. Since the modulus of elasticity of the diploe layer is in the range of an order of magnitude less than that of the compact bone, the diploe layer does most of the deforming during the test. This leads to two difficulties. Due to variations in the table thicknesses, a series of specimens, all of the same overall height, will have different diploe thichnesses. This leads to different strain rates in the diploe at a given crosshead speed and also different structural stiffness due to the variable amount of diploe present. To alleviate these problems all testing for basic information is now done on specimens consisting of diploe layer only which are machined to a constant height. Specimens with tables intact are still being tested, but as a structural test as opposed to a basic test.

The testing of the compression specimens has been done on a Instron 10,000 lb. universal testing machine with the crosshead pushing upward against a 1,000 lb. capacity load cell at rates up to 20 inches per minute. Because of the very short time duration of the test at high crosshead rates, extra circuitry was designed to prevent overloading of the load cell. The short test duration also necessitated the use of a recording oscilloscope in place of the strip chart recorder used in the static tests. Load is displayed versus time on the scope face. Since the crosshead moves at a constant speed the load-time trace can easily be converted to a load-deflection trace. The scope trace is

triggered by an adjustable microswitch to facilitate optimum trace display. A typical trace and data sheet are shown in Fig. 1. Before the test, the specimen dimensions are measured and the specimen is weighed. The loading curve shown in Fig. 1 is typical of the majority of the specimens tested. Failure of the specimen is considered to occur when the load falls off abruptly indicating collapse of the spongy structure. The modulus of elasticity of the specimen can be calculated from the slope of the fairly linear region between where the load picks up rapidly and failure occurs. The strain rate is calculated by dividing the crosshead rate by the height or gage length of the specimen.

The compression test is in many ways the most structure-sensitive test of the three basic mechanical tests on skull bone. In order to correlate the compressive mechanical properties of the diploe layer with structural features, a number of histological observations are made on the specimens. As noted, the weight and volume of each specimen is measured to allow the density to be calculated. Each specimen is photographed at suitable magnification before testing to record structural features. After testing, the specimen is sectioned on the hard tissue slicer and stained to bring out the regions of structural failure. The section is photographed and examined for modes of failure. A region of a failed compression specimen is shown in Fig. 2. Note the variety of cracks present, both clean breaks and local multiple cracks.

A series of compression tests planned according to the two way analysis of variances discussed in Appendix D have been run to study the relative effects of strain rate and skull to skull variation on crushing strength and modulus of elasticity of fresh skull bone. The two strain rates were 0.218 in/in/sec and

2.208 in/in/sec. Plugs from four skulls were used for both strength and modulus data and a fifth skull plug for strength data alone. In all 50 specimens were tested. The results shown by the analysis were that both skull to skull effects and rate effects are significant but interaction between the two effects was not significant. The raw data found in the test series is shown in Table 1 and a summary of the results of the analysis is shown in Table 2.

TABLE 1. COMPRESSION TEST RAW DATA

Specimen Number	Strain Rate	Compressive Modulus of Elasticity	Compressive Strength, psi
VA-5-PL-1	0.218 in/in/sec	1.27×10^5	3,100
VA-5-PL-3	"	1.25×10^5	3,230
VA-5-PL-5	"	1.21×10^5	3,380
VA-5-PL-8	"	2.12×10^5	5,010
VA-5-PL-9	"	1.02×10^5	3,260
VA-5-PL-11	"	2.27×10^5	5,420
VA-6-PR-1	"	0.76×10^5	1,940
VA-6-PR-3	"	0.24×10^5	755
VA-6-PR-5	"	0.635×10^5	1,990
VA-6-PR-7	"	0.59×10^5	1,860
VA-6-PR-10	"	0.63×10^5	2,300
VA-6-PR-12	"	0.57×10^5	1,820
VA-8-PL-1	"	3.39×10^5	9,700
VA-8-PL-4	"	2.28×10^5	5,640
VA-8-PL-7	"	3.63×10^5	9,240
VA-8-PL-13	"	3.72×10^5	11,600
VA-8-PL-16	"	3.81×10^5	11,000
VA-8-PL-17	"	3.94×10^5	
VA-8-PL-22	"	2.49×10^5	5,590

Specimen Number	Strain Rate	Compressive Modulus of Elasticity	Compressive Strength, psi
VA-9-PL-1	"		7,280
VA-9-PL-2	"	2.92×10^5	8,550
VA-9-PL-5	"	3.48×10^5	8,990
VA-9-PL-8	"	3.91×10^5	10,000
VA-9-PL-9	"	3.99×10^5	6,180
VA-9-PL-4	"	3.72×10^5	5,640
VA-29-PL-13	"		6,580
VA-29-PL-16	"		6,950
VA-29-PL-22	2.218 in/in/sec		6,650
VA-5-PL-4	2.208 in/in/sec	1.80×10^5	5,230
VA-5-PL-6	"	1.85×10^5	4,760
VA-5-PL-7	"	1.60×10^5	4,850
VA-5-PL-10	"	1.68×10^5	3,520
VA-5-PL-12	"	2.24×10^5	5,360
VA-6-PR-2	"	0.74×10^5	2,060
VA-6-PR-4	"	0.825×10^5	2,520
VA-6-PR-6	"	0.84×10^5	2,460
VA-6-PR-9	"	0.95×10^5	3,190
VA-6-PR-11	"	0.875×10^5	2,590
VA-8-PL-3	"	3.98×10^5	11,800
VA-8-PL-6	"	3.76×10^5	8,130
VA-8-PL-8	"	12.4×10^5	40,300

Specimen Number	Strain Rate	Compressive Modulus of Elasticity	Compressive Strength, psi
VA-8-PL-9	"	4.23×10^5	13,080
VA-8-PL-12	"	3.81×10^5	10,170
VA-8-PL-15	"	4.08×10^5	13,050
VA-8-PL-21	"	2.98×10^5	6,480
VA-9-PL-3	"	3.52×10^5	9,070
VA-9-PL-6	"	3.26×10^5	8,200
VA-9-PL-7	"	3.54×10^5	11,350
VA-9-PL-10	"	3.95×10^5	10,400
VA-9-PL-12	"	3.94×10^5	9,200
VA-29-PL-4	"		11,300
VA-29-PL-5	"	2.48×10^5	10,300
VA-29-PL-7	"	2.82×10^5	8,500
VA-29-PL-10	"	2.44×10^5	9,950
VA-29-PL-15	"	1.98×10^5	9,550
VA-29-PL-19	"	2.84×10^5	8,600
VA-29-PL-23	2.208 in/in/sec	2.79×10^5	9,600

TABLE 2. SUMMARY OF COMPRESSION TEST DATA OF THE DIPLOE LAYER

A. Averages of all data

Compressive Modulus of Elasticity, E_D

	Strain Rate = 0.218 in/in/sec	Strain Rate = 2.208 in/in/sec
Mean Value	2.178×10^5 psi ($1.53 \times 10^8 kg/m^2$)	2.511×10^5 psi ($1.77 \times 10^8 kg/m^2$)
Standard Deviation	1.35×10^5 psi ($0.95 \times 10^8 kg/m^2$)	1.57×10^5 psi ($1.11 \times 10^8 kg/m^2$)
High Value	3.99×10^5 psi ($2.81 \times 10^8 kg/m^2$)	4.08×10^5 psi ($2.88 \times 10^8 kg/m^2$)
Low Value	0.24×10^5 psi ($0.168 \times 10^8 kg/m^2$)	0.74×10^5 psi ($0.52 \times 10^8 kg/m^2$)

Compressive Strength, σ_D

	Strain Rate = 0.218 in/in/sec	Strain Rate = 2.208 in/in/sec
Mean Value	5736 psi ($4.03 \times 10^6 kg/m^2$)	7363 psi ($5.16 \times 10^6 kg/m^2$)
Standard Deviation	3090 psi ($2.17 \times 10^6 kg/m^2$)	3430 psi ($2.42 \times 10^6 kg/m^2$)
High Value	11,600 psi ($8.15 \times 10^6 kg/m^2$)	13,050 psi ($9.15 \times 10^6 kg/m^2$)
Low Value	755 psi ($5.3 \times 10^6 kg/m^2$)	2060 psi ($1.44 \times 10^6 kg/m^2$)

B. Two way Analysis of Variance Results

	Mean Value of data from both strain rates.	Standard deviation with main effects of strain rate and skull to skull variance accounted for.
Compressive Modulus of Elasticity	2.34×10^5 psi ($1.65 \times 10^8 kg/m^2$)	0.405×10^5 psi ($0.284 \times 10^8 kg/m^2$)
Compressive Strength	6550 psi ($4.60 \times 10^6 kg/m^2$)	1565 psi ($1.10 \times 10^6 kg/m^2$)

MECHANICAL PROPERTIES DATA SHEET

SPECIMEN NO. VA-29-PL-14

DATE TESTED 5/1/68

CROSSHEAD RATE 10"/Min

I.M. FREQUENCY ----------

TEST SECTION DIMENSIONS 0.098" x 0.184"

ADDITIONAL DATA

Specific Weight = 0.0461 lb/in^3

Height = 0.138 in

CALCULATED DATA

STRAIN RATE 1.18 in/in/sec.

MODULUS OF ELASTICITY 1.96 x 10^5 psi

ULTIMATE STRESS 8,520 psi

ULTIMATE STRAIN ----------

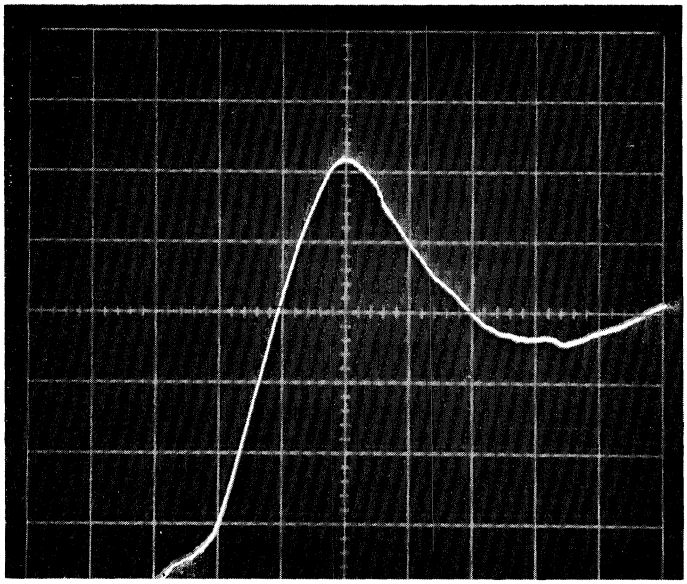

Fig. 1. Typical Compression Test Data Sheet

HISTOLOGICAL COMMENTS

Specimen consisted of diploë layer only.

TEST COMMENTS

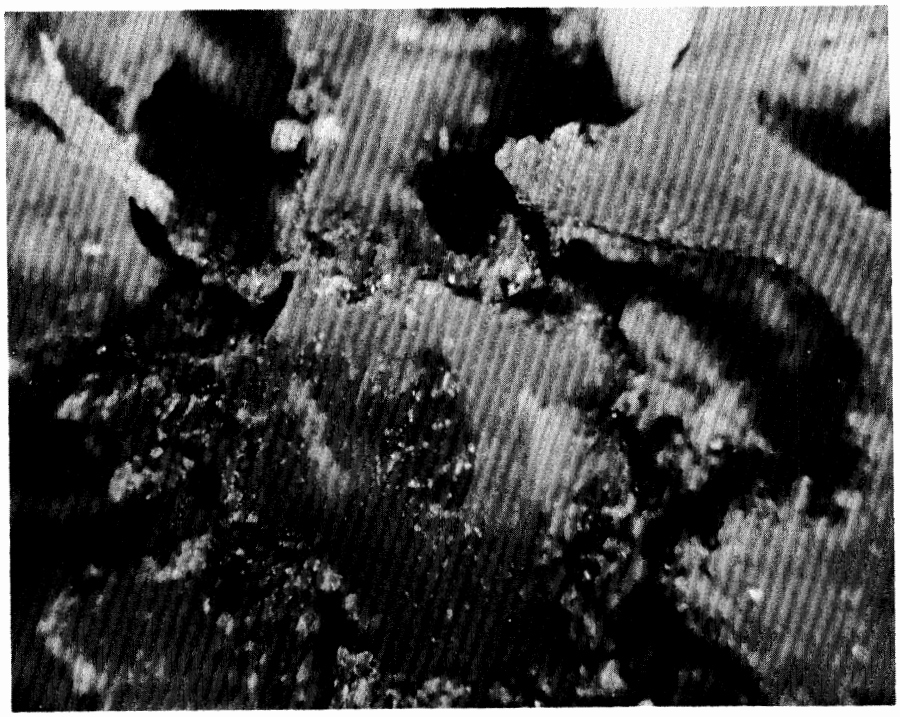

Fig. 2. Micrograph of Failed Region of Diploe Layer Compression Specimen (40X)

APPENDIX C

SHEAR TESTS

DYNAMIC SHEAR TEST

The dynamic shear test is a relatively simple test that measures the shear strength of the diploe layer of skull bone. The test is a quick, easy-to-run test which is being used to develop statistical analyses applicable to the other mechanical tests. So far, nearly all the shear tests have been run on specimens taken from the embalmed calvariums of medical school cadavers. A short series of tests on fresh bone material from autopsy is mentioned in the section on test results. Since the entire calvarium is available for testing, a large number of specimens (about 150) can be taken from the same source. Accordingly it is possible to study location effects within skull quite effectively.

An improved technique of obtaining shear specimens has been developed with the result that more uniform specimens may be obtained faster. Previously, the Stryker Autopsy Saw with 3/8" I.D. Bone Plug Cutter was hand held. Now it is mounted on a drill press stand as shown in Fig. 1. The specimens are taken as cylinders of bone with their axis perpendicular to the skull surface. Water is allowed to run over the cutter to prevent burning of the plug.

The shear test grips have also been redesigned since the description in the six month report. The grips are shown in Fig. 2. Note that by surrounding the moveable portion of the grips with the fixed upper part the possibility of spreading of the sliding surface under load is eliminated. The sliding faces of the grips are coated with Alpha Molykote to minimize friction effects. The plug is inserted on one side only with the diploe layer centered on one of the sliding planes. The grips, loaded and ready to test are shown in Fig. 3.

Because of the narrow gap between the two surfaces (0.005 inches) the nominal shear strain rate is magnified considerably. For given crosshead velocity, the strain rate is the velocity divided by the gap of 0.005 inches or effectively 200 times the crosshead velocity. The test can be performed both on the Instron 10,000 lb. universal testing machine and the Plastechon high speed universal testing machine. The load versus time trace for the test is obtained on an oscilloscope and the peak load recorded. The shear strength is calculated by dividing the peak load by the circular cross sectional area of the plug. A typical failed specimen is shown in Fig. 4.

Presently, the shear test is being used to develop a three way analysis of variance statistical model described in Appendix D. The statistical model will be used to determine the relative importance of strain rate effects, skull to skull variation, and position within the skull effects. A scheme for choosing the strain rate that a particular plug will be run at is shown in Fig. 5. The letters W, X, Y, Z represent four different strain rates and the regions bounded by the double lines represent locations of groups of four plugs considered to be a position. The individual plugs are identified by the scheme detailed in the six month report. Fig. 6 shows the conversion of this scheme to the regions of the unified location system for all contractors of the Head Injury Model Project.

Over 1,000 shear tests have been performed at high rates both on the Instron and the Plastechon testing machines. At this time, however, not all of these tests have been incorporated into the statistical analysis techniques presently under developement. Thus, the results discussed here will be concerned with some 600 shear tests involving four embalmed calvariums of similar structural features, run at four different strain rates (1.66, 6.66, 16.6, 66.6 in/in/sec) and analyzed by the initial three way analysis of variance statistical mode. The skull information is listed in Table 1 and simple

averaging of all the data for each rate and skull is shown in Table 2. It has been noted that there is fair correspondence of shear strengths of the left and right halves of the skull at corresponding positions. This information was used to provide replication for the model as a first run. Because the computer program allows only complete data at each position at this time, the system was reduced to a study of 6 replicated positions in 4 different skulls with 4 strain rates represented in each skull at each position, a total of 288 tests incorporated in the analysis. The results of the analysis are a mean shear strength of 3124 psi with a standard error of 582 psi. The most significant factor was skull to skull variation, the next most significant factor was position and the interaction between skull and position was third most important. Other interactions were present at low levels, but most interesting was that the main effect of strain rate was judged not significant by the analysis. Further testing will be done at higher strain rates for there is indication that rate sensitivity does show up at higher rates in embalmed bone.

A limited study of a series of shear tests on a frozen, fresh bone plug from autopsy proved very informative. Six shear specimens were taken from the plug and 3 were tested at 6.66 in/in/sec and 3 were tested at 66.6 in/in/sec. The results are tabulated in Table 3. The average shear strength at 6.66 in/in/sec was 3272 psi and the average shear strength at 66.6 in/in/sec was 4386 psi, an increase of 31%.

TABLE 1

Skull #99

Age: 82

Sex: Male

Race: Caucasian

Cause of Death: Pneumonia

Skull #108

Age: 60

Sex: Male

Race: Caucasian

Cause of Death: Bleeding Ulcer

Skull #106

Age: 63

Sex: Male

Race: Caucasian

Cause of Death: Myocardial Infarction

Skull #95

Age: 55

Sex: Male

Race: Caucasian

Cause of Death: Acute Coronary

TABLE 2. AVERAGE SHEAR STRENGTH VALUES FOR 4 SKULLS AT 4 STRAIN RATES

	Shear Strain Rate	
Skull	1.66 in/in/sec	6.66 in/in/sec
#95	3474 psi (2.44 x 10^6kg/m^2)	3559 psi (2.50 x 10^6kg/m^2)
#99	3044 psi (2.14 x 10^6kg/m^2)	3422 psi (2.40 x 10^6kg/m^2)
#106	2879 psi (2.02 x 10^6kg/m^2)	2972 psi (2.09 x 10^6kg/m^2)
#108	3828 psi (2.69 x 10^6kg/m^2)	3578 psi (2.60 x 10^6kg/m^2)

	Shear Strain Rate	
Skull	16.6 in/in/sec	66.6 in/in/sec
#95	3389 psi (2.38 x 10^6kg/m^2)	3671 psi (2.58 x 10^6kg/m^2)
#99	3080 psi (2.16 x 10^6kg/m^2)	3108 psi (2.19 x 10^6kg/m^2)
#106	3196 psi (2.25 x 10^6kg/m^2)	2889 psi (2.03 x 10^6kg/m^2)
#108	3885 psi (2.73 x 10^6kg/m^2)	3875 psi (2.72 x 10^6kg/m^2)

TABLE 3. SHEAR TESTS ON AUTOPSY MATERIAL

Bone Plug No. VA-42-PL

Age: 73

Sex: Male

Race: Caucasian

Cause of Death: Cancer

Plug Position: Centered on boundary between regions 11 and 13

Tests at 6.66 in/in/sec		Tests at 66.6 in/in/sec	
Spec. I	3555 psi ($2.50 \times 10^6 kg/m^2$)	Spec. 4	4354 psi ($3.06 \times 10^6 kg/m^2$)
Spec. 2	3025 psi ($2.13 \times 10^6 kg/m^2$)	Spec. 5	4516 psi ($3.17 \times 10^6 kg/m^2$)
Spec. 3	3236 psi ($2.28 \times 10^6 kg/m^2$)	Spec. 6	3987 psi ($2.81 \times 10^6 kg/m^2$)
Avg.	3272 psi ($2.30 \times 10^6 kg/m^2$)	Avg.	4286 psi ($3.01 \times 10^6 kg/m^2$)

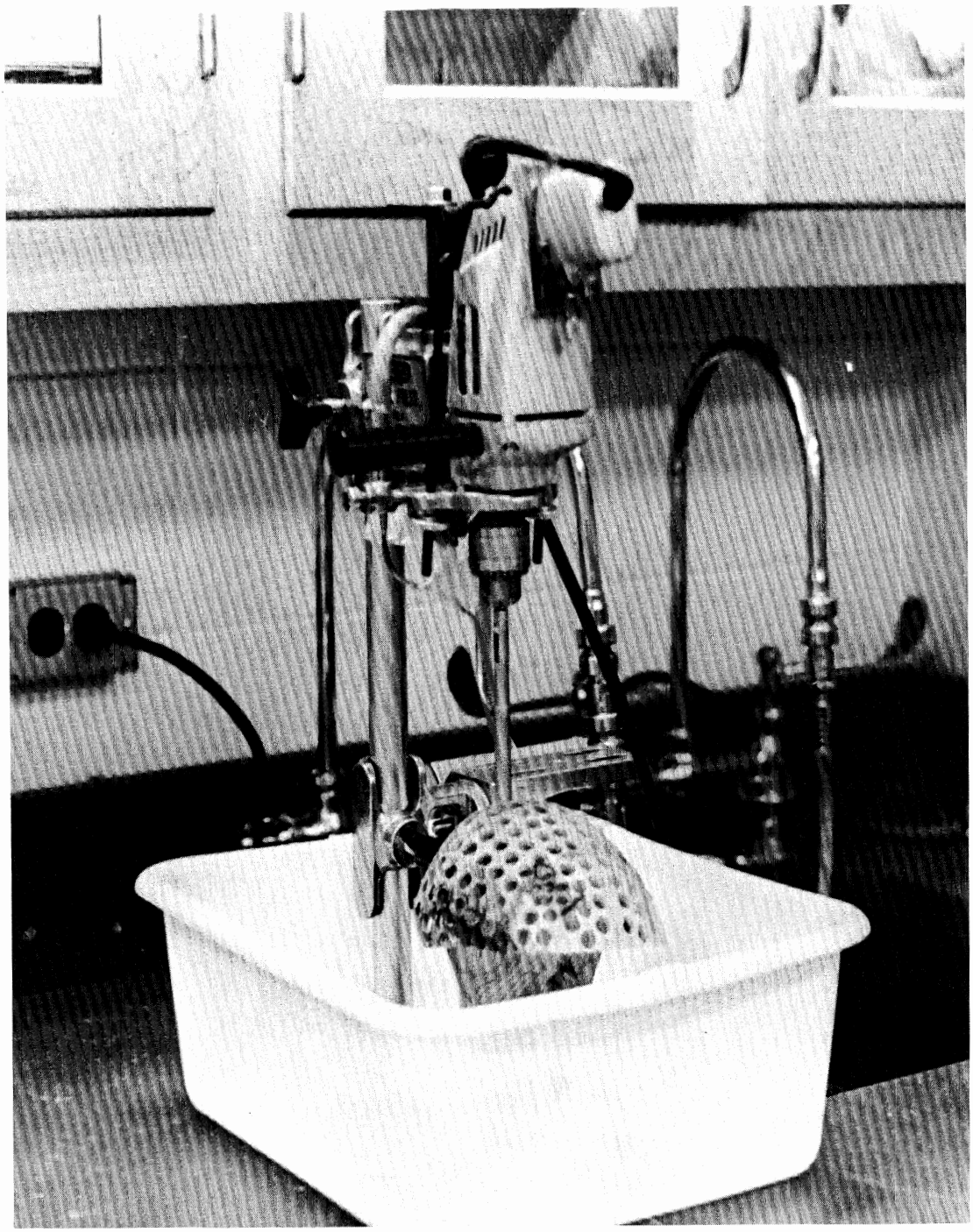

Fig. 1. Apparatus for Cutting Shear Test Specimens from Embalmed Calvarium

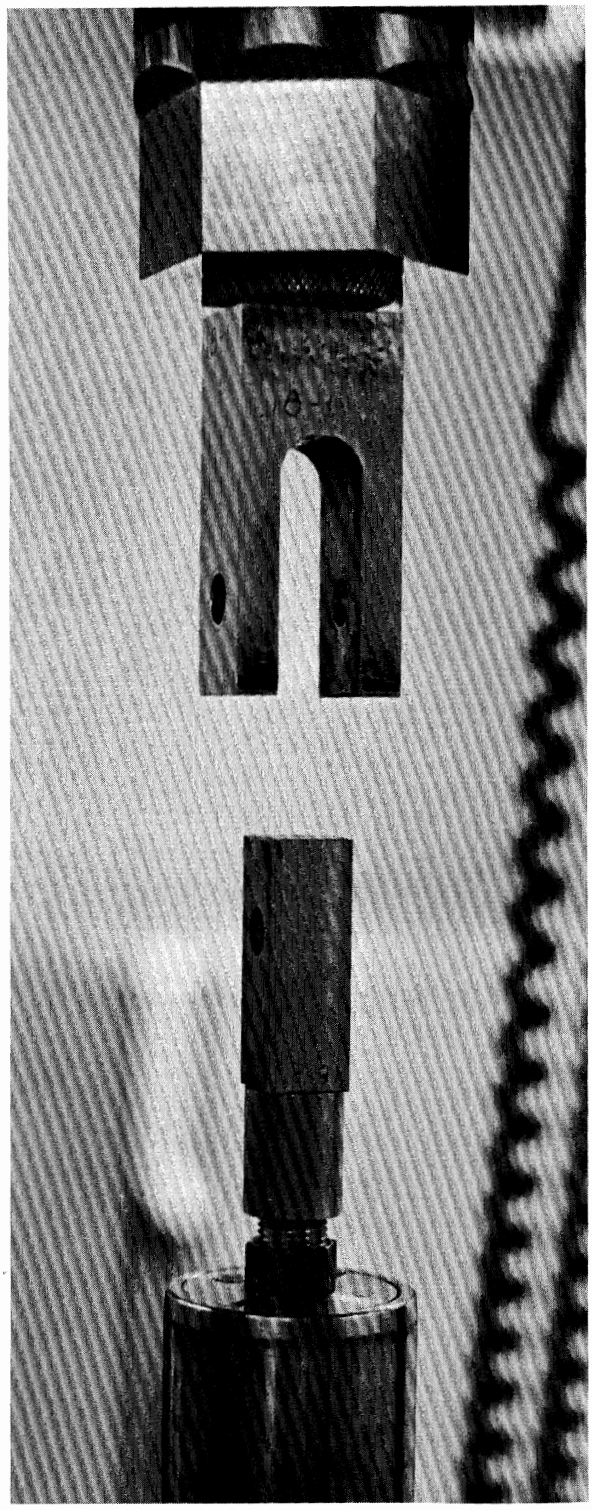

Fig. 2. Shear Test Grips

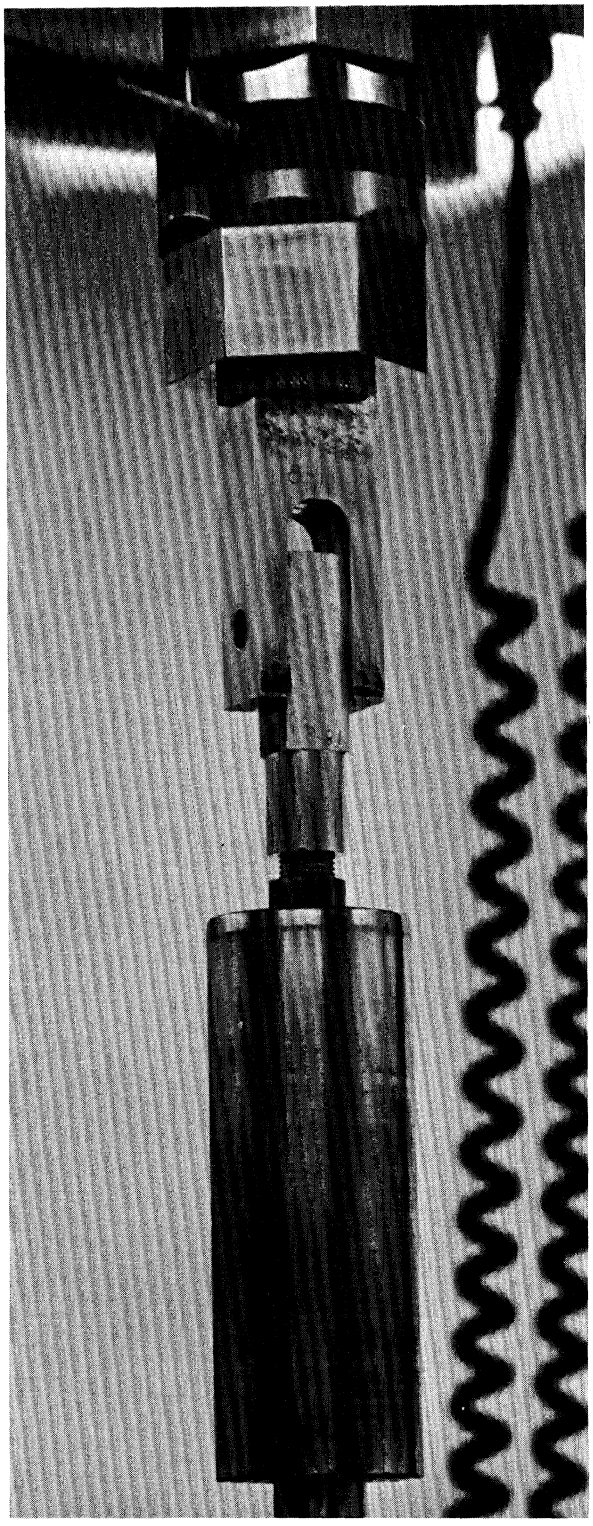

Fig. 3 Shear Test Grips With Specimen In Place

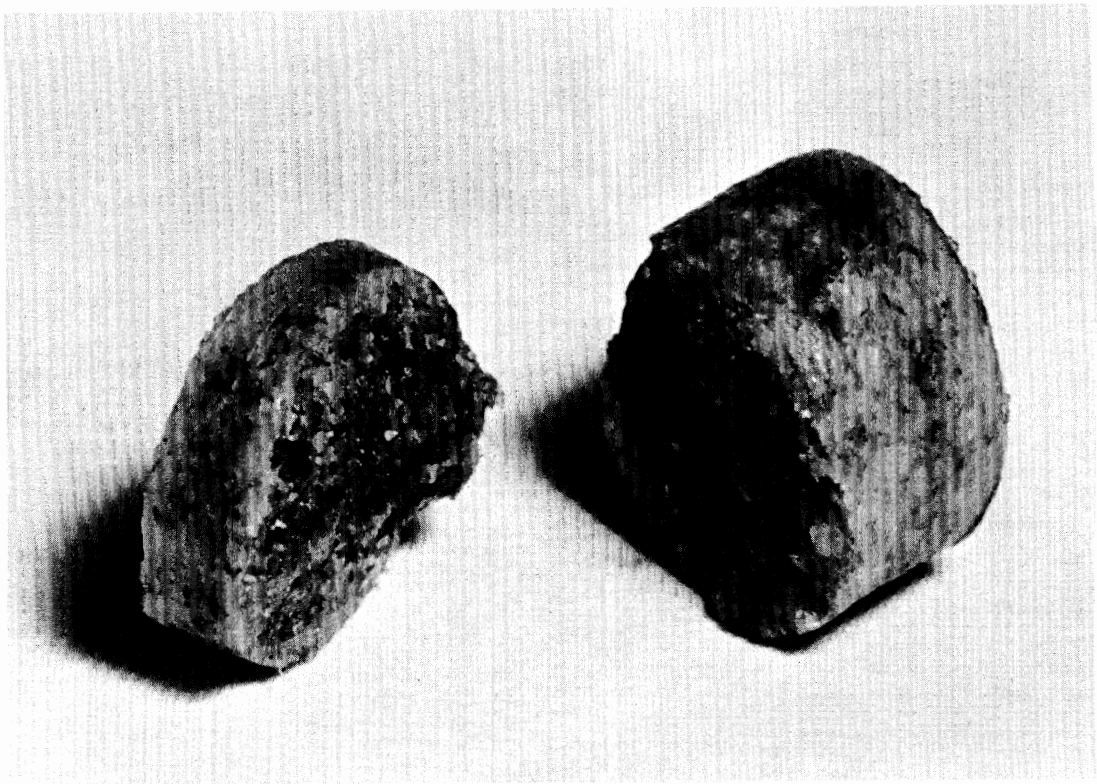

Fig. 4 Typical Shear Specimen Failure

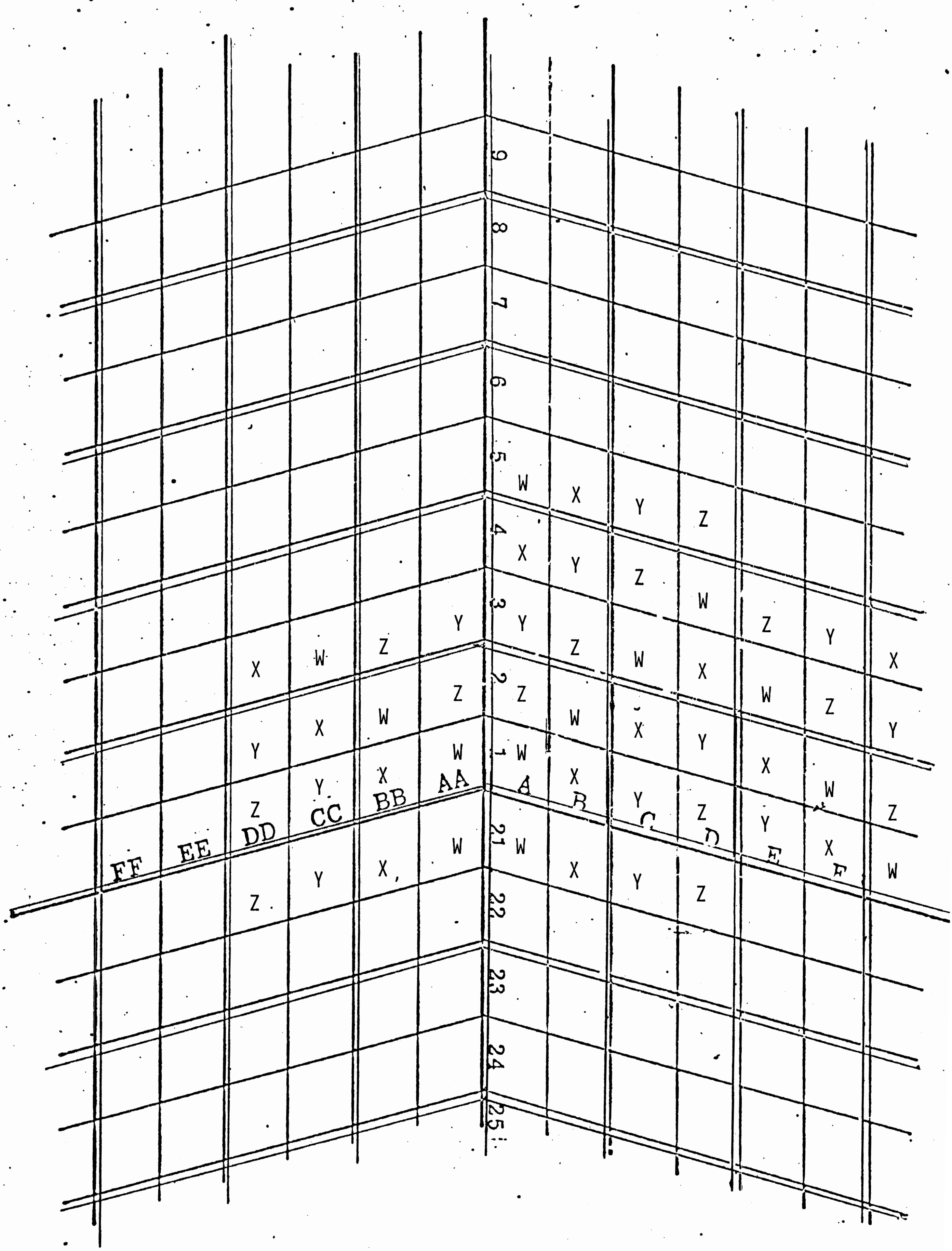

Fig. 5 Latin Square Arrangement for Assigning Strain Rates to Shear Test Specimens.

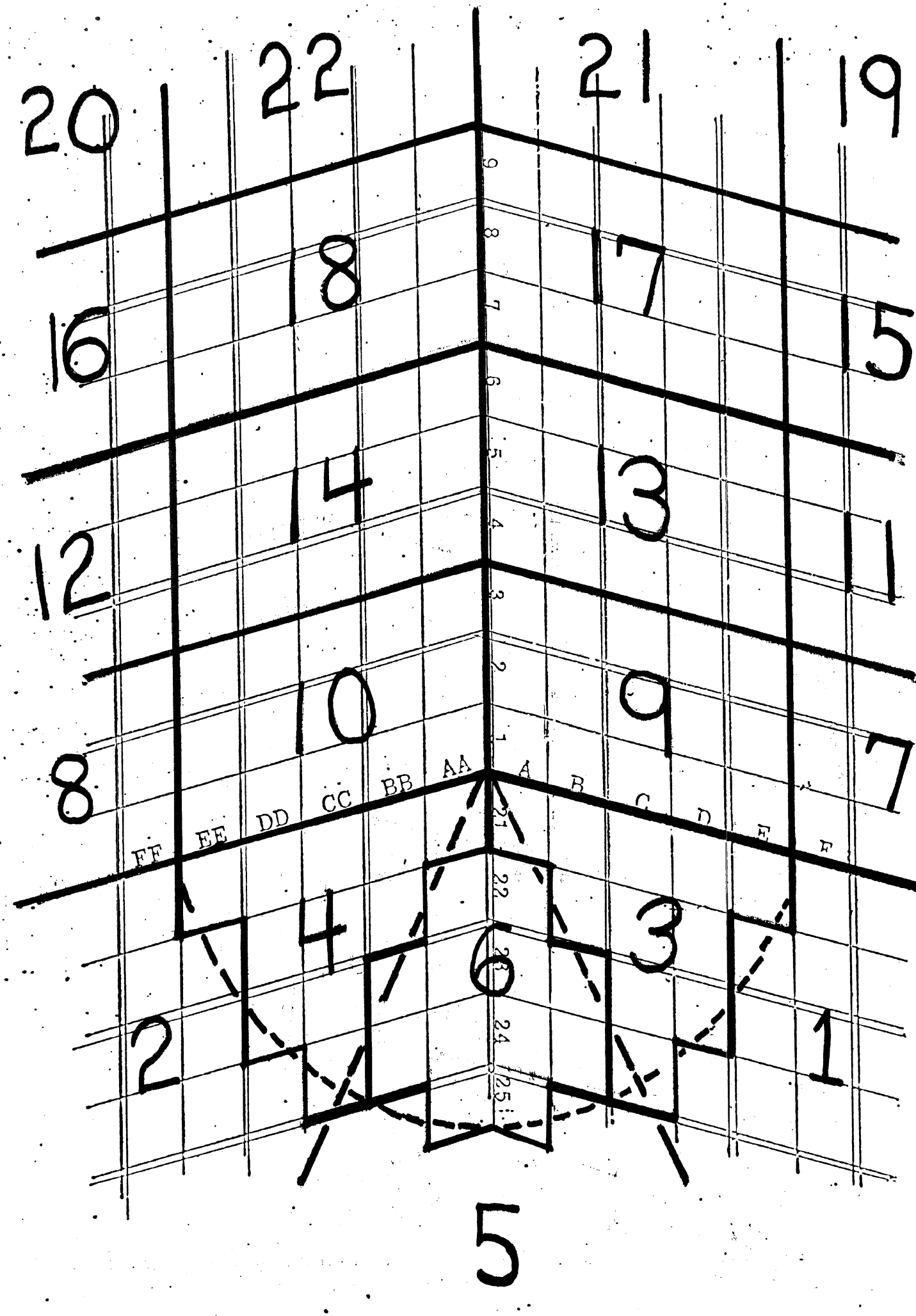

Fig. 6 Conversion of Calvarium Reference System to Uniform Reference System.

APPENDIX D

STATISTICAL ANALYSIS

STATISTICAL ANALYSIS

The object of the careful testing procedures and the histological analysis of the test specimens in this project is to minimize and explain the so-called "biological variation" that occurs in the mechanical properties of biological materials. It is realized, however, that all variations can not be explained away and, in fact, the mechanical properties of interest will most likely be characterized by a distribution of values in a statistical sense. Thus, along with the development of the testing procedures there have been parallel developments of statistical procedures to fit the tests. The statistical models described here are initial formulations. The development of statistical models is viewed as an iterative process and the models will grow in sophistication as the tests progress.

In the tension and compression tests the main emphasis has been put on strain rate effects and skull to skull effects since not enough material is available from any one skull to study position effects. Thus, a two-way analysis of variance model has been worked out for assessing the relative importance of strain rate and skull to skull variations.

The basic model is given by

$$y_{ijk} = \mu + \alpha_i + \beta_j + \gamma_{ij} + \varepsilon_{ijk} \qquad \begin{matrix} i = 1, \cdots, I \\ j = 1, \cdots, J \\ k = 1, \cdots, K_{ij} \end{matrix}$$

where

y_{ijk} = the observed value for the $i^{\underline{th}}$ skull, $j^{\underline{th}}$ rate and the $K^{\underline{th}}$ replication

μ = overall mean effect

α_i = main effect of the $i^{\underline{th}}$ skull

β_j = main effect of the $j^{\underline{th}}$ skull

γ_{ij} = interaction between the $i^{\underline{th}}$ skull and the $j^{\underline{th}}$ rate

ε_{ijk} = the error in the $ijk^{\underline{th}}$ observed value

Due to the relative abundance of specimens from whole embalmed calvariums, the shear test allows the variable of position in the skull to be studied in addition to the variables studied in the tension and compression tests. The statistical model for including the effect of position is a three way analysis of variance.

The basic model is given by

$$y_{ijkl} = \mu + \alpha_i^A + \alpha_j^B + \alpha_k^C + \alpha_{ij}^{AB} + \alpha_{ik}^{AC} + \alpha_{jk}^{BC} + \alpha_{ijk}^{ABC} + \varepsilon ijkl$$

where

yijkl = the observed value for the $i^{\underline{th}}$ skull, $j^{\underline{th}}$ rate, $k^{\underline{th}}$ position and $l^{\underline{th}}$ replication

μ = overall mean effect

α_i^A = main effect of the $i^{\underline{th}}$ skull

α_j^B = main effect of the $j^{\underline{th}}$ rate

α_k^C = main effect of the $k^{\underline{th}}$ position

α_{ij}^{AB} = interaction between $i^{\underline{th}}$ skull and $j^{\underline{th}}$ rate

α_{ik}^{AC} = interaction between $i^{\underline{th}}$ skull and $k^{\underline{th}}$ position

α_{jk}^{BC} = interaction between $j^{\underline{th}}$ rate and $k^{\underline{th}}$ position

α_{ijk}^{ABC} = three way interaction

$\varepsilon ijkl$ = the error in the $ijkl^{\underline{th}}$ observed value

APPENDIX E

DYNAMIC PROPERTIES OF BRAIN TISSUE

Table of Contents

List of Illustrations

List of Tables

Complex Dynamic Shear Modulus

Test Description and Objectives

The effort to determine the complex dynamic shear modulus of human brain tissue was continued as stated in the Appendices Concerning the Experimental and Analytical Research Program (Volume IV of the Interim Report on Contract PH-43-67-1136). Dow Corning's Dynamic Mechanical Apparatus (DMA) was utilized for testing. The tests were conducted to - (1) increase the sample population; and (2) evaluate and reduce errors in the measured modulus due to drying of the test specimen during actual testing. The mechanical procedure remained the same as was reported in the interim report. Primary emphasis was placed on longer test series conducted on one specimen rather than total number of specimens. The test series were designed to show modulus variation due to previous shear history and also involved various sample preparation techniques. All tests were conducted at 37°C.

Variations of two techniques were utilized to reduce water loss from the test specimen during actual testing. The first effort involved coating the entire sample surface with Dow Corning® Medical Adhesive 'B'. This product is a solvent-dispersed silicone adhesive in aerosol form. Samples were coated by either spray-coating them with adhesive direct from the aerosol can or by brush-coating the surfaces with the silicone-solvent mixture which had been reduced to approximately 50% of the original percentage solids (when in aerosol form).

The second technique consisted of isolating the sample from the exterior environment by means of a thin plastic case approximately 1/4-3/8 inch from the vertical walls of the sample. This technique was also used in conjunction with the above-mentioned silicone coating. This technique assumes that little or no water will be lost from the sample once the case humidity is equilibrated with the sample.

The shear rates (denoted by $\dot{\theta}s$) were continued at approximately the same level as had been utilized previously. Similar test sequences were conducted on several specimens in conjunction with various sample preparation procedures.

Test Equipment and Instrumentation

The equipment described in the interim report was utilized for all testing. The above-mentioned sample isolation chamber was the only modification. This chamber was constructed of 0.1 inch thick Plexiglas and was integrated into the existing Plexiglas cover plate.

A precision 50-ohm resistor in the amperage measurement circuit was found to have been defective throughout the period covered in the interim report. The G" and tan δ values which were reported are 22% less than the true experimental values. The values presented in this report were obtained with the new resistor in place.

Data Reduction

Minor modifications in the data reduction procedure were adopted to reduce the number of necessary steps. The revised procedure follows.

(1) Determine the shear angle, θs, for each sample measurement and also for each unloaded measurement using the following equation -

$$\theta s = \tan^{-1} \frac{E}{0.00415 \times f \times h}$$

$$= \frac{56.97\ E}{0.00415 \times f \times h}$$

where f is the frequency, h is the sample height in mils, 0.00415 is a machine constant determined experimentally for the DMA, and 56.97 is a linear conversion factor which replaces $\tan^{-1}$.

(2) Curves of the resonant frequency (f_o) and corresponding input amperage (I_o) are plotted versus Θs for the unloaded machine.

(3) f_o and I_o are read from the above curves for each sample Θs and recorded.

(4) The sample area is scaled from the photograph of the sample using a planimeter, with the aid of a calibrated grid scored on the cover plate and visible in the photograph.

(5) The moduli and supporting parameters are calculated from the following formulas, which are applicable to operation at resonant conditions.

$$G' = h_o/A\ (\omega^2 M - K_o) \qquad (a)$$
$$= (4\pi^2 M h_o/A)\ (f^2 - f_o^2)$$
$$= K_1 (f^2 - f_o^2)$$

$$G'' = \omega h_o/A\ \left(\frac{C_1 I}{E} - Rm_o\right) \qquad (b)$$
$$= (2\pi C_1 h_o/A)\ (f/E)\ (I - I_o)$$
$$= K_2\ (f/E)\ (I - I_o)$$

$$G^* = [(G')^2 + (G'')^2]^{1/2} \qquad (c)$$

$$\tan \delta = G''/G' \qquad (d)$$

where: h_o = Sample height, cm

A = Sample area, cm^2

K_o = Volume spring constant of machine, $gm\text{-}sec^{-2}$

M = Vibrating mass, 243 grams

f = Resonant frequency with sample in place, Hertz

f_o = Resonant frequency without sample and at same apparent Θs as f, Hertz

$\omega = 2\pi f$

C_1 = Force constant of machine, 1.53×10^6 gram-ohm-sec^{-1}

E = Output voltage, volts

Rm_o = Mechanical resistivity of machine, $(C_1 I_o / E)$

I = Driving amperage with sample in place, amperes

I_o = Driving amperage without sample and at same apparent θs as I, amperes

These modifications to the previously reported procedure were made to allow the data to be reduced on a semi-automatic calculator, thus lowering data reduction time. They are mathematically identical to the previous procedure.

Data and Discussion

Complete test results are included in tabular form (Tables I through IV) for all materials tested and also in graphic form (Figures 1 through 7) for selected test series that are felt to demonstrate observations not discussed in the interim report. The code system for the tests remains the same and identifies each test as to - (1) type of brain and sex (as - HBM - Human Brain, Male); (2) the specific brain (5-7 or 9); (3) hours post-mortem at the beginning of testing; and (4) the individual test, denoted by a letter, where a series of tests was conducted with the same specimen in a short time period. An individual test includes either - (1) one measurement isolated from other measurements by a recordable amount of time (as, for example, five minutes); or (2) a scan, or group of approximately 6-8 measurements at various shear rates conducted in rapid sequence.

All test series involving human brains 5-7 were coated with Dow Corning® Medical Adhesive 'B' as was test series HBM-9-96. With the exception of series HBM-5-28, which was spray-coated, all the above series were brush-coated with a solvent-diluted version of the same adhesive. The brush-coating technique is considered better as it apparently places a thinner and more uniform coating on the sample surface than does the spray-coat technique.

All test series of human brains 5-7 were conducted with the previously-reported humidifier in the test chamber, whereas those series of human brain 9 were tested in an unhumidified chamber.

Graphs of various modulus components from tests HBM-6-20, HBM-9-25 and HBM-9-96 are presented as they illustrate the pertinant results and observations. It had been previously noted that G' is far more susceptable to drying than is G". Figure 1 shows G' for test HBM-6-20. The sample had been brush coated with the adhesive-solvent mixture and was in a high-humidity environment. Scan A produced a G' value decreasing with increasing shear rate. Scans B and C produced a most constant G' value. After a 15 minute rest period, scans D-F essentially repeated the performance observed in A-C. Test G, conducted immediately after 10 minutes of shearing at θs ~14° would tend to indicate some thixotropic mechanism as the G' value is lower than had been observed in scans A-F. G' increased some 30% in test H, which was conducted some 20 minutes after test G, the interim period being occupied by a static (rest) sample position. Tests I-M were conducted after a five minute period of shear at θs ~14°. These tests are notable in that G' tends to increase with increasing shear angle.

Figures 2 and 3 illustrate G' for test series HBM-9-25 and HBM-9-96, respectively. Both of these series employed a test sequence very similar to HBM-6-20. HBM-9-25 was conducted without any sample coating or humidity control, but was enclosed in the above-described Plexiglas chamber which isolated it from the DMA sample chamber. Series HBM-9-96 was conducted with the same sample preparations as HBM-9-25 and additionally brush-coating the sample as in HBM-6-20. Examination of these graphs reveals similar trends but with considerably more variation in G' values for the latter scans in any given sequence of scans conducted in rapid order.

Figures 4 and 5 illustrate G" values for test series HBM-9-25 and HBM-9-96, respectively. Taken collectively, they indicate that G" is far more constant than is G' for the particular test series. Tan δ values for the same tests are illustrated in Figures 6 and 7 . The large variations are primarily the result of G' fluctuations.

One notable set of variations in tan δ was seen during test series HBM-7-47 and HBM-7-48. These two test series were conducted on brain tissues that were immediately adjacent to each other <u>in vivo</u>. HBM-7-48 was conducted on a sample whose major axis lay in an anterior-posterior plane of the brain rather than in a lateral plane as had all the other samples. The G" values were extremely low and yielded tan δ values approximately one order of magnitude lower than was recorded for the rest of the test population. As there are no other test parameters which suggest such a drastically decreased tan δ, it may well be an indication of the anisotropy of the human brain. Future tests will be designed to resolve this issue.

In summation, it appears that isolating the test specimen from the general test environment is not as effective as providing a high relative humidity for the test chamber. G' values are probably not noticeably dependent on shear angle for the range of shear angles utilized in all of the tests. Based on the available experimental results, it is believed that G' lies

in the range 6-11 x 10^3 dynes/cm^2; G", 3.5-6.0 x 10^3 dynes/cm^2; and tan δ, 0.40-0.55.

Dynamic Probe Apparatus

Test Description and Objectives

While the DMA has been deemed suitably sensitive for measuring the complex dynamic shear modulus of human brain, it does lack the ability to measure the modulus of the brain *in vivo*. An *in vivo* measurement on a live specimen essentially eliminates such potential variables as drying, aging post mortem, and lack of perfusion. One should also be able to determine the change in modulus from living to several hours post mortem, thus showing a correlation of the present data (DMA tests) to the modulus of the living (*in vivo*) brain. Desirable features for an *in vivo* test include:

(1) Variable frequency and amplitude

(2) The ability to test a small segment of tissue in order to observe any difference in modulus at various points of the brain.

(3) Portability

(4) Ease of data reduction

The above criteria indicated that a forced, non-resonant tester would provide the best approach. A transfer inpedance method was selected due to the increased sensitivity over a subtractive method (as employed on the DMA) when working with low-modulus test materials such as the brain. A small, sensitive impedance head driven by a sinusoidal vibration generator provides the mechanical input for such a system.

The test geometry to be employed consists of a small-diameter rod (probe) attached to the impedance head and vibrated perpendicular to, and in contact with, the surface of the brain. A probe diameter of approximately 1/8 inch was deemed appropriate for measurement of material properties rather than those of the system. A final diameter of 0.135" was selected in order to yield a contact area of 0.1 cm^2.

This machine, together with its accompanying electronics, has been termed the Dynamic Probe Apparatus, or DPA. Its purpose is to measure and display a stress-strain plot for a test material sinusoidally excited by the flat end of the probe tip. Utilizing an oscilloscope, this plot may be recorded photographically either as - (1) an x-y plot (Lissajou's trace); or (2) a time base plot consisting of separate force and displacement signals. Both types of plots yield themselves to the same analysis. The Lissajou's trace also allows determination of the percentage damping. This type of analysis is applied to the well-known Roelig Test Machine, designed to test elastomeric specimens.

Test Procedure

The test procedure consists of seven steps:

(1) The relative signal strengths from the force gages and the accelerometer are adjusted to yield a null signal when the impedance head is drived, without contact with the test specimen.

(2) The force signal is calibrated statically by measuring the change in the d.c. signal output when a known weight is added to the probe tip assembly.

(3) The displacement signal, from the accelerometer, is calibrated dynamically for the test frequency by vibrating the impedance head through a known displacement and adjusting the gain on the oscilloscope to yield the desired calibration. The displacement level is measured by a mechanically grounded micrometer mounted on the axis of motion of the impedance head. It is brought into light contact with the base disc of the impedance head with the system in static condition. This micrometer setting is recorded as the static

reading. After removing the micrometer tip from the base disc, the impedance head is sinusoidally driven at near maximum amplitude. The micrometer is then readjusted to yield light contact with the base disc during the peak amplitude. This condition is assumed to occur simultaneously with the first distortion of either the force or displacement signals being displayed on the oscilloscope. The single amplitude displacement is the difference in micrometer settings for the static and dynamic conditions.

(4) The DPA is brought into close proximity with the test specimen. (Normal operation is in a vertical plane normal to the surface of the test specimen.) The system vibration amplitude is adjusted to approximately the desired test condition.

(5) The DPA is slowly lowered onto the test specimen surface far enough to insure a complete trace, i.e. the probe must contact the specimen throughout the sinusoidal cycle. Note that this requires a static depression, of the probe tip on the test specimen, at least equal to the single amplitude of vibration.

(6) The amplitude is fine-adjusted to the desired level.

(7) A photograph of the resulting Lissajou's trace is taken. Optionally, a photograph of the linear (time-based) traces is also taken.

Data Reduction

Inasmuch as the flat-ended probe appears to operate on the sample in both the shear and compressive modes simultaneously, one can not determine either the complex dynamic shear or complex dynamic Young's modulus, G* and E* respectively, until a rather thorough analysis of the induced stresses is performed. One should be able, however, to determine the elastic (M') and viscous loss (M") components of a complex dynamic modulus M*,

and tan δ, or M''/M'. M', M'', and M^* are analogous to G', G'', and G^*, respectively.

See Figure 9a. In order to analyze the photograph of the Lissajou's trace resulting from a test, one must first determine:

(1) The force on the probe at maximum amplitude, y_2

(2) The maximum amplitude, x_2

(3) The force on the probe at zero amplitude, y_1

(4) A shape factor, equal to the effective specimen thickness (h) divided by the cross-sectional area of the probe tip (A), or h/A.

The forces involved are not the total forces on the probe but rather those due to the motion of the probe on the test specimen. The initial static forces are not present in the oscilloscope traces due to the fact that the signals were channeled through the oscilloscope's a.c. inputs.

These values are then substituted in the following equations -

$$M' = \frac{h}{A}\,\frac{y_2}{x_2} \qquad (a)$$

$$\tan \delta = \frac{y_1}{y_2} \qquad (b)$$

$$M'' = M' \tan \delta \qquad (c)$$

$$= \frac{h}{A}\,\frac{y_1}{x_2}$$

Note also, in Figure 9b, that the following equations may be utilized:

$$M' = \frac{h}{A}\,\frac{f}{d} \qquad (d)$$

$$\% \text{ Damping} = \frac{a}{b} \qquad (e)$$

All of the above equations assume the occurrence of a perfect, or near-perfect ellipse except equation (e) which is valid for distorted ellipses as well.

The effective sample thickness, h, is considered to be less than the diameter of the brain, i.e. the intact brain represents a semi-infinite sample thickness.

It is expected that h will be determined experimentally and related to tan δ, test amplitude, or a combination of the two.

Experimental

The DPA was used without calibration, to test a silicone gel and one sample of human brain tissue. The purpose of the tests was to determine the feasibility of in vivo testing with the apparatus. Qualitative results indicated that the sensitivity was sufficient for testing brain tissue. It was also noted that the relaxation time of brain tissue is rather long. This causes the force on the probe tip to be less on that portion of the amplitude cycle nearest the sample surface (i.e. when the least static compression is indicated). This causes the Lissajou's trace to be skewed rather than a perfect ellipse. This effect was not observed when testing the silicone gel.

Two in vivo test series have been conducted on live squirrel monkeys at the Highway Safety Research Institute labs (Ann Arbor). Both test series were very similar. The monkey, weighing about one kilogram, was anesthetized with sodium pentabarbital and placed on a custom-design jig which held its head firmly in an upright position. Transducers for EKG and respiration monitoring were attached to the monkey. A 1/4-inch hole was cut through the skull, being positioned over the right frontal lobe of the brain immediately anterior to the frontal sulcus and close to the midline. The dura was then removed with a scalpel. The DPA was positioned vertically over the hole and operated according to the above-described test procedure. Both Lissajou's

trace and linear trace photographs were taken. A series of tests was conducted over a period of about one hour. (The probe tip remained in the same static position on the brain between tests.) The monkey was then sacrificed with a lethal dose of sodium pentabarbital. Tests were now continued for about 1-1/2 hours after death.

Slow relaxation of the brain matter is evident in the test photos. Also, the dynamic force on the probe tip was reduced to about one-half its "living" value only a few minutes post mortem. The static force on the probe, due to its initial depression on the brain, decreased also. The photographic results are currently being more thoroughly analyzed.

The monkey brain from the first test was fixed in 10% Formalin and later examined grossly and by light-microscopic histological methods. Gross examination indicated an apparent abnormality (color change) under the trephined area. Histological results showed this color change to be due to drying. The only abnormality under the test area was edema of cortical parenchyma and pia vascularization. All neurons remained intact and there was no damage to glial structures.

Secant Bulk Modulus

Test Description and Objectives

As stated in the interim report, work in the bulk modulus area was continued, with the primary effort concentrated on low-pressure effects. As previously defined, the secant bulk modulus (β) of a compressible material is the ratio of stress to strain for the case of hydrostatic compression and is, therefore, the inverse of compressibility. The test procedure consists of placing the test material in a cylinderical compression cell and compressing it. A stress-strain record of the test provides the necessary data for the calculation of β from the equation -

$$\beta = \frac{V_o \Delta p}{\Delta V_o}$$

where: V_o = original volume of test material

Δp = applied hydrostatic pressure

ΔV_o = change in volume produced by Δp

Equipment and Instrumentation

The same compression cell and Baldwin Tate-Emory Universal Tester as described in the interim report were utilized for high pressure data collection. Low pressure tests were conducted on a Model TM Instron tensile machine and an Instron CCT compression load cell (200 pounds maximum load). The maximum test pressure with this assembly is 1000 psi. A compression rate of 0.5%/minute was utilized. The Instron employs a recording system similar to that of the Baldwin Tate-Emory machine.

Test Specimens and Procedures

Tissue specimens for high pressure tests were prepared as previously reported. Specimens for low pressure tests were prepared by one of four methods. After cutting the tissue in small pieces and measuring its volume (by displacement in the carrier fluid to be employed in the test) it was either:

(1) tested with silicone fluid or water as the carrier fluid, or

(2) degassed in the carrier fluid (silicone or water) and then tested.

The degassing step was included to determine if air trapped within the vasculature of the sample tissues was responsible for the apparently low modulus at pressures up to 300-500 psi. Water was used as the carrier fluid in some tests to determine if the silicone carrier fluid allows air bubbles to remain on the cut tissues due to lack of wetting associated with silicone fluids.

It was necessary to add a very small amount of silicone fluid to the top of the water column in the compression cell in order to achieve a good seal with the piston. The amount of silicone fluid in the test volume was negligible and, therefore, not considered in calculations.

Only minor changes in the established test procedure were necessary for those tests conducted on the Instron tensile machine: The recording system of the Instron does not require an external position transducer. A compression rate of 0.5%/minute was utilized. The other steps of the established procedure were observed without modification. In general, multiple compression-decompression cycles were recorded for each sample loading for an increased test population and also to ascertain if any irreversible strains were present.

Data Reduction

Minor modifications in the established data reduction procedure were observed in order to lessen the total data reduction time. This was possible as only two-phase systems (brain plus carrier fluid) were tested.

The secant bulk modulus (β) is obtained from the equation -

$$\beta = \frac{\% \text{ Br} \times \Delta p}{C_T - C_F}$$

where: % Br = percentage of brain in the test column

Δp = applied hydrostatic stress, psi

C_T = total observed percentage compression of the test volume at Δp

C_F = percentage compression due to the carrier fluid at Δp

Data and Discussion

Complete results from all tests are presented in Tables V through IX. Graphic results are included as necessary to illustrate pertinent results.

The high pressure tests conducted on the Baldwin Tate-Emory machine show no significant variations from the previously reported results. The secant bulk modulus appears to be very similar to published values for water.

The results obtained from tests conducted on the Instron tensile machine are most interesting in that they include the variables of carrier fluid and sample degassing. Figure 10 shows secant bulk modulus values obtained at pressures up to 1000 psi with the following test parameters.

	Sample Preparation	Carrier Fluid
(a)	Not degassed	Silicone
(b)	Not degassed	Water
(c)	Degassed	Silicone
(d)	Degassed	Water

Also included is a low pressure test conducted on the Baldwin Tate-Emory machine. Three samples, 8-HBM-33, 8-HBM-57 (degassed in silicone fluid), and 9-HBM-121 (degassed in water), yielded low modulus values due to their extreme compressibility at pressures under ~200 psi. See Figure 11. The remaining two samples, 8-HBM-149 and 9-HBM-141, yielded much higher modulus values and did not exhibit extreme compressibility at under 200 psi. See also Figure 11. Of the three low modulus samples, two had been degassed:

(1) 8-HBM-57 - 65 mm Hg for 15 minutes

(2) 9-HBM-121 - 8 mm Hg for 30 minutes

Both samples were resting in their carrier fluids (silicone and water, respectively) while subjected to the low pressures. Qualitative observations indicated that the sample volumes had increased during the low pressure conditions. It is felt that the extended degassing procedure created gaseous voids within the interior of the tissues. These gaseous voids caused the large amount of compression at relatively low pressure (under ~200 psi). The remaining low-modulus sample, 8-HBM-33, is felt to have had air bubbles trapped on the sample surfaces. These three tests were summarily deemed invalid. Notice that the modulus slope is very similar for all samples at pressures >200 psi. This is still another indication that the inability to measure the true amount of compression at low pressures (<200 psi) is the prime cause of differences in the modulus from sample-to-sample at low pressures. Therefore, the higher modulus values obtained in tests 8-HBM-149 and 9-HBM-141 are considered to be the true values. Figure 12 shows how these values appear on an extended pressure range when compared with high pressure tests.

Future Work

The DMA will find continued usage coupled with a better sample environment to further reduce the physiological effects now connected with testing. A physiological saline solution will be flowed over the exposed sample surfaces during testing. The internal temperature of the samples will be monitored with a thermocouple. The feasibility of an impulse test will be explored.

The DPA will be utilized for continued in vivo tests on monkeys. Test procedures will be revised as necessary. In order to reduce the number of test parameters, the monkey brains will be perfused with physiological saline at the normal internal vascular pressure upon sacrifice. It is hoped that this same technique can be applied to a human brain immediately preceding autopsy. Newly developed pressure transducers may well replace the custom-fabricated impedance head now in use.

The secant bulk modulus will be investigated at all pressures for the range of 0-100,000 psi stress. It is expected that the predominance of the effort will be concentrated on low pressure (0-1000 psi) and very-high pressure (40,000-100,000 psi) tests. The feasibility of impulse loading will be studied.

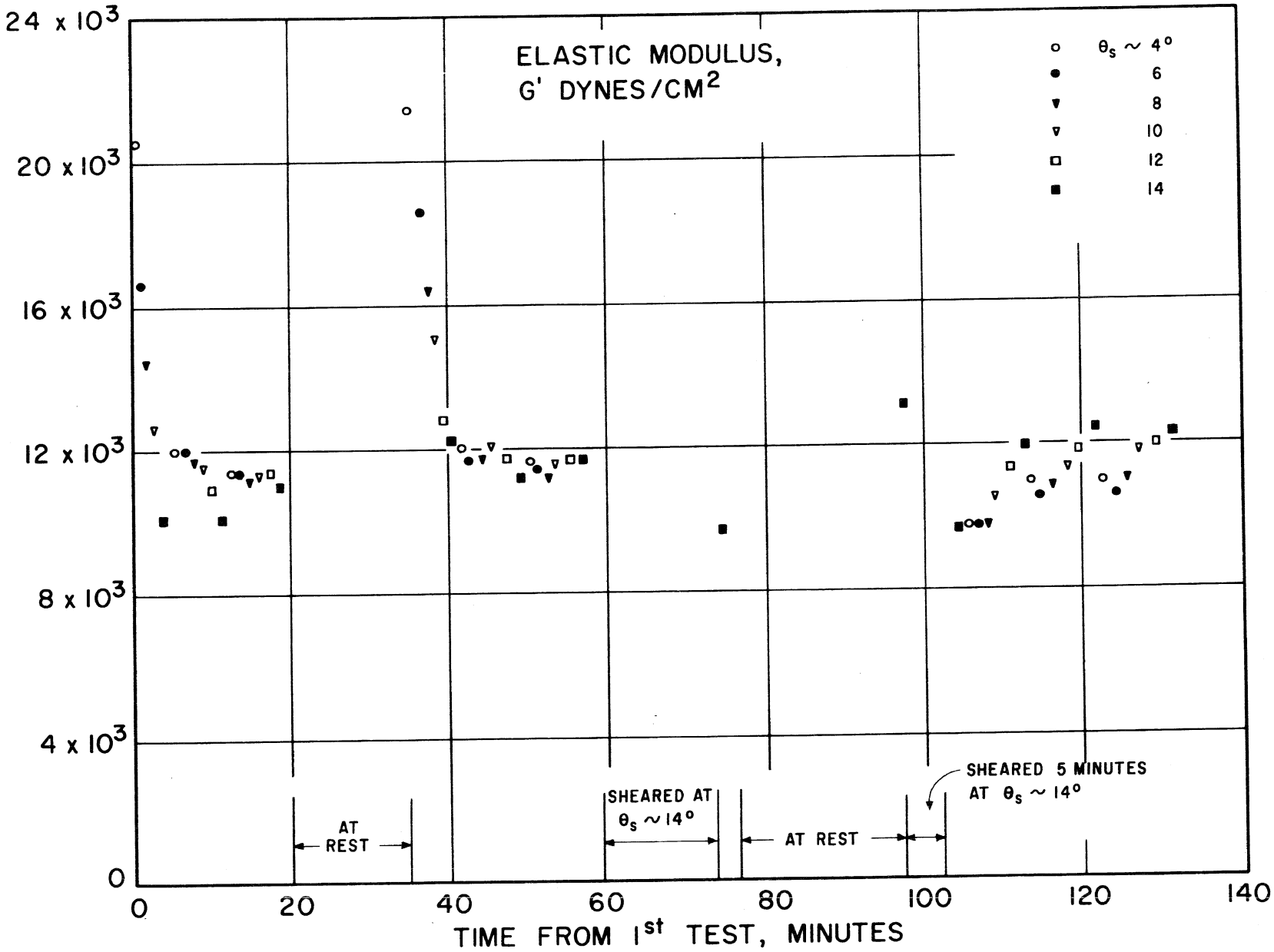

Figure 1 - Variables in Measurement of Dynamic Elastic Modulus. I. HBM-6-20. Time on Test, Displacement, Vibration History

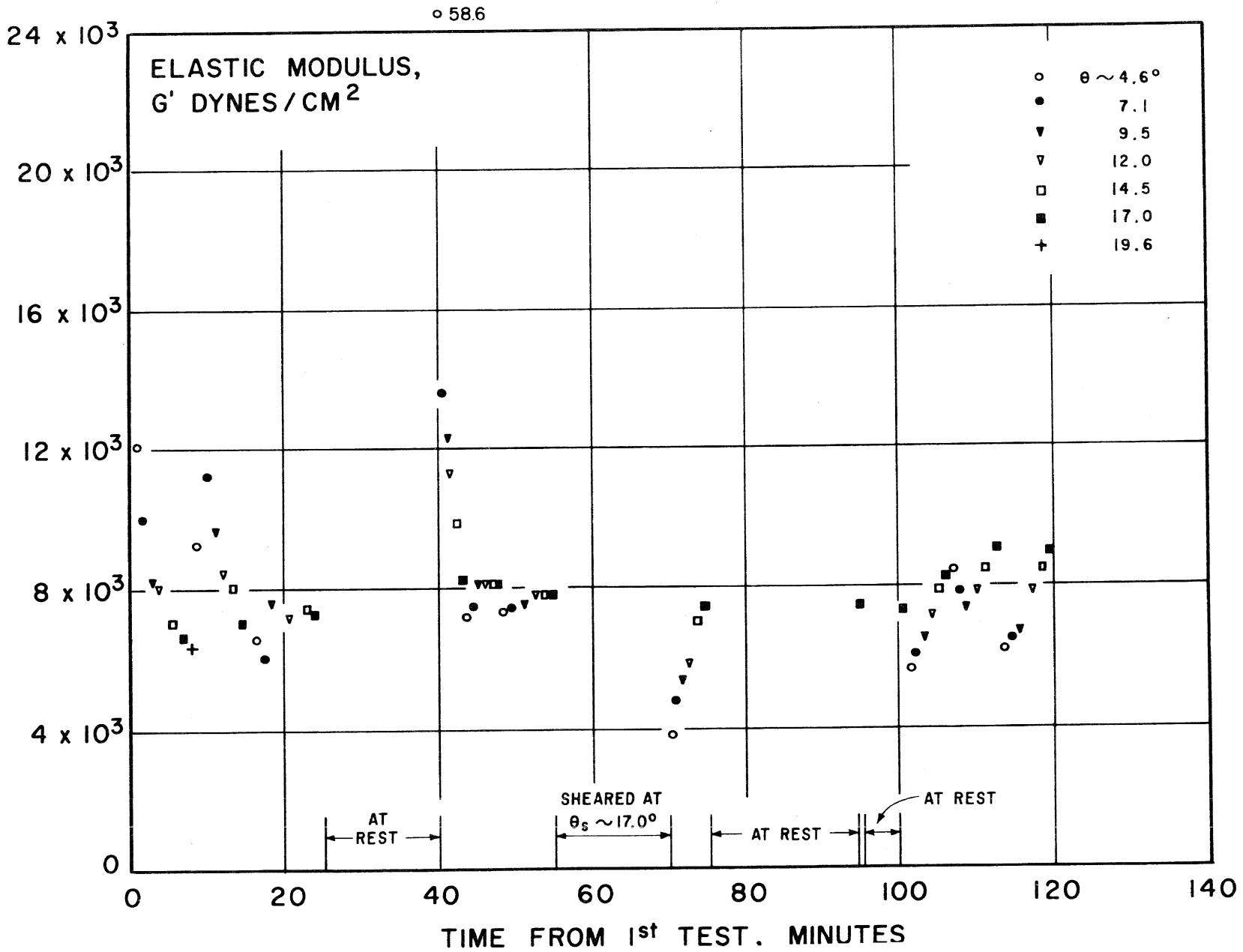

Figure 2 - Variables in Measurement of Dynamic Elastic Modulus. II. HBM-9-25. Time on Test, Displacement, Vibration History

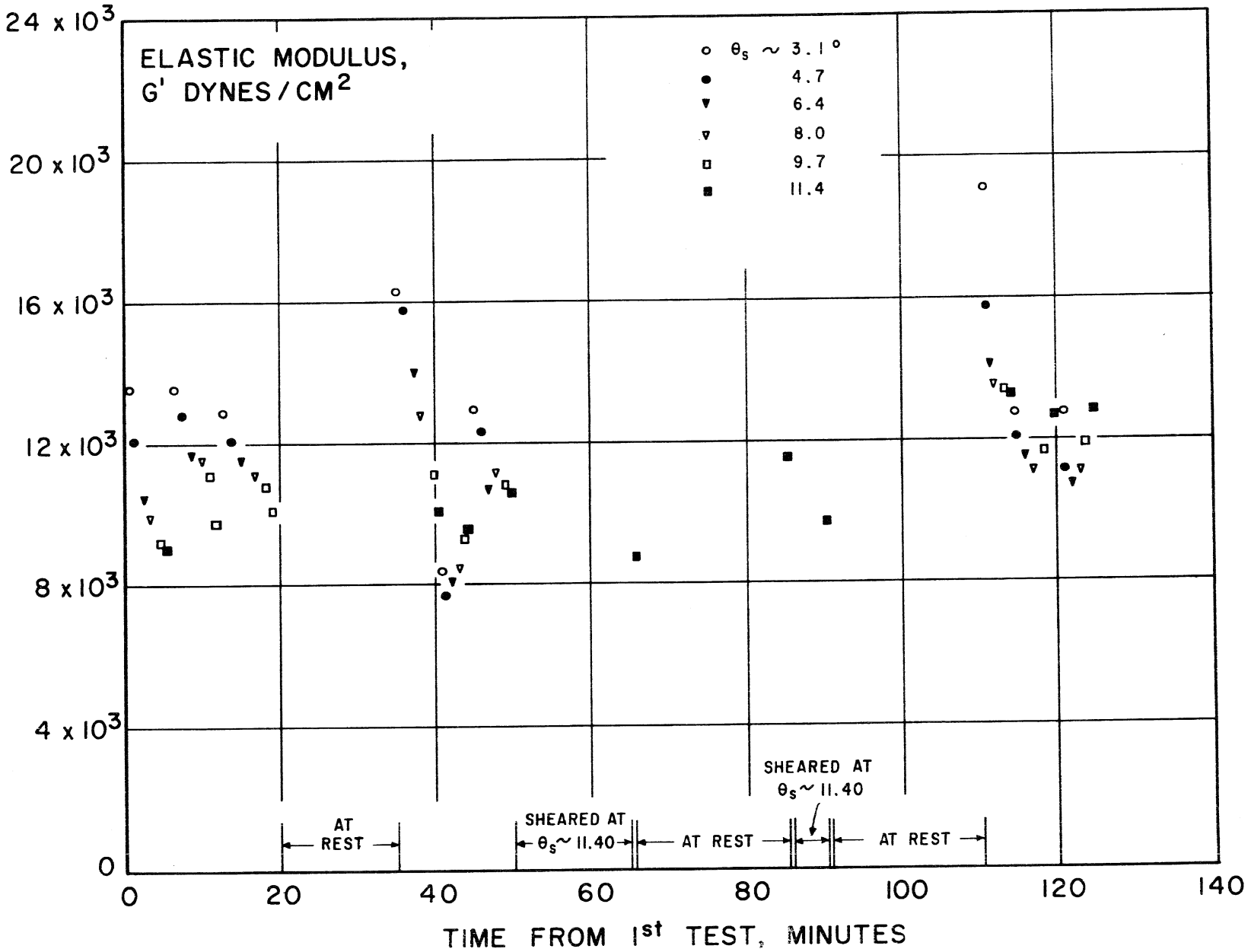

Figure 3 - Variables in Measurement of Dynamic Elastic Modulus. III. HBM-9-96. Time on Test, Displacement, Vibration History

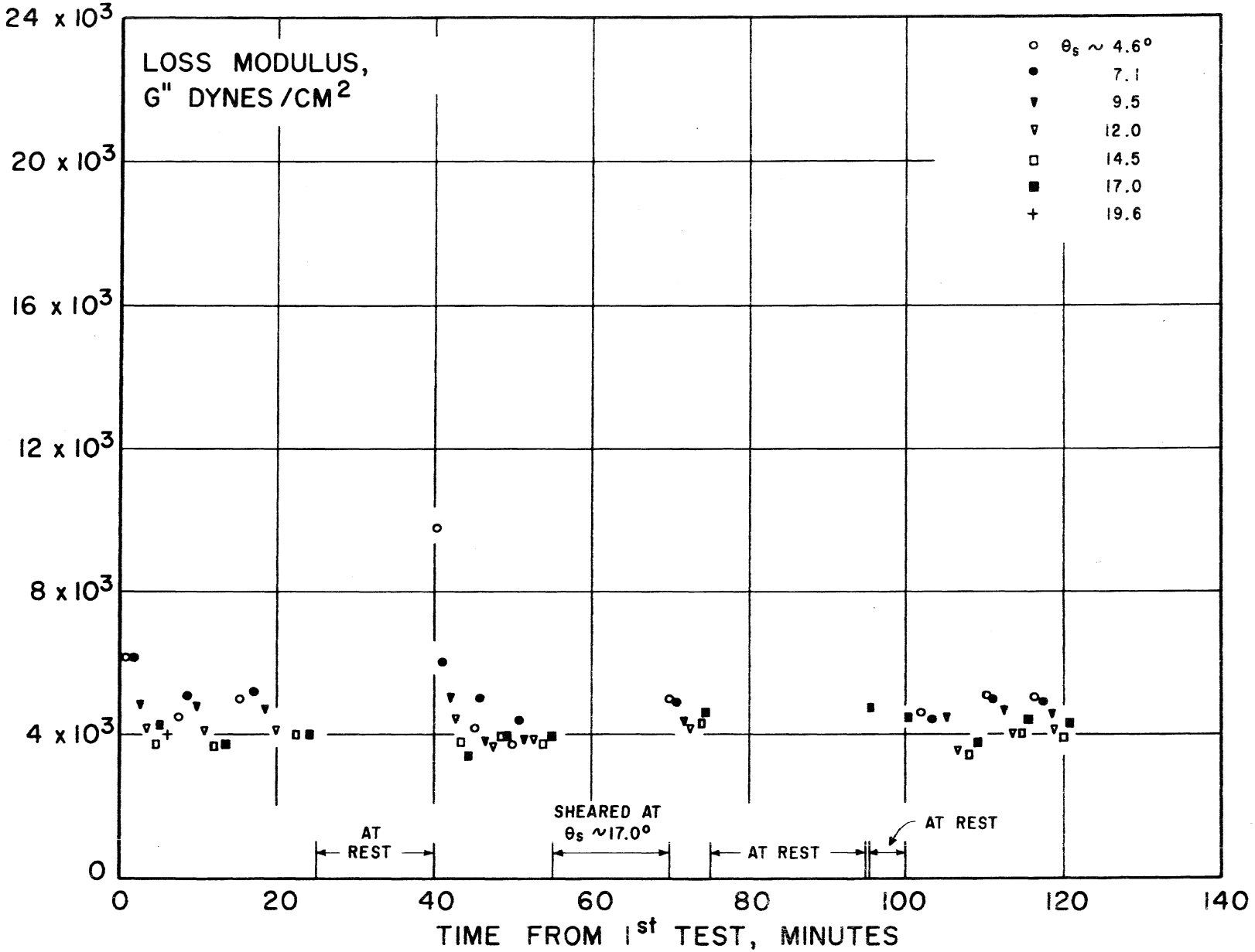

Figure 4 - Variables in Measurement of Dynamic Loss Modulus. I. HBM-9-25. Time on Test, Displacement, Vibration History

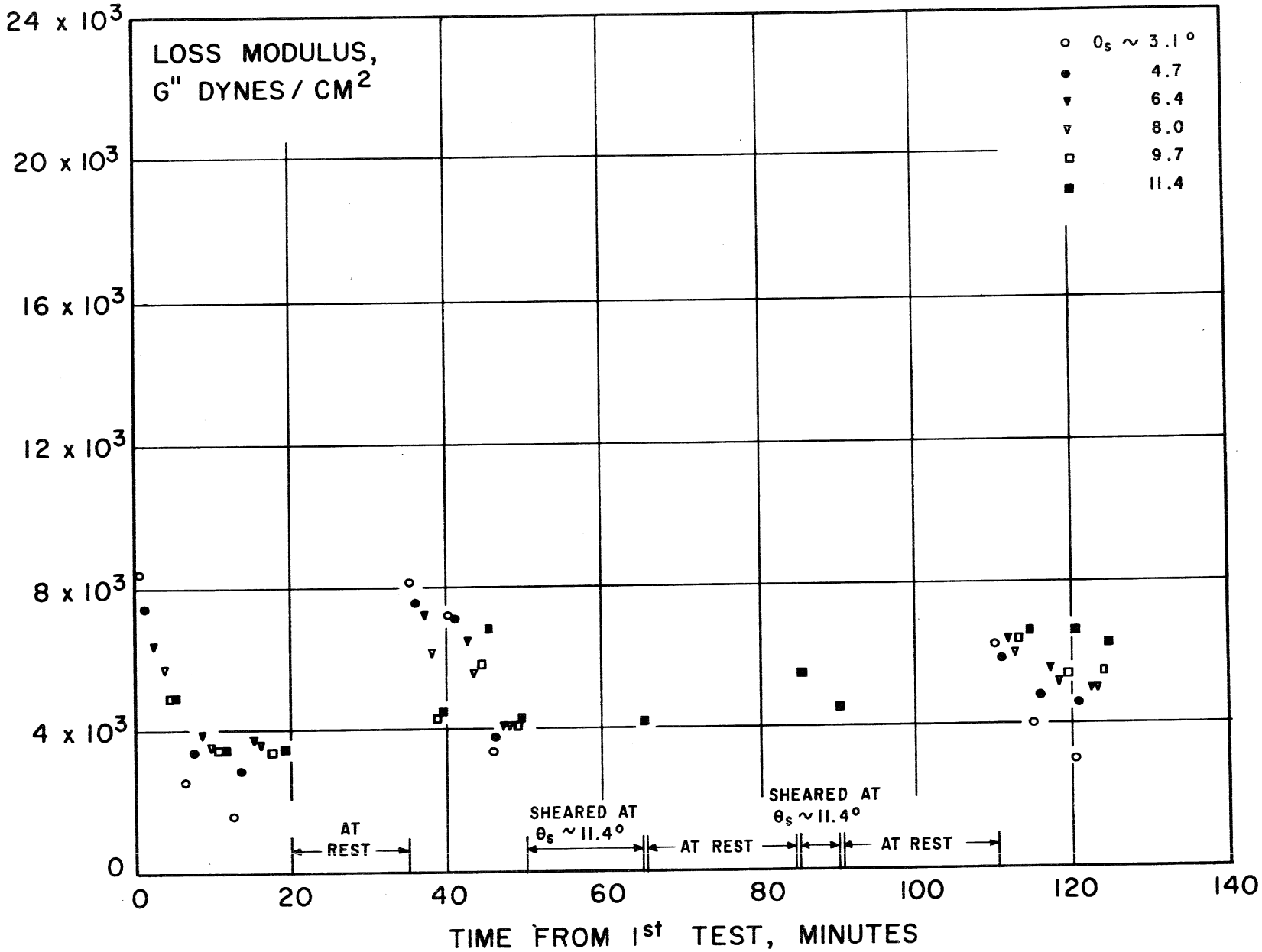

Figure 5 - Variables in Measurement of Dynamic Loss Modulus. II. HBM-9-96. Time on Test, Displacement, Vibration History

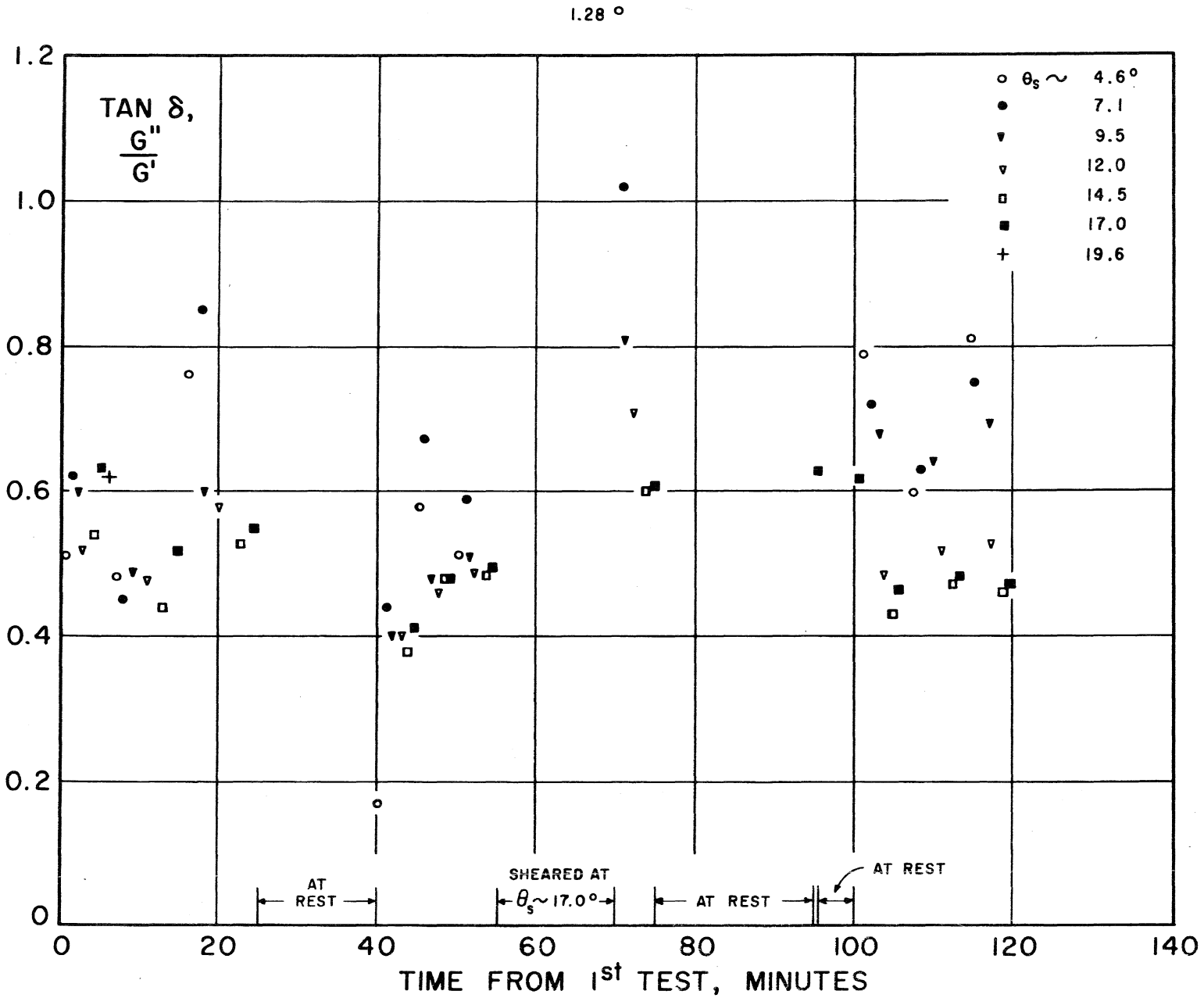

Figure 6 - Variables in Measurement of tan δ. I. HBM-9-25. Time on Test, Displacement, Vibration History

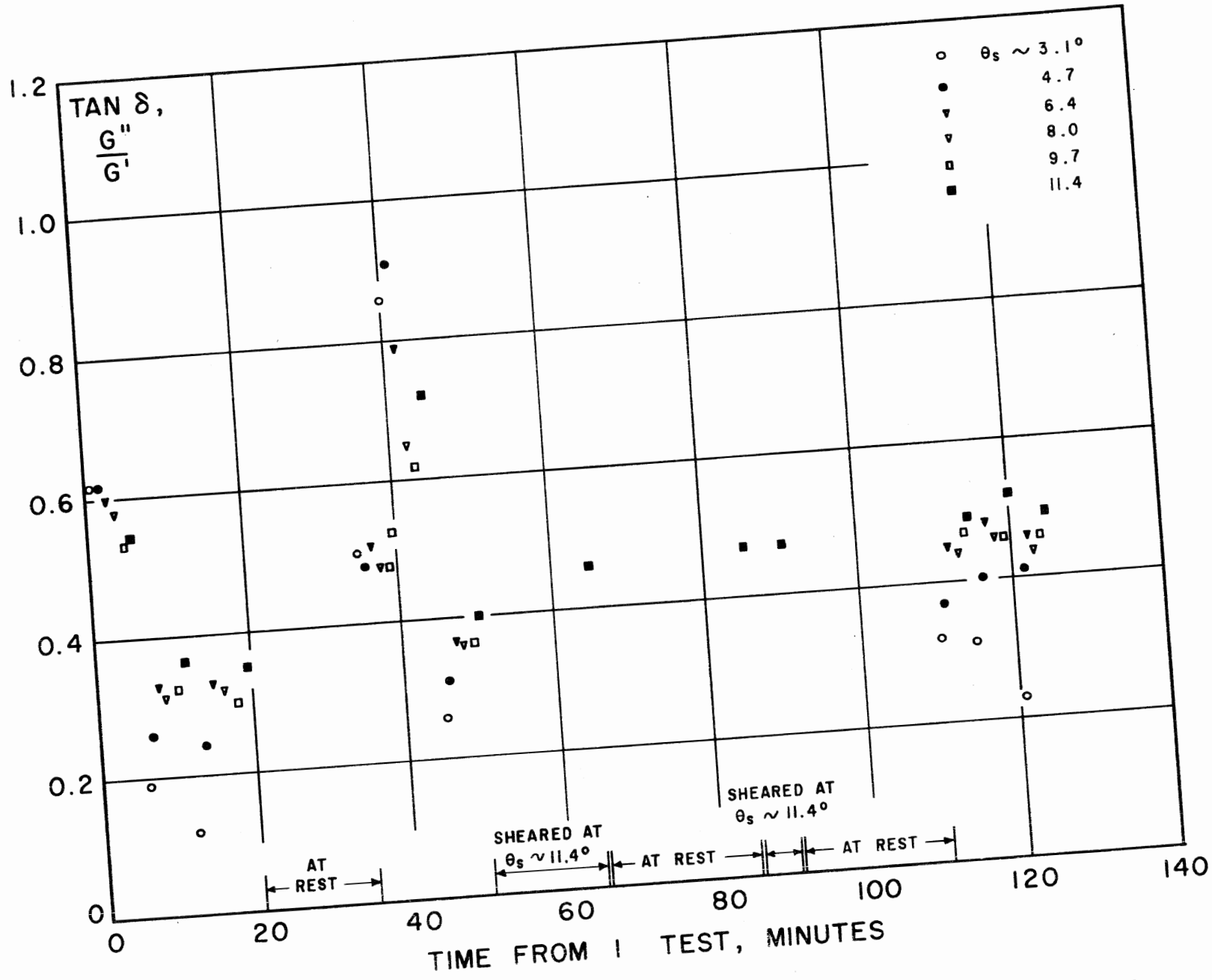

Figure 7 - Variables in Measurement of tan δ. II. HBM-9-96. Time on Test, Displacement, Vibration History

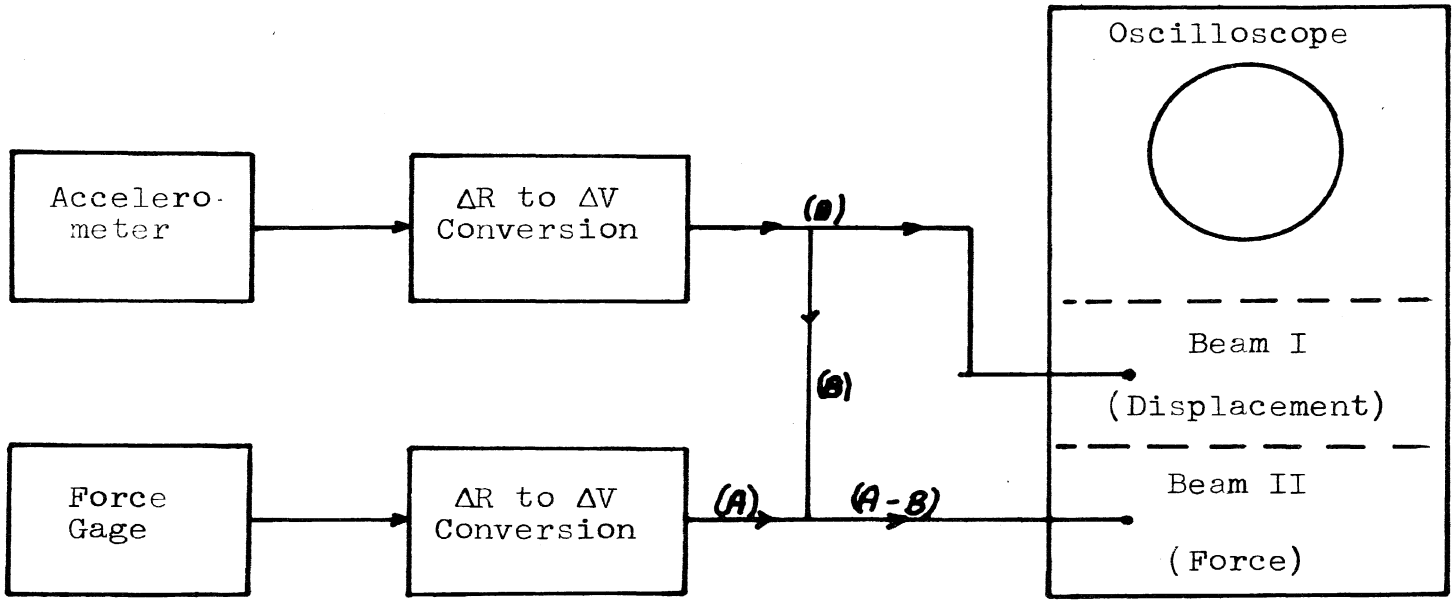

Figure 8 - Schematic Diagram of Dynamic Probe Apparatus

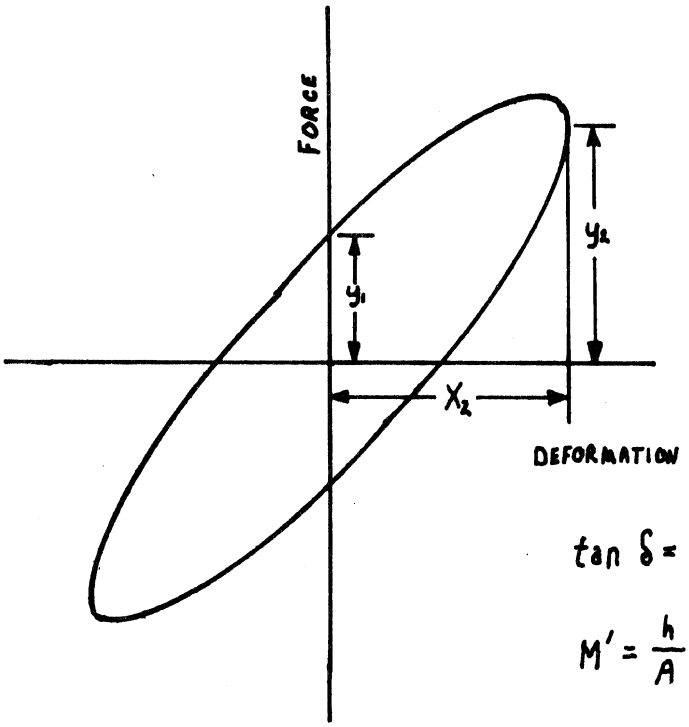

$$\tan \delta = \frac{y_1}{y_2}$$

$$M' = \frac{h}{A} \frac{y_2}{x_2}$$

$$M'' = M' \tan \delta = \frac{h}{A} \frac{y_1}{x_2}$$

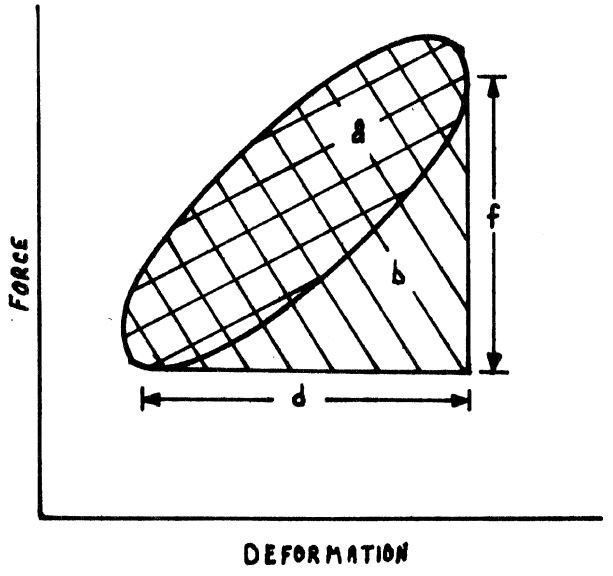

$$M' = \frac{h}{A} \frac{f}{d}$$

$$\% \text{ Damping} = \frac{a}{b}$$

Figure 9 - Analysis of Lissajou's Figure

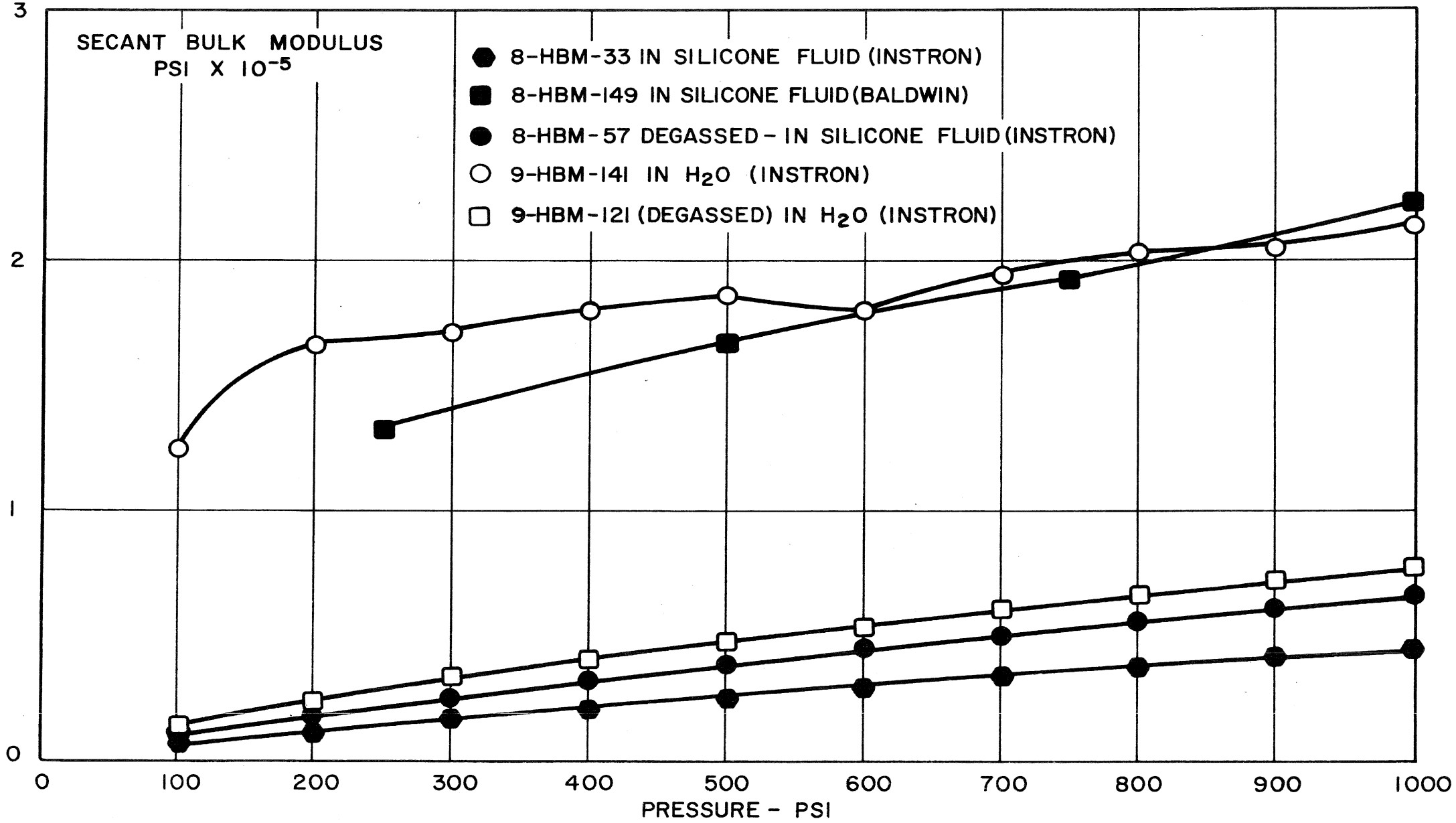

Figure 10 - Variables in Measurement of Secant Bulk Modulus of Human Brain Tissue for 0-1000 psi. Carrier fluid, sample degassing

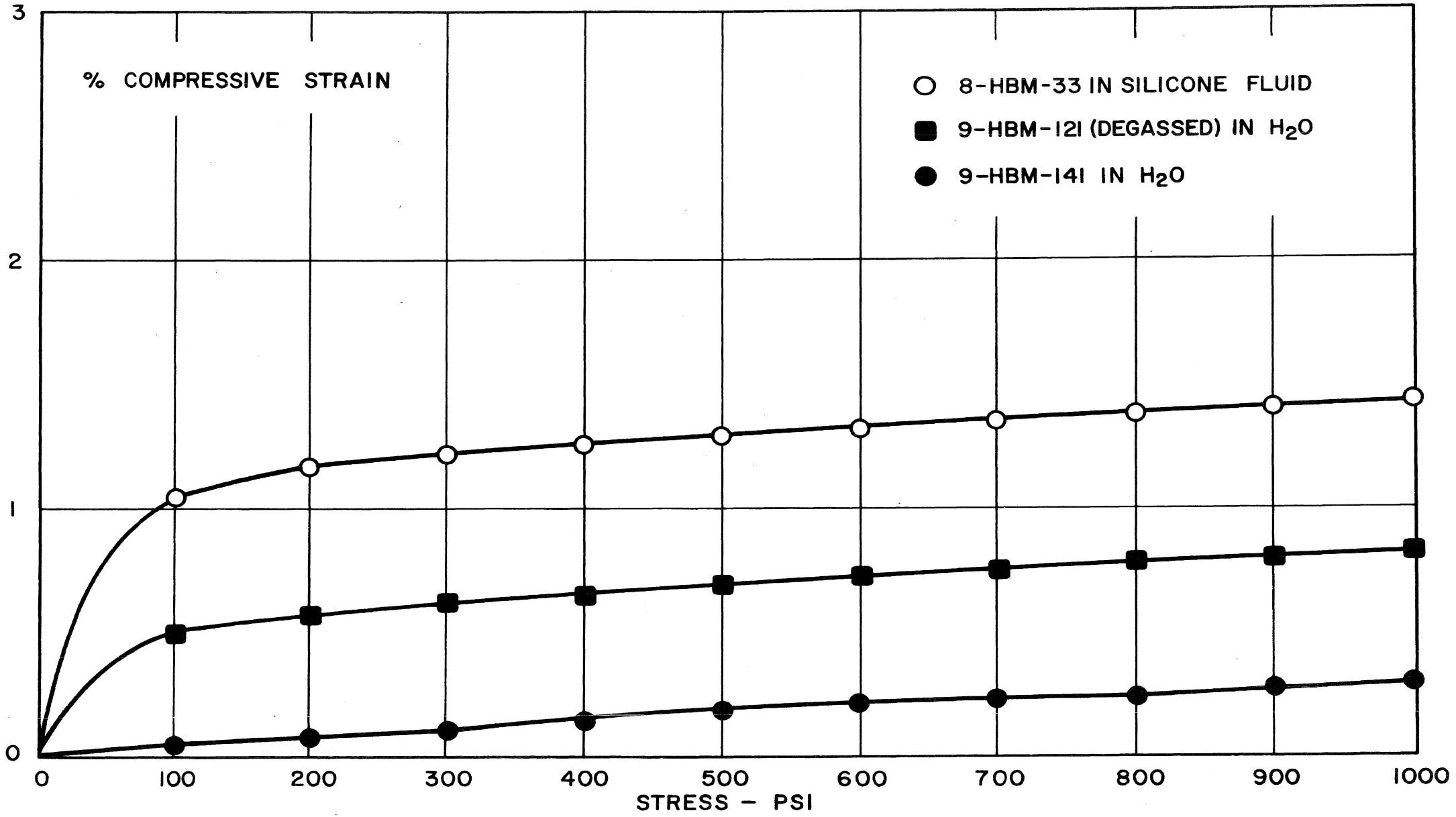

Figure 11 - Stress-Strain Relationship for Human Brain Tissues Subjected to 0-1000 psi Hydrostatic Stress

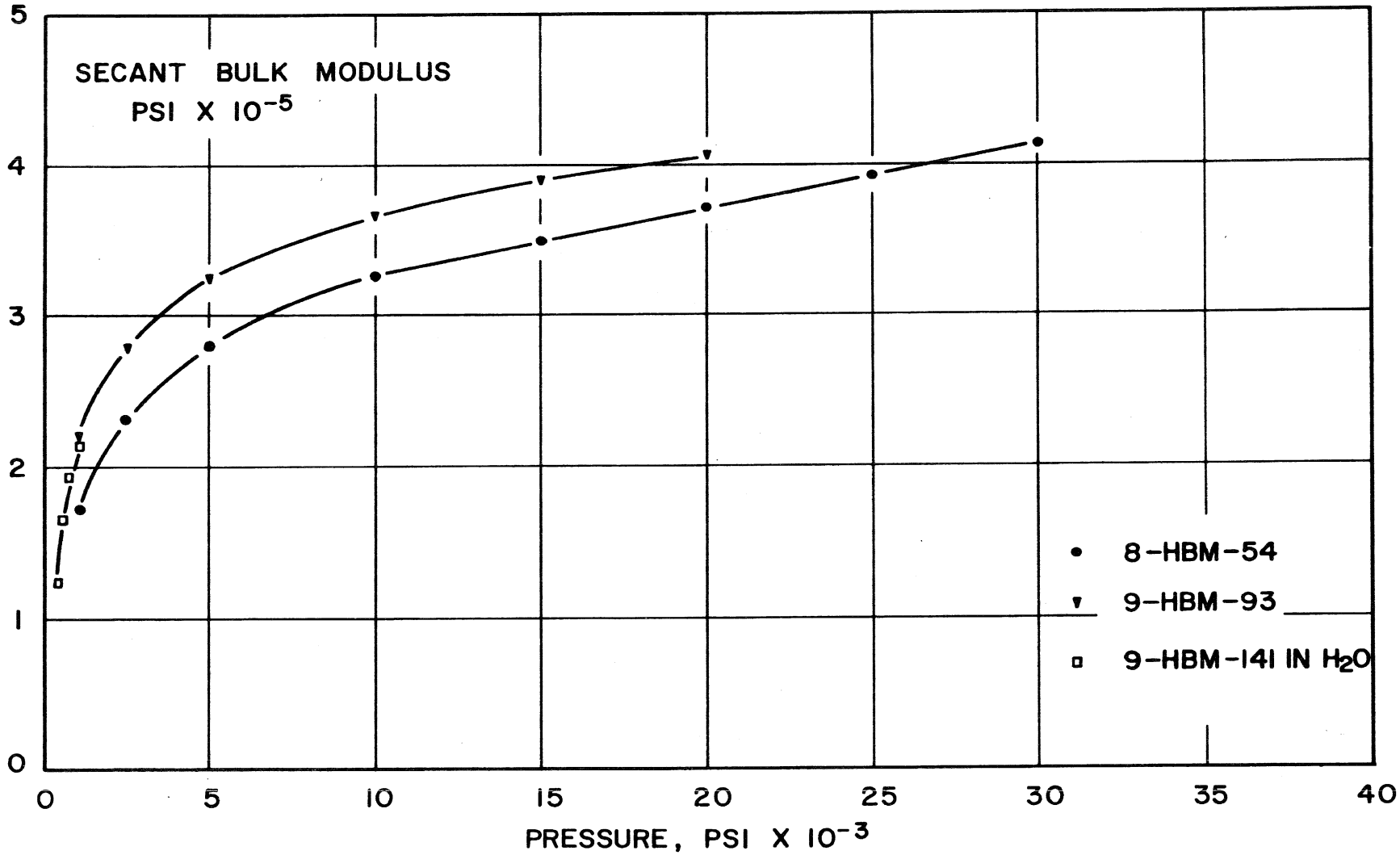

Figure 12 - Secant Bulk Modulus of Human Brain Tissue - 0-30 x 10^3 psi

Table I

Dynamic Shear Modulus
Human Brain No. 5

Sample History - Time of death: 12:15 P.M., 23 Jan. 68
Age: 80
Sex: M
Race: C
Cause of death: Overdose of Plascidel: Developed pneumonia
Time specimen removed at autopsy: 10:50 A.M., 24 Jan. 68
Location of test specimen: Frontal lobe
Transfer conditions: Packed in polyethylene bags and carried in ice and water

Test No.	Freq (Hz)	θs	G' dynes/cm^2	G" dynes/cm^2	tan δ
HBM-5-28A	9.73	2.5°	19.3 x 10^3	9.2 x 10^3	0.48
28 Jan. 68	9.51	3.9	16.7	7.5	0.45
Temp. - 37°C	9.32	5.3	13.0	7.5	0.58
White matter	9.23	6.7	12.4	5.9	0.48
h_o - 0.70 cm	9.11	8.2	9.3	4.9	0.53
A = 2.86 cm^2	9.07	9.6	9.3	4.4	0.47
h_o/A = 0.246 cm^{-1}	9.04	11.0	9.3	4.3	0.46

HBM-5-28B	9.49	2.6°	8.8 x 10^3	6.3 x 10^3	0.72
	9.35	4.0	10.0	6.2	0.62
	9.23	5.4	9.5	6.1	0.64
	9.18	6.7	10.2	5.2	0.51
	9.13	8.1	10.2	4.9	0.48
	9.07	9.6	9.3	4.4	0.47
	9.04	11.0	9.3	4.1	0.44

Table I (Continued)

Test No.	Freq (Hz)	θs	G' dynes/cm²	G'' dynes/cm²	tan δ
HBM-5-28C	9.49	2.6°	8.8 x 10^3	5.8 x 10^3	0.66
	9.33	4.0	9.1	5.9	0.65
	9.21	5.4	8.6	6.1	0.71
	9.15	6.8	9.0	5.2	0.58
	9.09	8.2	8.5	4.9	0.58
	9.06	9.6	8.9	4.6	0.52
	9.04	11.0	9.3	4.3	0.46

Sample remained in static condition for 15 minutes at 37°C between tests C and D					

HBM-5-28D	9.80	2.5°	22.5 x 10^3	10.2 x 10^3	0.45
	9.53	3.9	17.6	8.4	0.48
	9.39	5.3	16.1	8.9	0.55
	9.28	6.7	14.6	7.0	0.48
	9.21	8.1	13.6	6.1	0.45
	9.12	9.5	11.4	5.2	0.46
	9.08	10.9	11.0	5.2	0.47

HBM-5-28E	9.53	2.6°	10.6 x 10^3	7.7 x 10^3	0.73
	9.39	4.0	11.8	7.1	0.60
	9.26	5.4	10.3	7.9	0.77
	9.21	6.7	11.6	5.9	0.51
	9.14	8.1	10.6	5.8	0.55
	9.09	9.5	10.1	5.4	0.53
	9.07	10.9	10.5	5.4	0.51

Table I (Concluded)

Test No.	Freq (Hz)	θs	G' dynes/cm^2	G'' dynes/cm^2	tan δ
Sample sheared at θs ~20° for five minutes at 37°C between tests E and F					
HBM-5-28F	8.87	11.2°	2.5×10^3	3.3×10^3	1.32

Table II

Dynamic Shear Modulus
Human Brain No. 6

Sample History - Time of death: 8:30 P.M., 28 Jan. 68
Age: 50
Sex: M
Race: C
Cause of death: Respiratory death
Time specimen removed at autopsy: 11:05 A.M., 29 Jan. 68
Location of test specimen: Parietal lobe
Transfer conditions: Packed in polyethylene bags and carried in ice and water

Test No.	Freq (Hz)	θs	G' dynes/cm^2	G" dynes/cm^2	tan δ
HBM-6-20A	10.47	3.7°	20.6 x 10^3	7.4 x 10^3	0.36
29 Jan. 68	10.14	5.7	16.7	6.1	0.36
Temp. - 37°C	9.92	7.8	14.5	5.8	0.40
White matter	9.73	9.9	12.7	4.9	0.38
h_o = 0.45 cm	9.50	14.0	10.1	3.6	0.36
A = 4.40 cm^2					
h_o/A = 0.102 cm^{-1}					
	---	---	---	---	---
HBM-6-20B	10.03	3.8°	12.0 x 10^3	5.9 x 10^3	0.49
	9.89	5.9	12.0	5.4	0.45
	9.76	8.0	11.8	5.4	0.46
	9.68	9.9	11.7	4.8	0.41
	9.59	11.6	10.9	4.8	0.44
	9.50	14.0	10.1	4.2	0.42
	---	---	---	---	---

Table II (Continued)

Test No.	Freq (Hz)	θs	G' dynes/cm²	G'' dynes/cm²	tan δ
HBM-6-20C	9.98	3.9°	11.4 x 10^3	4.7 x 10^3	0.41
	9.84	6.2	11.4	5.1	0.45
	9.73	8.0	11.2	5.1	0.46
	9.66	10.0	11.3	4.7	0.42
	9.61	12.0	11.4	4.4	0.38
	9.55	14.0	11.0	4.6	0.42

Sample remained in static condition for 15 minutes at 37°C between tests C and D					

HBM-6-20D	10.51	3.7°	21.4 x 10^3	9.5 x 10^3	0.44
	10.23	5.7	18.5	8.3	0.45
	10.02	7.7	16.5	7.3	0.44
	9.86	9.8	15.0	6.6	0.44
	9.68	11.9	12.8	5.4	0.42
	9.61	13.9	12.2	5.2	0.43

HBM-6-20E	10.02	3.9°	12.1 x 10^3	6.3 x 10^3	0.52
	9.87	5.9	11.6	5.7	0.49
	9.79	7.3	11.7	6.1	0.52
	9.70	9.9	12.1	5.0	0.41
	9.63	11.9	11.8	5.0	0.42
	9.56	14.0	11.2	4.6	0.41

Table II (Continued)

Test No.	Freq (Hz)	θs	G' dynes/cm^2	G" dynes/cm^2	tan δ
HBM-6-20F	9.99	3.9°	11.6 x 10^3	6.3 x 10^3	0.54
	9.86	5.9	11.4	5.7	0.50
	9.74	8.0	11.2	5.5	0.49
	9.68	10.1	11.7	5.0	0.43
	9.63	11.9	11.8	5.2	0.44
	9.59	13.9	11.8	5.2	0.44
	---	---	---	---	---
Sample sheared at θs ~14° for ten minutes at 37°C					
	---	---	---	---	---
HBM-6-20G	9.48	14.2°	9.7 x 10^3	4.2 x 10^3	0.43
	---	---	---	---	---
Sample remained in static condition for 20 minutes at 37°C between tests G and H					
	---	---	---	---	---
HBM-6-20H	9.67	13.8°	13.1 x 10^3	5.7 x 10^3	0.44
	---	---	---	---	---
Sample sheared at θs ~14° for 10 minutes at 37°C between tests H and I					
	---	---	---	---	---
HBM-6-20I	9.48	14.2°	9.7 x 10^3	4.4 x 10^3	0.45
	---	---	---	---	---
HBM-6-20J	9.90	3.9°	9.8 x 10^3	5.8 x 10^3	0.59
	9.77	6.0	9.8	5.1	0.52
	9.67	8.0	9.9	5.3	0.54
	9.62	10.0	10.6	5.1	0.48
	9.60	12.0	11.3	4.9	0.43
	9.60	13.9	12.0	5.3	0.44
	---	---	---	---	---

Table II (Concluded)

Test No.	Freq (Hz)	θ_s	G' dynes/cm^2	G" dynes/cm^2	tan δ
HBM-6-20K	9.96	3.9°	11.0 x 10^3	5.8 x 10^3	0.53
	9.82	5.9	10.6	5.4	0.51
	9.72	8.0	10.9	5.3	0.49
	9.66	10.0	11.3	5.1	0.45
	9.63	11.9	11.8	5.1	0.43
	9.63	13.9	12.5	5.5	0.44
HBM-6-20L	9.96	3.9°	11.0 x 10^3	5.8 x 10^3	0.53
	9.82	5.9	10.6	5.6	0.53
	9.73	8.0	11.1	5.5	0.50
	9.69	10.0	11.9	5.3	0.44
	9.64	11.9	12.0	5.4	0.45
	9.64	13.9	12.7	5.6	0.44
	9.59	15.9	12.1	5.6	0.46

Table III

Dynamic Shear Modulus

Human Brain No. 7

Sample History - Time of death: 8:45 P.M., 27 Jan. 68
Age: 49
Sex: M
Race: C
Cause of death: Emphysema and Pneumothorax
Time specimen removed at autopsy: 11:45 A.M., 29 Jan. 68
Location of test specimen: Frontal lobe
Transfer conditions: Packed in polyethylene bags and carried in ice and water

Test No.	Freq (Hz)	θs	G' dynes/cm^2	G" dynes/cm^2	tan δ
HBM-7-47A	10.03	4.0°	13.4 x 10^3	6.2 x 10^3	0.46
29 Jan. 68	9.81	6.1	11.6	5.0	0.43
Temp. - 37°C	9.62	8.2	10.1	4.3	0.42
White matter	9.46	10.5	8.5	3.1	0.36
h_o = 0.439 cm	9.35	12.7	7.5	2.8	0.37
A = 3.98 cm^2	9.29	15.0	6.9	2.5	0.36
h_o/A = 0.110 cm^{-1}					
	---	---	---	---	---
HBM-7-47B	9.77	4.1°	8.0 x 10^3	4.2 x 10^3	0.52
	9.64	6.2	8.2	3.7	0.45
	9.52	8.3	8.0	3.5	0.44
	9.49	10.5	9.1	3.3	0.36
	9.41	12.7	8.7	3.0	0.34
	9.32	14.9	7.5	2.7	0.36
	---	---	---	---	---

Table III (Continued)

Test No.	Freq (Hz)	θ_s	G' dynes/cm^2	G'' dynes/cm^2	tan δ
HBM-7-47C	9.73	4.1°	7.2 x 10^3	4.1 x 10^3	0.57
	9.58	6.2	7.0	4.2	0.60
	9.49	8.4	7.4	3.7	0.50
	9.43	10.5	7.9	3.1	0.39
	9.39	12.7	8.2	3.0	0.36
	9.34	14.9	7.9	2.8	0.35
HBM-7-48A	10.18	5.6°	13.1 x 10^3	1.8 x 10^3	see text
29 Jan. 68	9.92	8.6	11.5	0.6	
Temp. - 37°C	9.69	11.7	9.7	0.4	
White matter	9.58	14.8	8.9	0.2	
h_o = 0.307 cm	9.44	18.0	7.3	0.1	
A = 3.98 cm^2	9.38	21.2	6.6	0.2	
h_o/A = 0.077 cm^{-1}					
HBM-7-48B	9.88	5.7°	8.9 x 10^3	0.6 x 10^3	see text
	9.73	8.8	8.9	0.4	
	9.60	11.8	8.5	0.4	
	9.52	14.9	8.0	0.2	
	9.47	18.0	7.8	0.3	
	9.38	21.2	6.6	0.3	
HBM-7-48C	9.81	5.8	7.9 x 10^3	0.6 x 10^3	see text
	9.66	8.8	7.9	0.4	
	9.55	11.9	7.8	0.4	
	9.50	14.9	7.8	0.2	
	9.44	18.0	7.3	0.3	
	9.40	21.1	6.9	0.4	

Table III (Continued)

Test No.	Freq (Hz)	θs	G' dynes/cm^2	G'' dynes/cm^2	tan δ
HBM-7-47C	9.73	4.1°	7.2 x 10^3	4.1 x 10^3	0.57
	9.58	6.2	7.0	4.2	0.60
	9.49	8.4	7.4	3.7	0.50
	9.43	10.5	7.9	3.1	0.39
	9.39	12.7	8.2	3.0	0.36
	9.34	14.9	7.9	2.8	0.35
HBM-7-48A	10.18	5.6°	13.1 x 10^3	1.8 x 10^3	see text
29 Jan. 68	9.92	8.6	11.5	0.6	
Temp. - 37°C	9.69	11.7	9.7	0.4	
White matter	9.58	14.8	8.9	0.2	
h_o = 0.307 cm	9.44	18.0	7.3	0.1	
A = 3.98 cm^2	9.38	21.2	6.6	0.2	
h_o/A = 0.077 cm^{-1}					
HBM-7-48B	9.88	5.7°	8.9 x 10^3	0.6 x 10^3	see text
	9.73	8.8	8.9	0.4	
	9.60	11.8	8.5	0.4	
	9.52	14.9	8.0	0.2	
	9.47	18.0	7.8	0.3	
	9.38	21.2	6.6	0.3	
HBM-7-48C	9.81	5.8	7.9 x 10^3	0.6 x 10^3	see text
	9.66	8.8	7.9	0.4	
	9.55	11.9	7.8	0.4	
	9.50	14.9	7.8	0.2	
	9.44	18.0	7.3	0.3	
	9.40	21.1	6.9	0.4	

Table III (Continued)

Test No.	Freq (Hz)	θ_s	G' dynes/cm^2	G'' dynes/cm^2	tan δ
Note that tests 47A-C and 48A-C were conducted on adjacent tissues that were oriented 90° from each other *in vivo*.					
HBM-7-62A	10.18	4.0°	19.0 x 10^3	4.2 x 10^3	0.22
30 Jan. 68	9.93	6.1	16.2	6.2	0.38
Temp. - 37°C	9.75	8.3	14.4	5.5	0.38
White matter	9.62	10.5	12.9	4.6	0.36
h_o = 0.432 cm	9.53	12.7	12.0	4.2	0.35
A = 3.00 cm^2	9.45	15.0	10.7	4.1	0.38
h_o/A = 0.144 cm^{-1}	9.38	17.2	9.6	4.0	0.42
HBM-7-62B	9.86	4.1°	10.3 x 10^3	3.0 x 10^3	0.29
	9.71	6.2	10.5	5.4	0.51
	9.60	8.4	10.4	5.6	0.54
	9.54	10.6	10.9	4.9	0.45
	9.49	12.8	11.0	4.6	0.42
	9.44	15.0	10.4	4.5	0.43
	9.40	17.2	10.2	4.6	0.45
HBM-7-62C	9.80	4.1°	8.8 x 10^3	6.0 x 10^3	0.68
	9.65	6.3	8.9	5.3	0.60
	9.57	8.4	9.6	5.6	0.58
	9.50	10.6	10.0	4.6	0.46
	9.48	12.8	10.7	4.6	0.43
	9.44	15.0	10.4	4.5	0.43
	9.42	17.2	10.7	4.7	0.44

Table III (Concluded)

Test No.	Freq (Hz)	θs	G' dynes/cm²	G'' dynes/cm²	tan δ
HBM-7-62D	9.84	4.1°	9.7×10^3	5.2×10^3	0.54
	9.57	8.4	9.6	5.3	0.55
	9.45	17.1	11.2	4.7	0.42

Sample remained in static condition for 15 minutes at 37°C between tests D and E					

HBM-7-62E	9.46	17.1°	11.5×10^3	5.4×10^3	0.47

Sample remained in static condition for 15 minutes at 37°C between tests E and F					

HBM-7-62F	9.58	16.9°	14.6×10^3	7.0×10^3	0.48

HBM-7-62G	9.98	4.0°	13.4×10^3	7.7×10^3	0.57
	9.81	6.2	13.1	7.1	0.54
	9.67	8.4	12.2	7.0	0.57
	9.52	10.6	10.5	5.7	0.54
	9.57	12.7	13.0	5.7	0.44
	9.56	14.8	13.6	5.9	0.43
	9.52	17.0	13.0	5.9	0.45

Sample remained in static condition for one hour at 37°C between tests G and H					

HBM-7-62H	9.61	16.8°	15.4×10^3	7.8×10^3	0.51

Table IV

Dynamic Shear Modulus
Human Brain No. 9

Sample History - Time of death: 1:25 P.M., 2 May 68
Age: 71
Sex: M
Race: C
Cause of death: Lung Cancer
Time specimen removed at autopsy: 10:30 A.M., 3 May 68
Location of test specimens: Frontal lobe
Transfer conditions: Packed in polyethylene bags and carried in ice and water

Test No.	Freq (Hz)	θs	G' dynes/cm²	G" dynes/cm²	G* dynes/cm²	tan δ
HBM-9-25A	9.98	4.5°	12.1 x 10^3	6.2 x 10^3	13.6 x 10^3	0.51
3 May 68	9.72	7.0	10.0	6.2	11.8	0.62
Temp. - 37°C	9.50	9.5	8.2	4.9	9.6	0.60
White matter	9.42	12.0	8.0	4.2	9.0	0.52
h_o = 0.386 cm	9.32	14.5	7.1	3.8	8.0	0.54
A = 3.43 cm^2	9.26	17.1	6.7	4.2	7.9	0.63
h_o/A = 0.112 cm^{-1}	9.23	19.6	6.4	3.9	7.5	0.62
HBM-9-25B	9.85	4.6°	9.3 x 10^3	4.5 x 10^3	10.3 x 10^3	0.48
	9.78	6.9	11.3	5.1	12.4	0.45
	9.58	9.4	9.7	4.8	10.8	0.49
	9.43	12.0	8.5	4.1	9.4	0.48
	9.36	14.5	8.1	3.6	8.9	0.44
	9.28	17.0	7.1	3.7	8.0	0.52

Table IV (Continued)

Test No.	Freq (Hz)	θs	G' dynes/cm^2	G" dynes/cm^2	G* dynes/cm^2	tan δ
HBM-9-25C	9.72	4.6°	6.6 x 10^3	5.0 x 10^3	8.3 x 10^3	0.76
	9.52	7.1	6.1	5.2	8.0	0.85
	9.49	9.5	7.8	4.7	9.1	0.60
	9.37	12.0	7.3	4.2	8.4	0.58
	9.33	14.5	7.5	4.0	8.5	0.53
	9.29	17.0	7.3	4.0	8.3	0.55

Sample remained in static condition for 15 minutes at 37°C between tests A-C and D						

HBM-9-25D	12.00	3.8°	58.6 x 10^3	9.8 x 10^3	59.4 x 10^3	0.17
	9.90	6.8	13.6	6.0	14.9	0.44
	9.71	9.3	12.4	5.0	13.4	0.40
	9.58	11.8	11.4	4.5	12.2	0.40
	9.45	14.3	9.9	3.8	10.6	0.38
	9.34	16.9	8.3	3.4	9.0	0.41

HBM-9-25E	9.75	4.6°	7.2 x 10^3	4.2 x 10^3	8.3 x 10^3	0.58
	9.59	7.1	7.5	5.0	9.0	0.67
	9.50	9.5	8.2	3.9	9.1	0.48
	9.41	12.0	8.1	3.7	8.9	0.46
	9.35	14.5	8.1	3.9	9.0	0.48
	9.30	16.9	8.1	3.9	9.0	0.48

Table IV (Continued)

Test No.	Freq (Hz)	θs	G' dynes/cm^2	G" dynes/cm^2	G* dynes/cm^2	tan δ
HBM-9-25F	9.76	4.6°	7.4 x 10^3	3.8 x 10^3	8.3 x 10^3	0.51
	9.59	7.1	7.5	4.4	8.7	0.59
	9.47	9.5	7.6	3.9	8.5	0.51
	9.40	12.0	7.9	3.9	8.8	0.49
	9.34	14.5	7.9	3.8	8.8	0.48
	9.32	17.0	7.9	3.9	8.8	0.49

Sample sheared at θs ~17.0° for 15 minutes at 37°C						

HBM-9-25G	9.58	4.7°	3.9 x 10^3	5.0 x 10^3	6.3 x 10^3	1.28
	9.46	7.2	4.8	4.9	6.8	1.02
	9.36	9.6	5.4	4.4	7.0	0.81
	9.30	12.1	5.9	4.2	7.2	0.71
	9.30	14.6	7.1	4.3	8.3	0.60
	9.30	17.0	7.5	4.6	8.8	0.61

Sample remained in static condition for 20 minutes at 37°C between tests G and H						

HBM-9-25H	9.30	17.0°	7.5 x 10^3	4.7 x 10^3	8.8 x 10^3	0.63

Sample remained in static condition for five minutes at 37°C between tests H and I						

HBM-9-25I	9.29	17.0°	7.3 x 10^3	4.5 x 10^3	8.6 x 10^3	0.62

Table IV (Continued)

Test No.	Freq (Hz)	θ_s	G' dynes/cm^2	G" dynes/cm^2	G* dynes/cm^2	tan δ
HBM-9-25J	9.68	4.7°	5.8 x 10^3	4.6 x 10^3	7.4 x 10^3	0.79
	9.52	7.1	6.1	4.4	7.5	0.72
	9.42	9.6	6.6	4.5	8.0	0.68
	9.37	12.0	7.3	3.6	8.1	0.49
	9.34	14.5	7.9	3.4	8.6	0.43
	9.34	16.9	8.3	3.8	9.1	0.46
HBM-9-25K	9.81	4.6°	8.5 x 10^3	5.1 x 10^3	9.9 x 10^3	0.60
	9.61	7.0	7.9	5.0	9.3	0.63
	9.47	9.5	7.4	4.7	8.8	0.64
	9.40	12.0	7.9	4.1	8.9	0.52
	9.38	14.4	8.5	4.0	9.4	0.47
	9.38	16.8	9.1	4.4	10.1	0.48
HBM-9-25L	9.70	4.7°	6.2 x 10^3	5.0 x 10^3	8.0 x 10^3	0.81
	9.54	7.1	6.5	4.9	8.1	0.75
	9.43	9.6	6.8	4.7	8.3	0.69
	9.40	12.0	7.9	4.2	8.9	0.53
	9.38	14.4	8.5	3.9	9.4	0.46
	9.38	16.8	9.1	4.3	10.1	0.47
HBM-9-96A	9.91	3.1°	13.6 x 10^3	8.4 x 10^3	16.0 x 10^3	0.62
6 May 68	9.69	4.7	12.1	7.5	14.2	0.62
Temp. - 37°C	9.50	6.4	10.5	6.3	12.2	0.60
White matter	9.41	8.1	10.0	5.8	11.6	0.58
h_o = 0.57 cm	9.33	9.8	9.3	4.9	10.5	0.53
A = 4.14 cm^2	9.28	11.5	9.0	4.9	10.2	0.54
h_o/A - 0.138 cm^{-1}						

Table IV (Continued)

Test No.	Freq (Hz)	θs	G' dynes/cm^2	G" dynes/cm^2	G* dynes/cm^2	tan δ
HBM-9-96B	9.91	3.1°	13.6 x 10^3	2.6 x 10^3	13.8 x 10^3	0.19
	9.72	4.7	12.9	3.4	13.3	0.26
	9.56	6.4	11.8	3.9	12.4	0.33
	9.48	8.0	11.7	3.6	12.2	0.31
	9.40	9.7	11.1	3.5	11.6	0.32
	9.32	11.4	9.8	3.5	10.4	0.36

HBM-9-96C	9.89	3.1°	13.0 x 10^3	1.6 x 10^3	13.1 x 10^3	0.12
	9.69	4.7	12.1	2.9	12.4	0.24
	9.55	6.4	11.6	3.8	12.2	0.33
	9.45	8.1	11.1	3.6	11.7	0.32
	9.39	9.7	10.9	3.3	11.4	0.30
	9.32	11.4	10.1	3.5	10.7	0.35

Sample remained in static condition for 15 minutes at 37°C between tests A-C and D						

HBM-9-96D	10.02	3.0°	16.4 x 10^3	8.2 x 10^3	18.3 x 10^3	0.50
	9.83	4.6	15.8	7.6	17.5	0.48
	9.64	6.3	14.0	7.2	15.7	0.51
	9.52	8.0	12.8	6.2	14.2	0.48
	9.40	9.7	11.1	5.3	12.3	0.48
	9.33	11.4	10.1	5.4	11.4	0.53

Table IV (Continued)

Test No.	Freq (Hz)	θs	G' dynes/cm²	G" dynes/cm²	G* dynes/cm²	tan δ
HBM-9-96E	9.72	3.1°	8.4 x 10^3	7.2 x 10^3	11.1 x 10^3	0.86
	9.52	4.8	7.8	7.1	10.5	0.91
	9.41	6.5	8.2	6.5	10.5	0.79
	9.35	8.2	8.6	5.6	10.3	0.65
	9.33	9.8	9.3	5.8	11.0	0.62
	9.30	11.5	9.6	6.9	11.8	0.72
HBM-9-96F	9.89	3.1°	13.0 x 10^3	3.4 x 10^3	13.4 x 10^3	0.26
	9.70	4.7	12.4	3.8	13.0	0.31
	9.51	6.4	10.8	4.0	11.5	0.37
	9.45	8.1	11.1	4.0	11.8	0.36
	9.39	9.7	10.9	4.0	11.6	0.37
	9.35	11.4	10.6	4.2	11.4	0.40
Sample sheared at θs ~11.4° for 15 minutes at 37°C						
HBM-9-96G	9.27	11.5°	8.8 x 10^3	4.1 x 10^3	9.7 x 10^3	0.46
Sample remained in static condition for 20 minutes at 37°C between tests G and H						
HBM-9-96H	9.39	11.4°	11.6 x 10^3	5.5 x 10^3	12.8 x 10^3	0.47
Sample sheared at θs ~11.4° for five minutes at 37°C						

Table IV (Concluded)

Test No.	Freq (Hz)	θs	G' dynes/cm²	G" dynes/cm²	G* dynes/cm²	tan δ
HBM-9-96I	9.31	11.5°	9.8 x 10^3	4.6 x 10^3	10.8 x 10^3	0.47
			---	---	---	
Sample remained in static condition for 20 minutes at 37°C between tests I and J						
			---	---	---	
HBM-9-96J	10.12	3.0°	19.1 x 10^3	6.2 x 10^3	20.1 x 10^3	0.32
	9.83	4.6	15.8	5.9	16.7	0.37
	9.65	6.3	14.2	6.4	15.6	0.45
	9.55	8.0	13.6	6.0	14.9	0.44
	9.49	9.6	13.5	6.4	14.9	0.47
	9.46	11.3	13.4	6.6	14.9	0.49
			---	---	---	
HBM-9-96K	9.88	3.1°	12.8 x 10^3	4.0 x 10^3	13.4 x 10^3	0.31
	9.69	4.7	12.1	4.8	13.0	0.40
	9.55	6.4	11.6	5.6	12.9	0.48
	9.46	8.1	11.2	5.2	12.3	0.46
	9.43	9.7	11.9	5.5	13.1	0.46
	9.43	11.3	12.7	6.6	14.3	0.52
			---	---	---	
HBM-9-96L	9.88	3.1°	12.8 x 10^3	3.0 x 10^3	13.1 x 10^3	0.23
	9.65	4.7	11.2	4.6	12.1	0.41
	9.51	6.4	10.8	5.0	11.9	0.46
	9.46	8.1	11.2	5.0	12.3	0.44
	9.43	9.7	11.9	5.5	13.1	0.46
	9.44	11.3	12.9	6.3	14.4	0.49

Table V

Secant Bulk Modulus

Human Brain No. 5

Sample History - Time of death: 12:15 P.M., 23 Jan. 68

Age: 80

Sex: M

Race: C

Cause of death: Overdose of Plascidel; developed pneumonia

Time specimen removed at autopsy: 10:50 A.M., 24 Jan. 68

Location of test specimen: Frontal lobe

Transfer conditions: Packed in polyethylene bags and shipped in ice and water

Test No.	Pressure	Total Compression	Brain Compression	Secant Bulk Modulus
5-HBM-27	5 x 10^3 psi	2.08%	1.18%	2.96 x 10^5 psi
Mixed grey and white matter	10	3.60	2.02	3.46
	15	4.95	2.83	3.70
24 Jan. 68	20	6.24	3.66	3.82
Temp. - 37°C				
69.9% brain				
30.1% carrier fluid (silicone)				
Test machine: Baldwin Tate-Emory				

Above values are the average of three (3) trials

Table VI

Secant Bulk Modulus
Human Brain No. 6

Sample History - Time of death: 2:30 P.M., 28 Jan. 68
Age: 50
Sex: M
Race: C
Cause of death: Respiratory death
Time specimen removed at autopsy: 11:05 A.M., 29 Jan. 68
Location of specimen: Parietal lobe
Transfer conditions: Packed in polyethylene bags and shipped in ice and water

Test No.	Pressure	Total Compression	Brain Compression	Secant Bulk Modulus
6-HBM-20	5 x 10^3 psi	2.01%	1.11%	2.94 x 10^5 psi
Mixed grey and	10	3.63	2.05	3.18
white matter	15	5.00	2.88	3.40
29 Jan. 68	20	6.20	3.62	3.60
Temp. - 37°C				
65.2% brain				
34.8% carrier fluid (silicone)				
Test machine: Baldwin Tate-Emory				

Above values are the average of three (3) trials

Table VII

Secant Bulk Modulus

Human Brain No. 7

Sample History - Time of death: 8:45 P.M., 27 Jan. 68
Age: 49
Sex: M
Race: C
Cause of death: Emphysema and Pneumothorax
Time specimen removed at autopsy: 11:45 A.M., 29 Jan. 68
Location of specimen: Frontal lobe
Transfer conditions: Packed in polyethylene bags and shipped in ice and water

Test No.	Pressure	Total Compression	Brain Compression	Secant Bulk Modulus
7-HBM-46	5 x 10^3 psi	2.08%	1.18%	2.57 x 10^5 psi
Mixed grey and white matter	10	3.74	2.16	2.81
29 Jan. 68	15	5.13	3.01	3.02
Temp. - 37°C	20	6.33	3.75	3.23
60.6% brain				
39.4% carrier fluid (silicone)				
Test machine: Baldwin Tate-Emory				

Above values are the average of three (3) trials

Table VIII

Secant Bulk Modulus
Human Brain No. 8

Sample History - Time of death: 4:07 A.M., 17 April 68
Age: 41
Sex: M
Race: C
Cause of death: Lung cancer
Time specimen removed at autopsy: 10:50 A.M., 17 April 68
Location of test specimen: Parietal lobe
Transfer conditions: Packed in polyethylene bags and carried in ice and water

Test No.	Pressure	Total Compression	Brain Compression	Secant Bulk Modulus
8-HBM-33	100 psi	1.08%	1.04%	0.06 x 10^5 psi
Mixed grey and	200	1.23	1.16	0.11
white matter	300	1.32	1.21	0.16
18 April 68	400	1.40	1.25	0.20
Temp. - 37°C	500	1.46	1.29	0.24
62.1% brain	600	1.52	1.31	0.29
37.9% carrier fluid	700	1.58	1.34	0.33
(silicone)	800	1.64	1.37	0.37
Test machine:	900	1.70	1.39	0.41
Instron	1000	1.76	1.43	0.44

Above values are the average of two (2) trials

Table VIII (Continued)

Test No.	Pressure	Total Compression	Brain Compression	Secant Bulk Modulus
8-HBM-54	1 x 10^3 psi	0.59%	0.43%	1.73 x 10^5 psi
Mixed grey and	2.5	1.22	0.79	2.32
white matter	5	2.11	1.30	2.81
19 April 68	10	3.65	2.24	3.27
Temp. - 37°C	15	5.03	3.13	3.50
73.0% brain	20	6.24	3.93	3.72
27.0% carrier fluid	25	7.33	4.66	3.92
(silicone)	30	8.30	5.31	4.13
Test machine:				
Baldwin Tate-				
Emory				

Above values are the average of five (5) trials

8-HBM-57	100 psi	0.70%	0.66%	0.10 x 10^5 psi
(degassed)	200	0.83	0.77	0.17
Mixed grey and	300	0.92	0.83	0.24
white matter	400	0.98	0.86	0.32
19 April 68	500	1.04	0.89	0.38
Temp. - 37°C	600	1.11	0.93	0.45
66.8% brain	700	0.96	0.75	0.49
33.2% carrier fluid	800	0.99	0.76	0.55
(silicone)	900	1.01	0.75	0.60
Test machine:	1000	1.05	0.76	0.64
Instron				

Above values are the average of three (3) trials

Table VIII (Concluded)

Test No.	Pressure	Total Compression	Brain Compression	Secant Bulk Modulus
8-HBM-149	250 psi	0.21%	0.12%	1.32×10^5 psi
Mixed grey and	500	0.36	0.19	1.66
white matter	750	0.50	0.26	1.91
23 April 68	1000	0.61	0.29	2.21
Temp. - 37°C				
63.7% brain				
36.3% carrier fluid				
(silicone)				
Test machine:				
Baldwin Tate-				
Emory				

Above values are the average of five (5) trials

Table IX

Secant Bulk Modulus

Human Brain No. 9

Sample History - Time of death: 1:25 P.M., 2 May 68

Age: 71

Sex: M

Race: C

Cause of death: Lung cancer

Time specimen removed at autopsy: 10:30 A.M., 3 May 68

Location of test specimen: Frontal lobe

Transfer conditions: Packed in polyethylene bags and carried in ice and water

Test No.	Pressure	Total Compression	Brain Compression	Secant Bulk Modulus
9-HBM-93	1 x 10^3 psi	0.53%	0.28%	2.17 x 10^5 psi
Mixed grey and	2.5	1.17	0.54	2.79
white matter	5	2.12	0.94	3.24
6 May 68	10	3.72	1.66	3.66
Temp. - 37°C	15	5.11	2.34	3.88
60.6% brain	20	6.37	2.99	4.05
39.4% carrier fluid (silicone)				
Test machine: Baldwin Tate-Emory				

Above values are the average of four (4) trials

Table IX (Concluded)

Test No.	Pressure	Total Compression	Brain Compression	Secant Bulk Modulus
9-HBM-121	100 psi	0.52%	0.49%	0.12 x 10^5 psi
(degassed)	200	0.61	0.56	0.22
Mixed grey and	300	0.68	0.61	0.30
white matter	400	0.73	0.64	0.39
7 May 68	500	0.78	0.67	0.46
Temp. - 37°C	600	0.83	0.71	0.53
62.1% brain	700	0.86	0.73	0.60
37.9% carrier fluid	800	0.92	0.77	0.65
(water)	900	0.95	0.78	0.72
Test machine:	1000	1.00	0.82	0.76
Instron				

Above values are the average of three (3) trials

9-HBM-141	100 psi	0.075%	0.05%	1.25 x 10^5 psi
Mixed grey and	200	0.13	0.08	1.66
white matter	300	0.18	0.11	1.71
8 May 68	400	0.23	0.14	1.78
Temp. - 37°C	500	0.27	0.17	1.86
62.1% brain	600	0.33	0.21	1.79
37.9% carrier fluid	700	0.36	0.23	1.94
(water)	800	0.40	0.24	2.03
Test machine:	900	0.44	0.28	2.03
Instron	1000	0.48	0.29	2.13

Above values are the average of seven (7) trials

APPENDIX F

IMPULSE LOADING OF A CLOSED SPHERICAL SHELL

INTRODUCTION

This appendix reports on the development of a mathematical model of head injury. In the six month report on this project, the analysis of the axisymmetric response of a closed spherical shell to a local radial impulse was stated.

The current report, entitled The Axisymmetric Response of a Fluid-Filled Spherical Shell to a local Radial Impulse, describes an impact model with the brain represented by a compressible, irrotational, inviscid fluid.

LIST OF SYMBOLS

A_o, A_{nm}, A_{nc}	Arbitrary constants (Constants of Integration)
E	Young's Modulus
F_e	External force distribution on the shell
M_z	Moment along polar axis
$P_n(\cos \xi)$	Legendre Polynomials of the first kind
$P_n(\cos \xi)$	Associated Legendre Polynomials of the first kind and first order
S	Midsurface of the shell
T	Kinetic Energy
V	Potential Energy
V_o,V_s	Volumes of fluid and shell respectively
U	Strain energy density
a	Radius of spherical shell
a_o,a_n	Coefficients of Legendre polynomial expansion of ζ
b_n	Coefficients of associated Legendre polynomial expansion of Ψ
c	Compressional wave speed in the fluid
c_s	Wave parameter, $[E/\rho_s(1-\nu^2]^{1/2}$
f	Shell-fluid parameter
h	Shell thickness
j_n	Spherical Bessel function
k	Wave number

P_a	Fluid pressure on the surface of the shell
r,θ,ϕ	Spherical coordinates of the deformed midsurface
s	Speed ratio, c/c_s
t	Time
$\bar{u}$	Meridional displacement with respect to center of mass of the shell
w	Radial displacement, a-r
$\bar{w}$	Radial displacement with respect to center of mass of the shell
z	Distance from the midsurface
α^2	Thickness parameter, $h^2/12a^2$
$\alpha_o,\alpha_{nc},\alpha_{nm}$	Phase angles (Constants of Integration)
β	Angle between midsurface normal and radial ray
γ_o	Midsurface shear strain
δ_{nc},δ_{nm}	Amplitude ratios
$\varepsilon_{o\xi},\varepsilon_{o\eta}$	Midsurface normal strains
$\varepsilon_\xi,\varepsilon_\eta$	Z-surface normal strains
ζ	Nondimensional radial displacement, 1/a(a-r)
ψ	Nondimensional angular meridional displacement $\phi-\xi$
a,η,ξ	Spherical coordinates of the undeformed midsurface
$k_{o\xi},k_{o\eta}$	Midsurface curvature
γ_n	n(n+1)
ν	Poisson's ratio
ρ_o,ρ_s	Mass density of fluid and shell respectively
σ_ξ,σ_η	Normal stresses
τ	Dimensionless time, ct/a

$\omega_o, \omega_{nc}, \omega_{nm}$ Angular frequencies of breathing, composite, and membrane modes respectively.

Ω Nondimensional frequency, ω_a/c

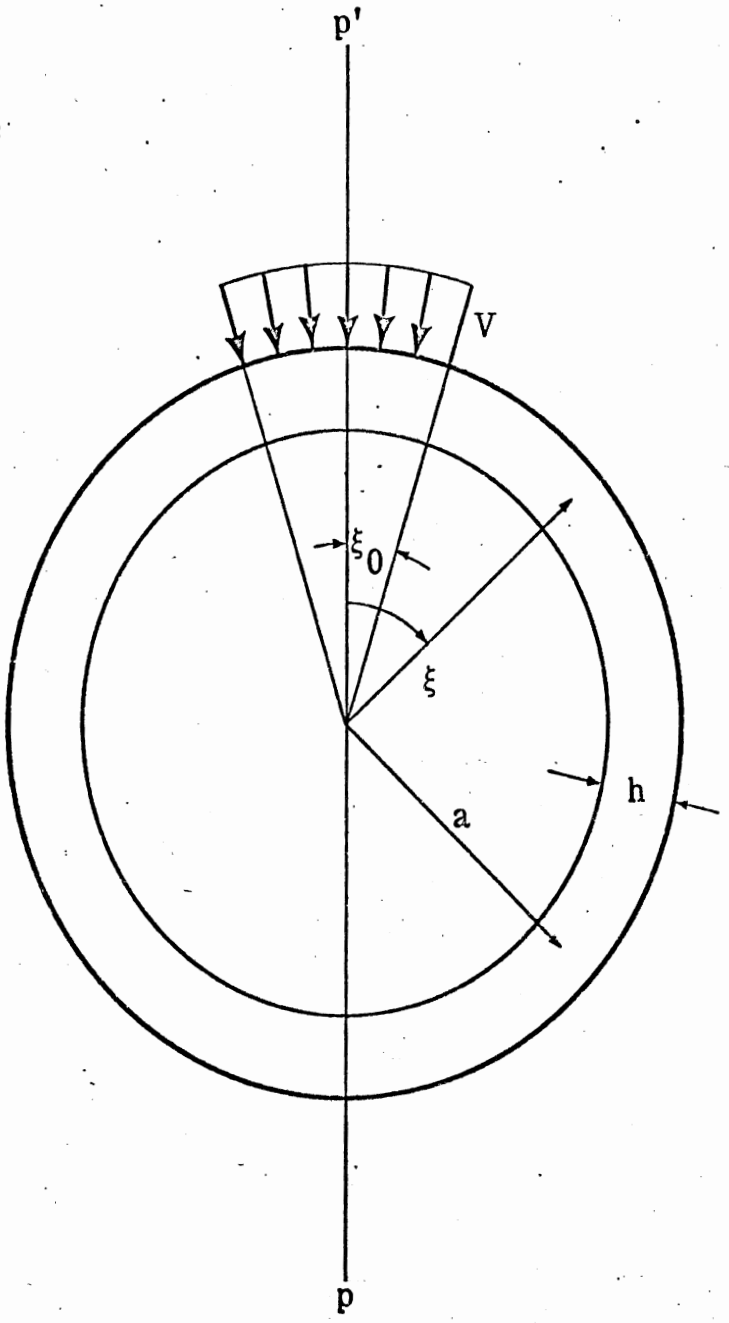

FIGURE 1. CLOSED SPHERICAL SHELL SUBJECTED TO LOCAL IMPULSE

THE AXISYMMETRIC RESPONSE OF A FLUID-FILLED SPHERICAL SHELL TO A LOCAL RADIAL IMPULSE

Impact problems involving spherical shells have been the subject of much research during the past one hundred years. Lamb,[1] Rayleigh,[2] Anzelius,[3] and Güttinger,[4] have studied the response of an acoustic fluid enclosed in a cavity with a rigid spherical wall. Others such as Love,[5] Baker,[6] Silberger,[7] Naghdi and Kalnins,[8] Kalnins,[9] McIvor and Sonstegard[10] have studied the vibration response of spherical shells. Coupled problems have been considered by Junger,[11] Goodman and Stern,[12] and Hickling,[13] all of whom worked with shells submerged in a fluid. In addition, Morse and Feshbach[14] as well as Rand and DiMaggio[15] have carried out the only vibration analyses of fluid-filled shells.

THE IN VACUO CASE

The equations of motion for free vibration of a closed spherical shell may be derived using an energy formulation as was done in Reference 10 where Lagrangian representation of spherical shell deformation was used. If the undeformed and deformed configurations of the midsurface are represented by spherical coordinates (a,η,ξ) and (r,θ,ϕ) respectively, the deformed coordinates are functions of initial configuration and time, i.e., $r = r(\xi,\eta,t)$, $\theta = \theta(\xi,\eta,t)$, and $\phi = \phi(\xi,\eta,t)$. The following dimensionless quantities may be defined.

$$\psi = \phi - \xi \quad \text{(angular meridional displacement)}$$

$$\zeta = (a-r)/a \quad \text{(radial displacement)}$$

$$\tau = \frac{1}{a}[E/\rho_s(1-\nu^2)]^{1/2} \quad \text{if} \quad c_s = [E/\rho_s(1-\nu^2)]^{1/2} \quad \text{then} \quad \tau = c_s t/a$$

$$\alpha^2 = h^2/12a^2 \quad \text{(a thickness parameter)}$$

For torsionless axisymmetric motion, $\psi = \psi(\xi,\tau)$ and $\zeta = \zeta(\xi,\tau)$ i.e., $\partial/\partial\eta = 0$. If $\partial/\partial\xi$ is represented by a dot, the system of equations reduces to two linear partial differential equations in the case where both the displacement and its derivative are assumed small.

$$\ddot{\psi} + \dot{\psi}\cot\xi - \psi(\nu + \cot^2\xi) - \dot{\zeta}(1+\nu) + \alpha^2[\dddot{\psi} + \ddot{\psi}\cot\xi - \dot{\psi}(\nu + \cot^2\xi) + \dddot{\zeta} + \ddot{\zeta}\cot\xi - \dot{\zeta}(\nu + \cot^2\xi)] = \partial^2\psi/\partial\tau^2 \tag{1}$$

$$(1+\nu)(\dot{\psi} + \psi\cot\xi - 2\zeta) - \alpha^2[\dddot{\psi} + 2\ddot{\psi}\cot\xi - \dot{\psi}(1+\nu+\cot^2\xi) + \psi\cot\xi(2-\nu+\cot^2\xi) + \dddot{\zeta} + 2\ddot{\zeta}\cot\xi - \ddot{\zeta}(1+\nu+\cot^2\xi) + \dot{\zeta}\cot\xi(2-\nu+\cot^2\xi)] = \partial^2\zeta/\partial\tau^2 \tag{2}$$

Assume the displacements ζ and ψ are represented by;

$$\zeta = \sum_{n=0}^{\infty} a_n(\tau)P_n(\cos\xi) \tag{3}$$

$$\psi = \sum_{n=1}^{\infty} b_n(\tau)\,P_n'(\cos\xi)\ , \tag{4}$$

where $P_n(\cos\ )$ are Legendre Polynomials of the first kind, and $P_n'(\cos\ )$ are associated Legendre Polynomials of the first kind and first order. It can be shown that[10] the square of the frequencies is:

$$\omega_o^2 = [2(1+\nu)] \tag{5a}$$

$$2\omega_n^2 = [1 + 3\nu - \alpha^2(1-\nu) + \lambda_n(1+\nu\alpha^2) + \alpha^2\lambda_n^2]$$
$$\pm \{[1 + 3\nu - \alpha^2(1-\nu) + \lambda_n(1+\nu\alpha^2) + \alpha^2\lambda_n^2]^2$$
$$- 4[-2(1-\nu^2)(1+\alpha^2) + \lambda_n(1-\nu^2) + \alpha^2\lambda_n(5-\nu^2) - 4\alpha^2\lambda_n^2$$
$$+ \alpha^2\lambda_n^3]\}^{1/2}\ , \tag{5b}$$

where positive and negative signs give frequencies ω_{nm} and ω_{nc} respectively and $\lambda_n = n(n+1)$. The amplitude ratios are:

$$\delta_{nm} = \frac{B_{nm}}{A_{nm}} = -\frac{P_1}{q_1-\omega_{nm}^2} = \frac{1+\nu-\alpha^2[1-\nu-n(n+1)]}{\omega_{nm}^2+(1+\alpha^2)[1-\nu-n(n+1)]} \tag{6a}$$

$$\delta_{nc} = \frac{B_{nc}}{A_{nc}} = -\frac{P_1}{q_1-\omega_{nc}^2} = \frac{1+\nu-\alpha^2[1-\nu-n(n+1)]}{\omega_{nc}^2+(1+\alpha^2)[1-\nu-n(n+1)]} \tag{6b}$$

The solutions for ζ and ψ are:

$$\zeta(\xi,\tau) = A_o\mathrm{Sin}(\omega_o\tau+\alpha_o) + \sum_{n=1}^{\infty}[A_{nm}\mathrm{Sin}(\omega_{nm}\tau+\alpha_{nm}) + A_{nc}\mathrm{Sin}(\omega_{nc}\tau+\alpha_{nc})]P_n(\cos\xi) \tag{7a}$$

$$\psi(\xi,\tau) = \sum_{n=1}^{\infty}[\delta_{nm}A_{nm}\mathrm{Sin}(\omega_{nm}\tau+\alpha_{nm}) + \delta_{nc}A_{nc}\mathrm{Sin}(\omega_{nc}\tau+\alpha_{nc})]P_n'(\cos\xi) \tag{7b}$$

For this problem the displacement initial conditions are:

$$\left.\begin{aligned}\zeta(\xi,0) &= 0 \qquad (8a)\\ \psi(\xi,0) &= 0 \qquad (8b)\end{aligned}\right\}$$

The two velocity initial conditions are not obvious. Their determination involves several steps.

First, the local velocity input may be expressed by a series expansion.

$$\text{If } w = a\text{-}r, \text{ let } \frac{\partial w}{\partial t} = \sum_{n=0}^{\infty} v_n P_n(\cos\xi) = \begin{cases} v & (0<\xi<\xi_o)\\ 0 & (\xi_o<\xi<\pi)\end{cases} \tag{9}$$

Both sides of equation (9) are then multiplied by $P_m(\cos \xi) \sin \xi$ and integrated

$$v_n = \frac{v \int_{\xi_o}^{o} P_n(\cos \xi) \sin \xi \, d\xi}{\int_{\pi}^{o} P_n^2 (\cos \xi) \sin \xi \, d\xi} \tag{10}$$

The norm of P_n; $N(P_n) = \int_{-1}^{+1} P_n^2(x)dx = \frac{2}{2n+1}$, $n = 0,1,2\ldots$

or

$$N[P_m(\cos \xi)] = \int_{\pi}^{o} -P_n^2 (\cos \xi) \sin \xi \, d\xi = \frac{2}{2n+1} . \tag{11}$$

From (3-10) and (3-11),

$$v_n = \frac{(2n+1)}{2} v \int_{o}^{\xi_o} P_n (\cos \xi) \sin \xi \, d\xi \tag{12}$$

However, using the transformation $x = \cos \xi$ in (3-12), it is easy to show that

$$\begin{aligned} v_o &= \frac{v}{2} (1 - \cos \xi_o) \\ v_n &= \frac{v}{2} [P_{n-1} (\cos \xi_o) - P_{n+1} (\cos \xi_o)] \end{aligned} \tag{13}$$

Hence, v_n is known for every n.

Second, the linear momentum along the polar axis PP', M_z, is defined to be the component of the radial momentum due to initial radial velocity v for $0 < \xi < + \xi_o$ (See Figure 2). Let v_z be the component of v along the polar axis PP', then the linear momentum along the polar axis is

$$M_z = \int_{p.s.v.} v_z \, \rho dV = \int_{p.s.v.} \frac{\partial w}{\partial t} \cos \xi \, \rho h dA,$$

where

$dA = 2\pi a^2 \sin \xi \, d\xi$

p.s.v. = partial shell volume.

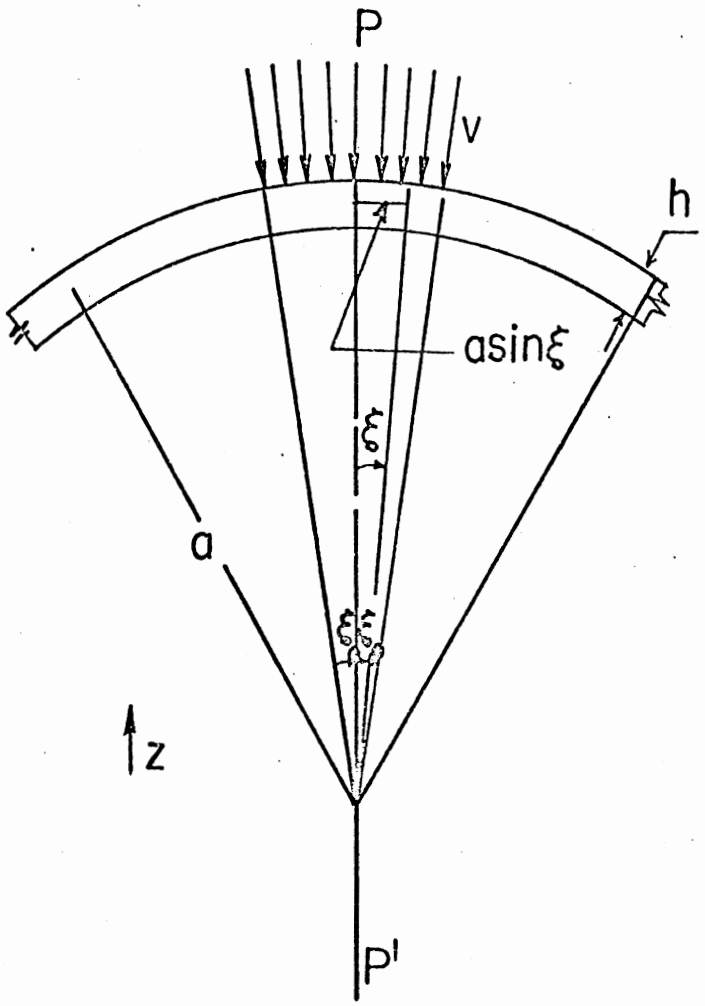

Figure 2. Momentum considerations for the shell.

Or in view of (9)

$$M_z = 2\pi a^2 \rho h \int_0^{\xi_0} \sum_{n=0}^{\infty} v_n P_n (\cos \xi) \sin \xi \cos \xi \, d\xi \quad . \qquad (14)$$

The mass of the shell, consistent with thin shell theory, is

$$m_{total} = \frac{4}{3} \rho\pi[3ha^2 + \frac{h^3}{4}] \simeq 4\pi\rho a^2 h \quad .$$

Hence, the velocity imparted to the center of mass of the shell (in the negative polar axis direction) is

$$v_z = \frac{1}{2} \int_0^{\xi_0} \sum_{n=0}^{\infty} v_n P_n (\cos \xi) \sin \xi \cos \xi \, d\xi \quad . \qquad (15)$$

Using the transformation $x = \cos \xi$, it can be shown after a little manipulation that

$$v_z = \frac{1}{8} v_o(1 - \cos 2\xi_o) + \sum_{n=1}^{\infty} \frac{v_n}{(2n+1)v} [v_n \cos \xi_o + \frac{v_{n-1}}{(2n-1)} - \frac{v_{n+1}}{(2n+3)}] \quad , \qquad (16)$$

where use was made of (13).

Third, the relative distribution of the deformation velocity is found by dividing closed spherical shell into two portions:

(A) $0 < \xi < +\xi_o$ (Region where the velocity input is applied)

(B) $+\xi_o < \xi < \pi$ (Region outside A)

For region (A) the deformation velocity in radial direction is called $\partial w/\partial t$ and in the meridional direction $\partial u/\partial t$, then,

$$\left.\begin{aligned} \frac{\partial \bar{w}}{\partial t} &= \frac{\partial w}{\partial t} - v_z \cos\xi = \frac{\partial w}{\partial t} - v_z P_1(\cos\xi) \\ \frac{\partial \bar{u}}{\partial t} &= 0 - v_z \sin\xi = -v_z P_1'(\cos\xi) \end{aligned}\right\} \tag{17}$$

Equation (17) may be written more explicitly using (9).

$$\frac{\partial \bar{w}}{\partial t} = v_o + (v_1 - v_z)\ P_1(\cos\xi) + \sum_{n=2}^{\infty} v_n P_n(\cos\xi) \tag{18a}$$

$$\frac{\partial \bar{u}}{\partial t} = -v_z P_1'(\cos\xi) \tag{18b}$$

where v_n is determined from (13) and v_z from (16). Initially, for region (B) the shell moves with the velocity, v_z, which is imparted to the center of mass of the shell in the negative polar-axis direction. Hence, the two velocity initial conditions in terms of the variables of the problem are

$$\frac{\partial \zeta(\xi,0)}{\partial \tau} = \frac{1}{c_s}\frac{\partial w}{\partial t} \quad \text{for } 0 < \xi < +\xi_o$$

$$\frac{\partial \psi(\xi,0)}{\partial \tau} = \frac{1}{c_s}\frac{\partial u}{\partial t} \quad \text{for } 0 < \xi < +\xi_o$$

This completes the determination of the initial conditions.

Application of the initial conditions (8a) and (8b) to solutions (7a,b) leads to $\alpha_o = \alpha_{nm} = \alpha_{nc} = 0$. Hence, from (7a,b),

$$\frac{\partial \zeta(\xi,0)}{\partial \tau} = A_o\omega_o + \sum_{n=1}^{\infty} [A_{nm}\omega_{nm} + A_{nc}\omega_{nc}] P_n(\cos \xi) = \frac{1}{c_s}\frac{\partial \bar{w}}{\partial t} \qquad (19a)$$

$$\frac{\partial \psi(\xi,0)}{\partial \tau} = \sum_{n=1}^{\infty} [\delta_{nm}A_{nm}\omega_{nm} + \delta_{nc}A_{nc}\omega_{nc}]P_n'(\cos \xi) = \frac{1}{c_s}\frac{\partial \bar{u}}{\partial t} \qquad (19b)$$

From equations (18a,b) and (19a,b) it can be concluded that

$$A_o = \frac{v_o}{c_s\omega_o} \quad \text{for } n = 0$$

$$\left.\begin{aligned} A_{1m}\omega_{1m} + A_{1c}\omega_{1c} &= \frac{1}{c_s}(v_1 - v_z) \qquad (20a)\\ \delta_{1m} A_{1m} \omega_{1m} + \delta_{1c} A_{1c} \omega_{1c} &= -\frac{1}{c_s} v_z \qquad (20b)\end{aligned}\right\} \text{for } n = 1$$

$$\left.\begin{aligned} A_{nm} \omega_{nm} + A_{nc} \omega_{nc} &= \frac{1}{c_s} v_n \qquad (21a)\\ \delta_{nm} A_{nm} \omega_{nm} + \delta_{nc} A_{nc} \omega_{nc} &= 0 \qquad (21b)\end{aligned}\right\} \text{for } n \geq 2$$

From (20a) and (20b)

$$A_{1c} = \frac{\delta_{1m}v_1 + v_z(1-\delta_{1m})}{c_s\omega_{1m}(\delta_{1m}-\delta_{1c})} \quad \text{and} \quad A_{1m} = \frac{\delta_{1c}v_1 + v_z(1-\delta_{1c})}{c_s\omega_{1m}(\delta_{1c}-\delta_{1m})}$$

Similarly, from (21a) and (21b), for $n \geq 2$,

$$A_{nc} = \frac{\delta_{nm}\, v_n}{\omega_{nc}\, c_s(\delta_{nm}-\delta_{nc})} \quad \text{and} \quad A_{nm} = \frac{\delta_{nc}\, v_n}{\omega_{nm}\, c_s(\delta_{nc}-\delta_{nm})}$$

Since all the A_{nc}, A_{nm}, δ_{nc}, δ_{nm}, ω_{nc} and ω_{nm} are known, the solutions (7a) and (7b) are completely determinate.

$$\zeta(\xi,\tau) = \frac{v_o}{c_o\omega_o}\sin\omega_o\tau + \frac{\delta_{1c}\,v_1 + v_z(1-\delta_{1c})}{c_s\,\omega_{1m}\,(\delta_{1c}-\delta_{1m})}\sin(\omega_{1m}\tau)\,P_1(\cos\xi)$$
$$+\sum_{n=2}^{\infty}\frac{v_n}{c_s}\left[\frac{\delta_{nm}}{\omega_{nc}(\delta_{nm}-\delta_{nc})}\sin(\omega_{nc}\tau) + \frac{\delta_{nc}}{(\delta_{nc}-\delta_{nm})\omega_{nm}}\sin(\omega_{nm}\tau)\right]P_n(\cos\xi) \tag{22a}$$

$$\psi(\xi,\tau) = -\delta_{1m}\frac{\delta_{1c}\,v_1 + v_z(1-\delta_{1c})}{c_s\,\omega_{1m}\,(\delta_{1c}-\delta_{1m})}\sin(\omega_{1m}\tau)\sin\xi$$
$$+\sum_{n=2}^{\infty}\frac{v_n\,\delta_{nc}\delta_{nm}}{c_s}\left[\frac{\sin(\omega_{nc}\tau)}{\omega_{nc}(\delta_{nm}-\delta_{nc})} + \frac{\sin(\omega_{nm}\tau)}{\omega_{nm}(\delta_{nc}-\delta_{nm})}\right]\left[\frac{n\cos\xi\,P_n(\cos\xi) - nP_{n-1}(\cos\xi)}{\sin\xi}\right] \tag{22b}$$

where v_z, v_n, $_{nm}$ and $_{nc}$, $_{nm}$ and $_{nc}$ are computed from Equations (16), (13), (6), and (5) respectively. It was shown in reference (10) that for $a/h \geq 20$ and $n \geq 2$, the coefficien- in the second term under the summation in (22) can be neglected.

The linear midsurface strain and rotation quantities, in terms of $\zeta(\xi,\tau)$ and $\psi(\xi,\tau)$, are

$$\left.\begin{aligned}\epsilon_{o\xi}(\xi,\tau) &= \frac{\partial\psi}{\partial\xi} - \zeta \qquad (23a)\\ \epsilon_{o\eta}(\xi,\tau) &= -\zeta + \psi\cot\xi \qquad (23b)\end{aligned}\right\}\ \text{midsurface normal strains}$$

$$\left.\begin{aligned}k_{o\xi}(\xi,\tau) &= \frac{1}{a}\left(1 + \zeta + \frac{\partial^2\zeta}{\partial\xi^2}\right) \qquad (24a)\\ k_{o\eta}(\xi,\tau) &= \frac{1}{a\sin\xi}(1 + \zeta - \psi\cot\xi) \qquad (24b)\end{aligned}\right\}\ \text{midsurface curvatures}$$

$$\beta(\xi,\tau) = -\frac{\partial\zeta}{\partial\xi} = \text{the angle between the surface normal and the radial ray.} \tag{25}$$

For an isotropic and homogeneous continuum, Hooke's Law yields the biaxial stress-strain relations

$$\sigma_\xi(\xi,\tau) = \frac{E}{1-\nu^2}(\epsilon_\xi + \nu\epsilon_\eta) \tag{26a}$$

$$\sigma_\eta(\xi,\tau) = \frac{E}{1-\nu^2}(\epsilon_\eta + \nu\epsilon_\xi) \tag{26b}$$

where ϵ_ξ and ϵ_η are the z-surface strain quantities

$$\epsilon_\xi(\xi,\tau) = \epsilon_{o\xi} + z(k_{o\xi}-\frac{1}{a})(1+\epsilon_{o\xi})(1-\frac{z}{a}) \tag{27a}$$

$$\epsilon_\eta(\xi,\tau) = \epsilon_{o\eta} + z[k_{o\eta}\sin(\phi-\beta)-\frac{1}{a}](1+\epsilon_{o\eta})(1-\frac{z}{a}) \tag{27b}$$

where

$$\phi(\xi,\tau) = \psi(\xi,\tau) + \xi$$

THE FLUID-SOLID INTERACTION

In order to use Hamilton's principle to obtain the governing differential equations of a fluid-filled spherical shell, it is necessary to calculate the kinetic and potential energies of the region occupied by an ideal fluid and the thin elastic shell surrounding it. The potential energy of the region is

$$V = \int_S \bar{U}dS - \int_S p_a w dS + \int_S F_e w dS + \int_{V_o} \frac{\rho_o}{2c^2}\left(\frac{\partial\Phi}{\partial t}\right)^2 dV_o \tag{28}$$

The first term in (28) is the strain energy of the shell, the second and third terms are the work done due to the internal fluid pressure and the external pressure pulse respectively while the last term is compressive strain energy stored in the fluid.

The strain energy per unit area of the thin shell is well-known.[16]

$$\bar{U} = \frac{Eh}{2(1-\nu^2)}[(\epsilon_\phi-\epsilon_\theta)^2 - 2(1-\nu)(\epsilon_\phi\epsilon_\theta - \frac{\bar{\omega}^2}{4})] + \frac{Eh^3}{24(1-\nu^2)}[(k_\phi+k_\theta)^2 - 2(1-\nu)(k_\phi k_\theta - \bar{\tau}^2)]. \tag{29}$$

The midsurface strain-displacement relations in the case of axisymmetric torsionless motion of the shell are

$$\begin{aligned} \epsilon_\phi &= \frac{1}{a}(\frac{\partial u}{\partial \phi} - w) & k_\phi &= \frac{1}{a^2}(\frac{\partial^2 w}{\partial \phi^2} + \frac{\partial u}{\partial \phi}) \\ \epsilon_\theta &= \frac{1}{a}(u\cot\phi - w) & k_\theta &= \frac{\cot\phi}{a^2}(\frac{\partial w}{\partial \phi} + u) \\ \bar{\omega} &= 0 & \bar{\tau} &= 0 \end{aligned} \tag{30}$$

The kinetic energy of the region is

$$T = \frac{1}{2}\int_{\forall_s} \rho_s[(\frac{\partial u}{\partial t})^2 + (\frac{\partial w}{\partial t})^2]d\forall_s + \frac{1}{2}\int_{\forall_o} \rho_o|\nabla\bar{\Phi}|^2\, d\forall_o \ , \tag{31}$$

Applying Hamilton's principle

$$\delta\int_{t_1}^{t_2}(T-V)dt = 0 \ ,$$

together with equations (28) to (31), results in the equations of motion of the region along with some natural boundary conditions

$$(1+\alpha^2)[-u_{\phi\phi}-u_\phi\cot\phi+(\nu+\cot^2\phi)u]-\alpha^2w_{\phi\phi\phi}-\alpha^2w_{\phi\phi}\cot\phi+[\alpha^2(\cot^2\phi+\nu)+1+\nu]w_\phi$$
$$+\frac{1-\nu^2}{E}\rho_s a^2u_{tt}=0 \tag{32}$$

$$\alpha^2u_{\phi\phi\phi}+2\alpha^2u_{\phi\phi}\cot\phi-[(1+\nu)(1+\alpha^2)+\alpha^2\cot^2\phi]u_\phi+[\alpha^2\cot^3\phi+3\alpha^2\cot\phi$$
$$-(1+\nu)(1+\alpha^2)\cot\phi]u+\alpha^2[w_{\phi\phi\phi\phi}+2\cot\phi\,w_{\phi\phi\phi}-(1+\nu+\cot^2\phi)w_{\phi\phi}$$
$$+(2\cot\phi+\cot^3\phi-\nu\cot\phi)w_\phi]+2(1+\nu)w+\frac{1-\nu^2}{E}\rho_s a^2w_{tt}$$
$$+\frac{1-\nu^2}{Eh}a^2[F_e(\phi,t)-\rho_o\Phi_t(a,\phi,t)]=0 \tag{33}$$

$$c^2[\frac{1}{r^2}(r^2\Phi_r)_r+\frac{1}{r^2\sin\phi}(\sin\phi\,\Phi_\phi)_\phi]-\Phi_{tt}=0 \tag{34}$$

where, as before, the subscript notation is used for partial differentiation. In (33), $P_a=-\rho_o\Phi_t(a,\phi,t)$ is the dynamic fluid pressure acting on shell surface.

From (34) the form of velocity potential Φ can be expanded as

$$\Phi(r,\phi,t)=\sum_{n=0}^{\infty}c_n(t)P_n(\cos\phi)j_n(kr) \tag{35}$$

The boundary conditicn between fluid and shell can be stated as the continuity of normal velocities, i.e.,

$$w_t(\phi,t)=\Phi_r(a,\phi,t) \tag{36}$$

Equations (32) and (33) are nondimensionalized by using $\psi=u/a$, $\zeta=-w/a$, $t=c_st/a$, where c_s is the wave velocity in the shell. They become

$$\ddot{\psi}+\dot{\psi}\cot\xi-\psi(\nu+\cot^2\xi)-(1+\nu)\dot{\zeta}+\alpha^2[\ddot{\psi}+\dot{\psi}\cot\xi-\psi(\nu+\cot^2\xi)+\dddot{\zeta}+\ddot{\zeta}\cot\xi$$
$$-\dot{\zeta}(\nu+\cot^2\xi)]=\partial^2\psi/\partial\iota^2 \tag{37}$$

$$(1+\nu)(\dot{\psi}+\psi\cot\xi - 2\zeta) - \alpha^2[\dddot{\psi}+2\ddot{\psi}\cot\xi - \dot{\psi}(1+\nu+\cot^2\xi) + \psi\cot\xi\,(2-\nu+\cot^2\xi)$$
$$+ \dddot{\zeta} + 2\ddot{\zeta}\cot\xi - \ddot{\zeta}(1+\nu+\cot^2\xi) + \dot{\zeta}\cot\xi\,(2-\nu+\cot^2\xi)]$$
$$+ \frac{\rho_o}{\rho_s}\frac{\partial\Phi}{\partial\tau}(a,\xi,\tau) - \frac{a^2(1-\nu^2)}{Eh}F_e(\xi,\tau) = \partial^2\zeta/\partial\tau^2 \qquad (38)$$

It should be noted that equations (37) and (38) are identical to (1) and (2) except for the two terms involving $\partial\Phi/\partial\tau$ and F_e in (38).

In the absence of the external pressure pulse, the frequency equation including the effect of the fluid can be obtained. Analogous to Section B, the nondimensional displacements, ζ and ψ, are expanded as in (3) and (4). The system of differential equations for the coefficients $a_n(\tau)$ and $b_n(\tau)$ are

$$\text{for } n = 0,\quad \frac{d^2a_o(\tau)}{d\tau^2} + \frac{2(1+\nu)}{1+\left[f\frac{j_o(\Omega)}{\Omega j_o'(\Omega)}\right]}a_o(\tau) = 0 \qquad (39)$$

$$\text{for } n \geq 1,\quad \left[1+f\frac{j_n(\Omega)}{\Omega j_n'(\Omega)}\right]\frac{d^2a_n(\tau)}{d\tau^2} + \left\{(1+\nu)\lambda_n + \alpha^2[\lambda_n^2 - \lambda_n(1-\nu)]\right\}b_n(\tau)$$
$$+ \left\{2(1+\nu) + \alpha^2[\lambda_n^2 - \lambda_n(1-\nu)]\right\}a_n(\tau) = 0 \qquad (40)$$

$$\frac{d^2b_n(\tau)}{d\tau^2} + \left\{(1+\nu) - \alpha^2[(1-\nu) - \lambda_n]\right\}a_n(\tau) - \left\{[(1-\nu) - \lambda_n](1+\alpha^2)\right\}b_n(\tau) = 0\,, \qquad (41)$$

where $f = \rho_o a/\rho_s h$ = nondimensional fluid-shell parameter and $\lambda_n = (n+1)n$.

The solution of (39), (40) and (41) are assumed to be of the form

$$a_n(\tau) = A_n e^{i\Omega s\tau}$$

$$b_n(\tau) = B_n e^{i\Omega s\tau} \quad , \tag{42}$$

where $s = c/c_s$ = ratio of the compressive wave speed in the fluid to the wave speed in bending. Substitution of (42) into (39) to (41) yields

$$\text{for } n = 0, \quad s^2\Omega^2 - \frac{2(1+\nu)}{\left[1+f\frac{j_0(\Omega)}{\Omega j_0'(\Omega)}\right]} = 0 \tag{43}$$

$$\text{for } n \geq 1 \quad s^4\Omega^4 + \left\{\frac{\left[1+f\frac{j_n(\Omega)}{\Omega j_n'(\Omega)}\right][1-\nu-\lambda_n](1+\alpha^2)-2(1+\nu)-\alpha^2[\lambda_n^2-\lambda_n(1-\nu)]}{\left[1+f\frac{j_n(\Omega)}{\Omega j_n'(\Omega)}\right]}\right\} s^2\Omega^2$$

$$-\left\{\frac{(1+\nu)\{2[1-\nu-\lambda_n](1+\alpha^2)+\lambda_n[1+\nu-\alpha^2(1-\nu-\lambda_n)]+\alpha^2[\lambda^2-\lambda_n(1-\nu)](2-\lambda_n)}{\left[1+f\frac{j_n(\Omega)}{\Omega j_n'(\Omega)}\right]}\right\} = 0 \tag{44}$$

It is interesting to note that the limiting cases of equations (43) and (44) agree with the results obtained previously, as it must.

Case 1 $f = 0$ corresponds to the absence of fluid, i.e., the in-vacuo case given by (35).

Case 2 $s \to 0$ corresponds to a rigid shell and the equation degenerates to

$$j_n'(\Omega) = 0 \quad , \tag{45a}$$

which is easily shown to be equal to

$$2\Omega J'_{n+(1/2)}(\Omega) = J_{n+(1/2)}(\Omega) \quad . \tag{45b}$$

Equation (45b) was obtained by Güttinger.[4]

Case 3 $\alpha^2 = 0$ yields the frequency equation corresponding to the membrane (extensional) theory.

REFERENCES

1. Lamb, H., "On the Vibrations of a Spherical Shell," Proceedings of the London Mathematical Society, Vol. 14, pp. 50-56, (1882).

2. Rayleigh, "On the Vibrations of a Gas Contained within a Rigid Spherical Envelope," Proceedings of the London Mathematical Society, Vol. 4, pp. 93-103, (1872)

3. Anzelius, A., "The Effect of an Impact on a Spherical Liquid Mass," Acta. Path. Microbiol. Scand., Sup. 48, pp. 153-159, (1943).

4. Güttinger, W., "Der Stosseffekt auf eine Flussigkeitskugel als Grundlage einer physikalischen Theorie der Entstehung von Gehirnverletzungen," Z. Naturforsch., 5a, pp. 622-628, (1950).

5. Love, A. E. H., "On Free and Forced Vibrations of an Elastic Spherical Shell Containing a Given Mass of Liquid," Proceedings of the London Mathematical Society, Vol. 19, pp. 170-207, (1887).

6. Baker, W. E., "Axisymmetric Modes of Vibration of Thin Spherical Shells," Journal of the Acoustical Society of America, Vol. 33, p. 1749, (1961).

7. Silbiger, A., "Free and Forced Vibrations of a Spherical Shell," ONR Report U-106-48, (1960).

8. Naghdi, P. M., and Kalnins, A., "On Vibrations of Elastic Spherical Shells," Journal of Applied Mechanics, Vol. 29, p. 65, (1962).

9. Kalnins, A., "Effect of Bending on Vibrations of Spherical Shells," Journal of the Acoustical Society of America, Vol. 36, p. 74, (1964).

10. McIvor, I. K., and Sonstegard, D. A., "Axisymmetric Response of a Closed Spherical Shell to a Nearly Uniform Radial Impulse," Journal of the Acoustical Society of America, Vol. 40, pp. 1540-1547, (1966).

11. Junger, M. C., "Vibration of Elastic Shells in a Fluid Medium and the Associated Radiation of Sound," Journal of Applied Mechanics, Vol. 74, pp. 439-445, (1952).

12. Goodman, R. R., and Stern, K., "Reflection and Transmission of Sound by Elastic Spherical Shells," Journal of the Acoustical Society of America, Vol. 34, pp. 338-344, (1962).

13. Hickling, R., "Analysis of Echoes from a Solid Elastic Sphere in Water," Journal of the Acoustical Society of America, Vol. 34, pp. 1582-1592, (1962).

14. Morse, P. M., and Feshbach, H., "Methods of Theoretical Physics, McGraw-Hill Book Co., New York, Part II, pp. 1469-1472, (1953).

15. Rand, R., and DiMaggio, F., "Vibrations of Fluid-Filled Spherical and Spheroidal Shells," Journal of the Acoustical Society of America, Vo. 42, pp. 1278-1286, (1967).

16. Novozhilov, V. V., "Thin Shell Theory," 2nd ed., Noordhoff Ltd., Groninger, Holland, (1964).